ไพโรไลซิสด้วยตัวเร่งปฏิกิริยาของซังข้าวโพดโดยใช้เอสบีเอ-15 รองรับโลหะ

นางสาวช่อมาลี กสิบาล

วิทยานิพนธ์นี้เป็นส่วนหนึ่งของการศึกษาตามหลักสูตรปริญญาวิทยาศาสตรมหาบัณฑิต
สาขาวิชาปิโตรเคมีและวิทยาศาสตร์พอลิเมอร์
คณะวิทยาศาสตร์ จุฬาลงกรณ์มหาวิทยาลัย
ปีการศึกษา 2554

CATALYTIC PYROLYSIS OF CORNCOB USING METAL SUPPORTED SBA-15

Miss Chomalee Kasiban

A Thesis Submitted in Partial Fulfillment of the Requirements
for the Degree of Master of Science Program in Petrochemistry and Polymer Science
Faculty of Science
Chulalongkorn University
Academic Year 2011

Thesis Title	CATALYTIC PYROLYSIS OF CORNCOB USING METAL SUPPORTED SBA-15
By	Miss. Chomalee Kasiban
Field of Study	Petrochemistry and Polymer Science
Thesis Advisor	Duangamol Tungasmita, Ph.D.

Accepted by the Faculty of Science, Chulalongkorn University in Partial Fulfillment of the Requirements for the Master‟s Degree

……..Dean of the Faculty of Science

(Professor Supot Hannongbua, Dr. rer. nat.)

THESIS COMMITTEE

……Chairman

(Professor Pattarapan Prasassarakich, Ph.D.)

……Thesis Advisor

(Duangamol Tungasmita, Ph.D.)

……Examiner

(Associate Professor Wimonrat Trakarnpruk, Ph.D.)

……External Examiner

(Gamolwan Tumcharern, Ph.D.)

ช่อมาลี กสิบาล : ไพโรไลซิสด้วยตัวเร่งปฏิกิริยาของซังข้าวโพดโดยใช้เอสบีเอ-15 ที่รองรับโลหะ (CATALYTIC PYROLYSIS OF CORNCOB USING METAL SUPPORTED SBA-15) อ.ที่ปรึกษาวิทยานิพนธ์หลัก: ดร. ดวงกมล ตุงคะสมิต, 150 หน้า

ในงานวิจัยนี้ได้เตรียมตัวเร่งปฏิกิริยาที่ถูกแบ่งออกเป็น 3 กลุ่ม ประกอบด้วย วัสดุที่มีรูพรุนขนาดเล็ก (ซีโอไลต์เบต้า) วัสดุที่มีรูพรุนขนาดกลาง (ซิลิกา เอสบีเอ-15 และอะลูมิเนียม-เอสบีเอ-15) และโลหะนิกเกิล และแพลเลเดียม บนตัวรองรับเอสบีเอ-15 และซีโอไลต์เบต้า ตัวเร่งปฏิกิริยาถูกตรวจสอบลักษณะเฉพาะด้วยเทคนิคการเลี้ยวเบนของรังสีเอกซ์ เทคนิคการดูดซับไนโตรเจน อะลูมิเนียมนิวเคลียร์แมกเนติกเรโซแนนซ์สำหรับสถานะของแข็ง กล้องจุลทรรศน์อิเล็กตรอนแบบส่องกราด และกล้องจุลทรรศน์อิเล็กตรอนแบบส่องผ่าน จากนั้นตัวเร่งปฏิกิริยาทั้งหมดถูกนำมาประยุกต์สำหรับกระบวนการไพโรไลซิสโดยใช้ความร้อนและตัวเร่งปฏิกิริยา ของวัสดุเหลือใช้ทางการเกษตรดังเช่นซังข้าวโพดในเครื่องปฏิกรณ์ท่อสแตนเลส ภายใต้บรรยากาศไนโตรเจน ปัจจัยที่ส่งผลต่อปฏิกิริยา ได้แก่ อุณหภูมิปฏิกิริยา ชนิดและปริมาณของตัวเร่งปฏิกิริยา อุณหภูมิไพโรไลซิสเป็นตัวแปรสำคัญที่มีผลต่อการสลายของชีวมวลที่อุณหภูมิต่ำ 300 องศาเซลเซียส และเวลาที่น้อยในปฏิกิริยาศึกษาการแตกตัวของซังข้าวโพดบนตัวเร่งปฏิกิริยาต่างๆ ผลิตภัณฑ์ก๊าซหลัก คือ มีเทน สารประกอบไฮโดรคาร์บอนที่มีจุดเดือดสูงกว่านอมัลเพนเทน (C_5^+) และคาร์บอนไดออกไซด์ ในขณะที่สารประกอบไฮโดรเจนชนิดเบาที่มีคาร์บอน 2-4 อะตอมเป็นผลิตภัณฑ์รอง สำหรับผลิตภัณฑ์ที่เป็นของเหลวกลั่น ถูกแบ่งเป็น 6 กลุ่มหมู่ฟังก์ชั่น ประกอบด้วย กรดและแอลกอฮอล์ กลุ่มสารประกอบอนุพันธ์ฟูแรน กลุ่มฟีนอลิก กลุ่มสารคีโตนชนิดเบา และกลุ่มสารเอสเตอร์ชนิดเบา ตัวเร่งปฏิกิริยาอะลูมิเนียม-เอสบีเอ-15(20) ให้ผลิตภัณฑ์ในกลุ่มเอสเตอร์ชนิดเบาสูง เช่น 2-เมทิลบิวทิล โพพาโนอิก เอซิด เอสเตอร์ และ 2-เมทิลเฟนิลอะซิเตท ซึ่งความสำคัญใช้เป็นสารขั้นกลางผลิตสารแต่งกลิ่นหวาน กลิ่นแอปเปิ้ล และกลิ่นกล้วยในอุตสาหกรรมอาหารได้

สาขาวิชา ปิโตรเคมีและวิทยาศาสตร์พอลิเมอร์ ลายมือชื่อนิสิต .....

ปีการศึกษา 2554 ลายมือชื่ออ.ที่ปรึกษาวิทยานิพนธ์หลัก .....

5172259623: MAJOR PETROCHEMISTRY AND POLYMER SCIENCE
KEYWORDS: AL-SBA-15 / CORNCOB / CATALYTIC PYROLYSIS

CHOIMALEE KASIBAN: CATALYTIC PYROLYSIS OF CORNCOB USING METAL SUPPORTED SBA-15.
ADVISOR: DUANGAMOL TUNGASMITA, Ph.D. 150 pp.

In this study, prepared catalysts were divided into three groups consisting of microporous material (beta zeolite), mesoporous materials (SBA-15 and Al-SBA-15) and metal (Ni and Pd) loading on supported SBA-15 and beta zeolite. The catalysts were characterized by X-ray powder diffraction, nitrogen sorption analysis, solid state ^{27}Al-nuclear magnetic resonance, scanning electron microscopy and transmission electron microscopy. All catalysts were applied for thermal and catalytic pyrolysis processes of agricultural waste as corncob in a stainless steel tube reactor under nitrogen atmosphere. Factors affected to reaction such as reaction temperature, catalytic type and amount of catalyst were studied. The pyrolysis temperature was the important parameter affected to the decomposition of biomass at low temperature as 300°C and short time were applied to be cracked corncob over various catalysts. The gas products were methane, the hydrocarbon having boiling point higher than *n*-pentane (C_5^+) and CO_2 whereas the light hydrocarbon gases having 2-4 carbon atoms (C_2-C_4) were minor products. The distillated liquid products were divided into six functional groups including acid and alcohol groups, furan derivative group, phenolic compound group, light ketone group, light ester group and others. The Al-SBA-15(20) catalyst gave high light ester group such as 2-methyl-butyl propanoic acid ester and 2-methoxy phenyl acetate which most important used as intermediate products in sweet flavor and apple, banana aroma in the food industry.

Field of Study: Petrochemistry and Polymer Science Student's Signature .....
Academic Year: 2011 Advisor's Signature .....

ACKNOWLEDGEMENTS

The success of this research can be attributed to the extensive support and assistance from Dr. Duangamol Tungasmita, my thesis advisor. I would like to sincere gratitude to her for valuable advice and guidance in this research as well as extraordinary experiences throughout the work.

I also would like to give my gratitude to the chairman and members of this research committee for all of their comment and useful suggestion about this research. Moreover, I would like to thank Department of Petrochemistry and Polymer Science, Faculty of Science, Chulalongkorn University for providing the convenience in laboratories and instrument. I would like to thank the Nakhon Sawan Field Crop Research Center for supporting as raw material in biomass. In addition, Thailand Japan Technology Transfer Project a loan supported by Japan Banks for International Cooperation (TJTTP-JBIC) for instrument support.

Many thanks go in particular to the members of Materials Chemistry and Catalysis Research Unit for their help and encouragement throughout the course of my research and study. Finally, I would like to express my deepest gratitude to my family for their entirely care and support. The usefulness of this thesis, I dedicate to my family and all teachers who taught me since my childhood.

CONTENTS

Page

Page

Page

Page

LIST OF TABLES

Page

Table

LIST OF FIGURES

Figure **Page**

Figure **Page**

Figure **Page**

Figure **Page**

LIST OF SCHEMES

Scheme **Page**

LIST OF ABBREVIATIONS

Å	Angstrom
a.u.	Arbitrary unit
BET	Brunauer-Emmett-Teller
BJH	Barret, Joyner, and Halenda
^{o}C	Degree Celsius
GC	Gas chromatography
g	Gram (s)
h	Hour
MAS-NMR	Magic angle spinning-nuclear magnetic resonance
MS	Mass spectroscopy
μm	Micrometer (s)
mg	Milligram (s)
ml	Milliliter (s)
min	Minute (s)
M	Molarity
nm	Nanometer (s)
ppm	Part per million
%	Percentage
SEM	Scanning electron microscopy
TEM	Transmission electron microscopy
TEOS	Tetraethyl orthosilicate
XRD	X-ray diffraction

CHAPTER I

INTRODUCTION

1.1 Motivation

In the present, the world has been confronting an environmental problem due to rapid society development and the increasing demands of energy worldwide. Department Energy of Energy Information Administration (EIA) has predicted demand trends for the global liquid fuel supply until 2030. Global demand for liquid fuel in 2006 was 85 million barrels per day and then the global demand seems to increase sharply until 2030 was expected to 106.6 million barrels per day [1]. The fossil fuel energy resources such as crude oil, nature gas and coal are limited. Thus, it is essential to seek for renewable energy to replace fossil fuel.

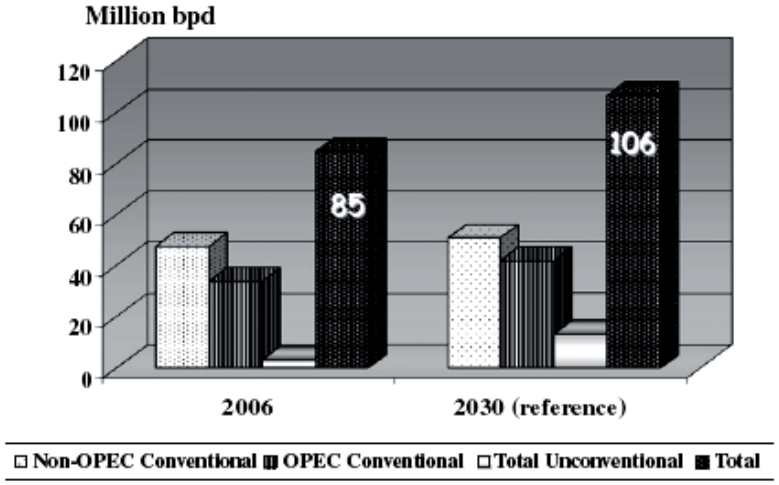

Figure 1.1 The global liquid fuel supply in 2006-2030.

The renewable energy is basic energy from natural resource which it derived from solar energy, wind energy, ocean energy, hydro-electric, geothermal energy, biomass and other sources. But biomass is the only renewable energy resource of carbon for the production of chemicals, materials and fuel. Figure 1.2 shows the global consumption for primary energy by sources in 2011. The total renewable energy demand was 98 kilo tonnes of oil equivalents (ktoe) and the proportion of renewable

energy was 8% from all energy sources. Biomass is a large source of renewable energy source. Biomass includes biofuels, wood and waste materials, municipal solid waste, straw, agricultural waste accounts for 48% of total renewable energy consumption [2]. Therefore, biomass is particularly suited a source abundant, low cost feedstock for production of bio based chemicals, fuels and energy to substitute fossil resource. Biomass is environmentally friendly and sustainable in nature. It has lower emissions of sulfur dioxide (SO_2), nitrogen oxides (NO_x) and soot less than fossil fuels [3]. Benefit of biomass energy including generating electricity, intermediate chemical, fueling vehicles and providing process heat for industrial. Thus, many counties have become interest in biomass energy.

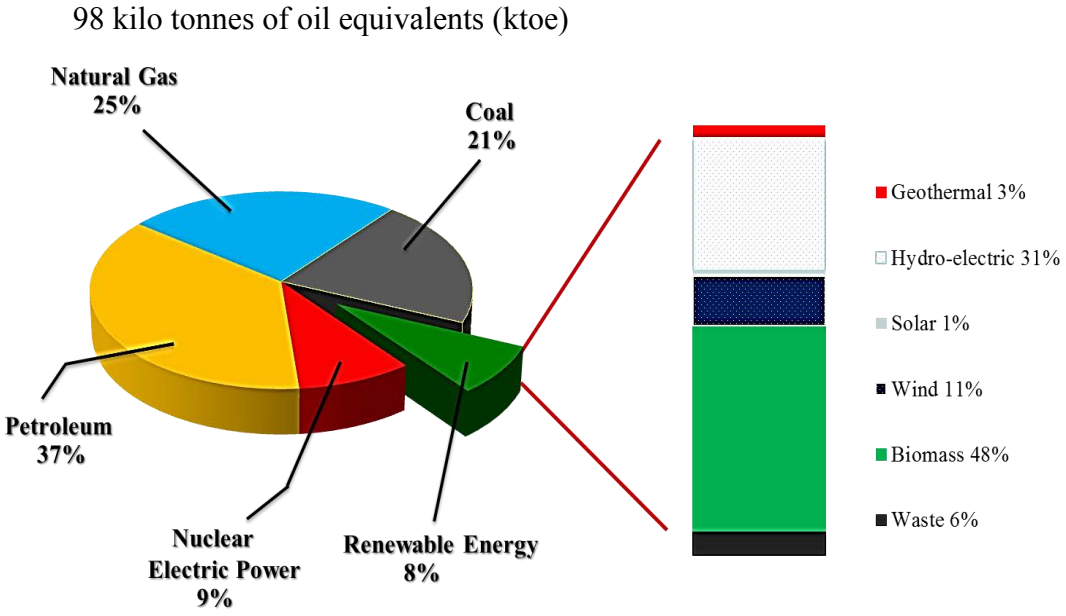

Figure 1.2 The primary energy consumption by source and renewable energy production consumption by source in 2011.

Thailand is an agricultural country. Therefore, there are varieties of agriculture residue products can be used as an energy source. The renewable energy resources have been developed continuously to respond the high energy demand in manufacturing, transport, commercial and residential sectors. The biomass residue of major crop in Thailand consists of rice husk, sugarcane, rubber wood, palm oil, cassava, corncob and eucalyptus residues is presented in Table 1.1. The amount crop

residues estimated to be about 68 million tons which indicated that potential there is a possibility for increasing the use of biomass as an energy source. The biomass energy is the second major energy source in Thailand which important energy source in households and up-country industries.

Table 1.1 Biomass residues of Thailand [4]

Type	**Production (million tons)**	**Agricultural residues**	**CRR***		**Amount crop residue (million tons)**
			%Yield	**Tons/ acres**	
Rice	25	husk	21%	-	5.25
Rice	25	rice straw	49%	-	12.25
Sugarcane	50	bagasse	28%	-	14
Sugarcane	50	leaf	17	-	8.5
Rubber wood	0.25	sawdust	-	1.2	0.75
Rubber wood	0.25	slab	-	4.8	3
Rubber wood	0.25	herb	-	2	1.25
Palm oil	5	fiber	19%	-	0.95
Palm oil	5	palm shell	4%	-	0.2
Palm oil	5	palm empty bunch	32%	-	1.6
Palm oil	5	palm leaf	141%	-	7.05
Palm oil	0.01	palm stalk	-	4	0.1
Cassava	10	cassava waste	37%	-	3.7
Cassava	10	cassava stalk	0.06%	-	0.01
Cassava	17	cassava root	20%	-	3.4
Corn	5	corncob	24%	-	1.2
Eucalyptus	0.6	stalk	-	1.2	1.8
Total					**68**

*CRR = Crop to residues ratios

Biomass materials is known as lignocellulosic biomass. Mainly compositions of lignocellulosic biomass consist of cellulose, hemicellulose, lignin and other compounds which the proportion via thermochemical or biochemical process. Biochemical process is general slowly process and yield single or specific products but thermochemical processes are rapid and yield multiple and complex products, which can be divided into combustion, gasification and pyrolysis. All of products from the thermo-chemical processes available for converting biomass to a more useful energy showed in Figure 1.3 [5]. Combustion is well-established commercial technology whereas combustion technologies lead to air pollution problem. Gasification has been practicing for previous years and there are many examples of demonstration and pre-commercial process. Pyrolysis process is a decomposition of materials that occurs in the absence of oxygen or less oxygen. This process can be converted biomass into non-condensable gases, liquid products or bio-oils and solid char depend on the optimum conditions. In addition, bio-oil obtained pyrolysis process cannot be used directly as fuel because of high oxygen content, high acidity and energy value is half that of petroleum fuels. Thus, catalyst adding in this process will promote high cracking activity and product selectivity in catalytic pyrolysis biomass [6].

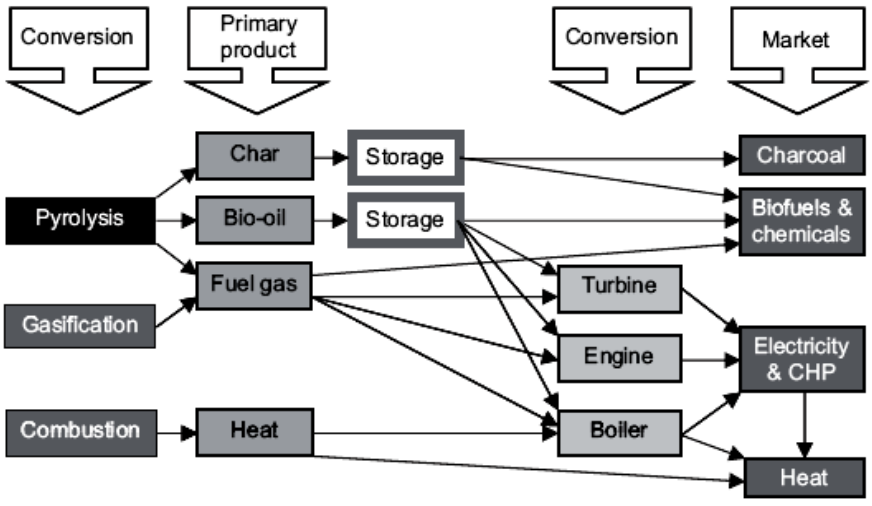

Figure 1.3 Summaries for the products from the thermo-chemical processes.

Generally, the heterogeneous catalysts used in the biomass are mesoporous and microporous materials. SBA-15 is a high hydrothermal stability mesoporous material [7], [8]. SBA-15 composes of parallel cylindrical pores with axes arrange in a hexagonal unit cell which is wider pores than other mesoporous materials. However, there are only few papers reported about the synthesis of Al-SBA-15 and using in pyrolysis process of biomass [9].

1.2 Objectives

1. To synthesize and characterize mesoporous material SBA-15 under hydrothermal condition.
2. To aluminate SBA-15 and characterize the Al-SBA-15 catalyst.
3. To prepare and characterize the metal supported SBA-15 by impregnation method.
4. To investigate the optimum condition for catalytic pyrolysis of corncob.

1.3 Scope of work

The synthesize SBA-15 [10] and Al-SBA-15 [11] under hydrothermal method was investigated using triblock copolymer as pore directing agent. The SiO_2/Al_2O_3 mole ratios in gel were varied as 20, 30 and 60. Moreover, nickel(II) nitrate and palladium(II) chloride were utilized as metal supported on SBA-15 by impregnation method. The optimum condition for pyrolysis of corncob over catalyst was determined by studying the effects of temperature, catalytic amounts, SiO_2/Al_2O_3 mole ratios in Al-SBA-15 and metal type. They were tested for their activity in the catalytic pyrolysis of corncob under optimum condition.

1.4 Literature

Pyrolysis of biomass material is operated at low oxygen atmosphere. The degradation of biomass is converted to gas, liquid and residues during pyrolysis which depends on the mode of pyrolysis condition and the type of biomass [12].

In 2004, Xie et al. [13] investigated the pyrolysis behavior of waste corncob in a tube-type stainless steel reactor at temperature 350-600°C under N_2 atmosphere. At temperature 350-400°C, the gas yield was about 27-40.96% (v/v) which CO and CO_2

were mainly composition of gas product about 80-95% (v/v) and other gases such as H_2, CH_4, C_2H_4 and C_4H_8. When temperature was increased at range 450-500°C, CO and H_2 were increased about 50% (v/v). The yield of liquid was about 34-40wt% which main components of liquid product were phenol, furanmethanol and related derivative compounds. The application of liquid from pyrolysis of corncob was oxygenated fuel and raw chemical material for refining process.

In 2008, Suneerat et al. [14] studied the behavior of three agricultural residues in Thailand including rice husk, rice straw and corncob using a drop-tube fixed-bed reactor with heating rate (>1,000°C/s) at temperature 850°C and holding time range from 1-10,800 seconds. The weight loss occurred within after injected into the reactor and accounted 70-90% of the initial weight. Corncob contained highest cellulose content but lowest lignin content which obtained high gas yield. Main gas product from pyrolysis of corncob was CO due to the decomposition of cellulose.

In 2010, Akeem M. et al. [15] studied the fast pyrolysis of five biomasses from sub-Sahara Africa and Europe including spruce, beech, iroko, albiza and corncob at temperature of 470°C for 60 min under N_2 flow gas and characterized physical properties of bio-oil. Main compositions of bio-oil from pyrolysis of biomass were acetic acid, hydroxyacetaldeyde, hydroxypropanone and levoglucosan. Meanwhile, bio-oil from corncob was found the highest yield of hydroxypropane and acidic because of the degradation of xylose from hemicellulose. In addition, 4-vinylphenol was found only in corncob bio-oil which lignin derived product.

Zeolite is known catalyst for catalytic cracking in the oil refining and petrochemical industries. Several zeolite catalysts are applied in the pyrolysis of biomass due to strong acidic catalyst such as ZSM-5, Y and beta zeolite which zeolite was affected selective to deoxygenation and synthesis of aromatic hydrocarbon of pyrolytic vapors [12].

In 2008, Murzin et al. [16] studied non-catalytic and catalytic pyrolysis of pine wood chips in a fluidized bed reactor at 450°C used zeolite with several SiO_2/Al_2O_3 mole ratios including H-beta(25), H-Y(12), H-ZSM-5(23) and H-MOR(20) as catalysts. The H-ZSM-5(23) zeolite gave low amount of alcohols and acids whereas the formation of ketones was high as compared with other zeolites. Moreover, H-MOR(20) lead to the formation of acids and alcohols whereas gave only small

amounts of polyaromatic hydrocarbons which no detected in the non-catalytic pyrolysis oils.

In 2008, Murzin et al. [17] investigated the acidity effect of the H-beta zeolite on the yield products from catalytic pyrolysis of pine wood in a fluidized bed reactor at 450°C. The SiO_2/Al_2O_3 mole ratios of beta zeolites in this studied were 25, 150 and 300. They observed the higher acidity amounts of H-beta zeolites were produced less organic oil yield whereas yield of char was increased which as a result of coke formation. Moreover, water was formed during catalytic pyrolysis and the increasing of water amount probably led to the formation of polyaromatic hydrocarbons.

In 2009, Xiao et al. [18] investigated fast pyrolysis of corncob in 2-in-1 process fluidized bed reactor and used HZSM-5 zeolite with Si/Al mole ratio 24 as catalyst. The optimal condition was at temperature 550°C, N_2 flow rate 3.4 L/min, static bed reactor height of 10 cm and 1-2 mm particle size of biomass. The high yield of liquid was 56.8% at 550°C and the yield of gas was increased from 12.1-21.3% with the increasing of temperature from 400-700°C. Under optimal condition with HZSM-5 catalyst investigated component of aromatic hydrocarbons in oil fraction and the decreasing of oxygen content was about 25% when compared with non-catalytic reaction.

In 2011, Akwasi et al. [19] studied the Py/GC-MS experiment of eight lignocellulose biomass with nine zeolite catalysts including H-Ferrierite (Si/Al was 20), H-Mordenite (SiO_2/Al_2O_3 was 40), H-Y (SiO_2/Al_2O_3 was 10), H-ZSM-5 (SiO_2/Al_2O_3 were 23, 50, 280) and H-Beta (SiO_2/Al_2O_3 were 25, 38, 360). Relative composition of pyrolytic products consists of non-condensable gas, condensable vapors and solid residues. The oxygenated compounds of all catalysts were decreased in pyrolytic vapors. The H-ZSM-5 (SiO_2/Al_2O_3 was 23) mostly produced aromatic hydrocarbons whereas H-Beta (SiO_2/Al_2O_3 was 25) increased amount of coke due to heavy hydrocarbons being produced within the pores of the zeolite during catalytic pyrolysis.

Mesoporous catalysts are widely used in biomass pyrolysis such as MCM-41, SBA-15 and modified mesoporous catalysts. SBA-15 is high surface areas and large pore size with hexagonal array of uniform mesopores material, wall thickness of pore size from 3-30 nm, and high hydrothermal and thermal stability [12]. These properties

of SBA-15 promising catalyst for treating biomass pyrolysis vapors which contain high water and large structure. Moreover, SBA-15 is a pure silica material lack of acidity. The development acid sites of SBA-15 can be incorporation of Al in framework of the mesoporous silica by post-synthesis.

In 2000, Samolda et al. [20] studied catalytic pyrolysis of Lignocell HBS 150-500 as biomass with commercial catalyst including HZSM-5, fluid catalytic cracking catalysts (FCC: ReUSY), alumina (α-, γ-Al_2O_3) and transition metal catalysts (Fe/Cr). The experimental was operated fixed bed reactor at reaction temperature 500°C using N_2 gas flow. The alumina catalyst such as α-, γ-Al_2O_3 were very low surface area without active site and they were found high liquid yield but they could not improve composition of liquid product. Meanwhile, HZSM-5 zeolite converted carbonyls compound to hydrocarbons whereas transition metal catalyst (Fe/Cr) converted heavy phenolic compounds to phenol and light phenolic.

In 2009, Zhu et al. [9] studied fast pyrolysis of sawdust by pyrolysis-gas chromatography/mass spectrometry with SBA-15 and Al-SBA-15 catalysts with several Si/Al mole ratios included 10, 20, 35 and 70. All Al-SB-15 catalysts were more active than SBA-15. After catalytic cracking, levoglucosan was decreased or completely eliminated. The increasing of light phenols, light furans, acetic acid and hydrocarbon yield were brought to the increasing of bio-oils heating value.

In 2009, Funda et al. [21] investigated the yields and product composition from pyrolysis of corncob in fixed-bed reactor at temperature 300-800°C with alumina as catalyst. In non-catalytic experiment gave the formation of char products at low temperature (300-400°C). At moderate temperature (600°C) produced high liquid oil products whereas high temperature (600-800°C) was converted to the cracking of the products into gas products. The optimal condition was at moderate temperature for alumina catalyst. After catalytic reaction, the total phenolic compounds were decreased and the polyaromatic hydrocarbons (PAHs) were increased. Moreover, the carboxylic acids were reduced in corncob liquid products.

Transition metal material is a good catalyst for biomass pyrolysis such as palladium (Pd) metal plays an important role in organic synthesis. Zero valence of palladium exhibited good catalytic activity in the formation of C-C bond. The palladium catalyst was problem for the recycle in large-scale application. Therefore, it

is necessary to develop heterogeneous catalysts which can be recovered from the reaction system by loading metal supported on mesoporous material [22]. Nickel (Ni) was widely used as catalyst for dehydrogenation and hydrogenation reactions due to low cost and high activity. However, nickel metal suffered from catalyst deactivation, sintering and coke deposition [23].

In 2005, Sineenat [24] studied the corncob pyrolysis in a circulating fluidized bed reactor with nickel supported on alumina as catalyst. The optimal condition was 850°C, 5wt% amount of catalyst which 9wt% Ni loaded on alumina. At this condition, biomass gave methane reforming and tar cracking and gas products as H_2 and CO about 52.0% and 18.0%, respectively.

In 2010, Zhu et al. [25] studied the palladium supported on SBA-15 in catalytic upgrading for pyrolysis vapors of poplar wood at temperature 600°C with heating rate of 20°C/millisecond. The Pd/SBA-15 (3wt%) cracked the lignin-derived oligomers to monomeric phenols and converted to phenols without the carbonyl compounds and unsaturated hydrocarbons on the side chain which phenol was useful in chemicals. In addition, the anhydrosugars were completely eliminated and linear aldehydes, acids were decreased.

Thus, in this research investigated thermal and catalytic pyrolysis of agricultural waste as corncob. The corncob pyrolysis in the presence of pure SBA-15, incorporated aluminum into SBA-15 and impregnated of metal on supported catalyst. The pyrolysis of corncob was determined by studying the effect of reaction temperature in the range 250-600°C, catalyst type, corncob to catalyst ratios and metal type.

CHAPTER II

THEORY

2.1 Biomass

2.1.1 Definition

The term of biomass (*bio* meaning *life* + *maza* meaning *mass*) refers to non-fossil fuels and biodegradable organic material derived from plants, animals and microorganisms. Biomass is resource of organic compounds from plant and animal material especially agricultural waste products and ago-industries residue which used as a fuel source [26].

2.1.2 Biomass feedstock

The biomass is organic materials that use as feedstock in pyrolysis process. Biomass resources are large amounts of energy of varying types and quality. Biomass resources can be divided into two categories, which are natural biomass and non-biodegradable organic from industrial. Natural biomass resources include wood crop, agricultural waste and by-product, herbaceous wood, municipal solid waste, animal wastes, bagasse, waste from food processing and aquatic plants and algae. Non-biodegradable organic resources include paper waste, industrial residue, plastic waste and other materials which they are not converting by biochemical processes. The main categories of biomass feedstock are showed in Table 2.1.

Table 2.1 The main categories of biomass feedstock

Source of residue	Type of residue
Forest products	Woods, logging residues, trees, sawdust, bark and other
Biorenewable wastes	Agricultural wastes, crop residues, mill wood wastes, urban organic wastes
Energy crops	Herbaceous wood crops, sugar crop, forage crops, grasses, oil-seed crops, starch crops, switchgrass, miscanthus
Aquatic plants	Algae, water weed, reed and ruches, water hyacinth
Food crops	Grains, oil crops
Sugar crops	Sugar cane, molasses, sugar beets
Algae	Prokaryotic algae, eukaryotic algae
Organic wastes	Industrial organic wastes, municipal solid waste, municipal sewage and sludge
Landfill	Hazardous waste, non-hazardous waste, liquid waste, inert waste

2.1.3 Biomass resources in Thailand [4]

The energy demand in Thailand increased rapidly as results of the economic development and population growth. In 2002, the total energy demand in Thailand was about 18,679 kilo tonnes of oil equivalents (ktoe) which increased from previous year at the rate of 4.93% shows in Table 2.2. However, among various energy supplies, the various sources of energy supply, petroleum products, coal and lignite dominated a main energy source which supplied energy to 4,235 million tonnes of oil

equivalents (ktoe) and 4,884 kilo tonnes of oil equivalents (ktoe), respectively. However, biomass energy supplied about 4,007 kilo tonnes of oil equivalents (ktoe) and accounting of 17.1% of the total energy consumption. Thailand is an agro-industry country which provides varieties of agriculture products residue that can be used as energy source. Biomass materials in Thailand were as used to generate electricity, heat, or liquid fuels such as ethanol for motor vehicles that substantially lower environmental impact than conventional fossil fuels.

Table 2.2 The energy consumption by sources in Thailand

Source (Unit: ktoe)[a]	**1998**	**1999**	**2000**	**2001**	**2002**
Coal and Lignite	3,237	3,876	3,627	4.377	4,884
Petroleum products	3,853	3,971	4,136	3,988	4,235
Natural gas	877	1,112	1,374	1,556	1,745
Electricity	2,566	3,012	3,346	3,494	3,808
Biomass	3,222	3,517	3,725	3,507	4,007
Total	13,754	15,488	16,208	16,922	18,679

[a] ktoe : kilo tonnes of oil equivalents

Biomass feedstock in Thailand is derived from various sources such as wood and wood residues, agricultural crop and residues, agro-industrial waste including:

- Agricultural crops such as sugarcane, cassava, corn are sources of carbohydrate, starch and sugar. These energy crops can be used for vegetable oil to energy fuel.

- Agricultural residues such as rice straw from rice fields, cassava rhizome from tapioca and corncob from cornfields.
- Wood and wood residues such as fast-growing trees, wood waste from wood mill are waste from pulp and paper mill.
- Waste stream such as rice husk from rice mills, molasses and bagasse from sugar refineries, residues from oil palm extraction plants, municipal solid waste and other waste.

2.2 Biomass characteristics

2.2.1 Physical characteristics [27]

The raw biomass is a large of moisture, organic compounds and minerals especially, solid materials. Thus, physical properties are important in the design and handling of reactor for processing plant and prepare raw biomass for use as fuel energy. The physical processes of raw biomass include dewatering and drying, size reduction, densification and separation. Dewatering and drying is removal of moisture from raw biomass. The dewatering process is removed moisture as liquid whereas the drying process is removed moisture as vapors. For the reduction size process is reduced physical size of raw biomass before direct use fuel. The size reduction technique consist of fabrication into fuel pellets, cubes and briquettes or small particles The advantages of size reduction process are storage volume, facilitate handling of the solid material and transport of the material. Furthermore, the density of raw biomass such as hays, straws and other agricultural crops, reduce storage space and transportation costs. For separation process of raw biomass is a physically separate potential biomass feedstock into two or more compounds for different application, for example the separation of agricultural biomass into foodstuffs and residues that serve as fuel or as raw material for fuel industry.

2.2.2 Chemical characteristics

2.2.2.1 Moisture content

The moisture content in biomass is the quantity of water per unit mass of the dry solid. Moisture content is described in two ways; wet basis and dry basis. The operation involved with power generation most often consider moisture content on a wet basis. The wet basis water content is the ratio of the total mass of moisture in the original sample to the original wet mass of sample. The dry basis moisture content is favored of the manufacturers of wood products. The dry basis moisture content is the fractional water content or the weight of water divided by the sample weight when sample is dry. In addition, all moisture contents refer to on a wet basis. The moisture contents of biomass feedstock are high value and resulted to reduce combustion efficiency [27].

2.2.2.2 Proximate analysis

The proximate analysis describes the characteristics of solid fuels and biomass materials in combustion process including the volatile matter, fixed carbon and ash content. In general, biomass materials are highly volatile compounds which need for specialized reactor designs to cope with the rapid evolution of gas. Fossil fuels such as coals with very high fixed carbon need to be burnt on a grate because they take a long time to burn out if they are not pulverized to a very small size. The highly of amounts volatile matter and fixed carbon directly affect to the heating value of bio-oil. The high of ash content in biomass materials is relatively difficult in the air pollution control. The wood biomass is lower ash content, higher volatiles and less fixed carbon compared with coal fuel shows in Table 2.3 [28].

Table 2.3 Proximate analysis of solid fuels and biomass materials

Fuels	Ash content (%)	Moisture (%)	Volatile matter (%)	Heating value (HHV, GJ $Mg^{-1)a}$
Anthracite coal	7.83	2.80	1.3	30.90
Bituminous coal	2.72	2.18	33.40	34.50
Sub-bituminous	3.71	18.41	44.3	21.24
Softwood	1.00	20.00	85.0	18.60

[a] On a moisture and ash free basis (maf).

2.2.2.3 Ultimate analysis

The ultimate analysis reports the elemental composition in the biomass. Usually, reports on the carbon (C), hydrogen (H), nitrogen (N), sulphur (S) composition and oxygen (O) which the ultimate analysis depend on several different raw materials fuels. An ultimate analysis is performed and reported on a dry basis, because the moisture is indicated as additional hydrogen and oxygen shows in Table 2.4. The advantages of biomass material are high volatile when comparison with solid fossil fuels, biomass contains less carbon and more oxygen and affect to the heating value of bio-oil products [29].

Table 2.4 Ultimate analysis for solid fuels and biomass materials [a]

Fuels	C	H	N	S	O	Ash	Heating value (HHV, GJ $Mg^{-1)}$
Bituminous coal	75.5	5.0	1.20	3.10	4.90	10.3	31.67
Charcoal	80.3	3.1	0.20	0.00	11.30	3.4	31.02

Douglas fir	52.3	6.3	0.10	0.00	40.50	0.8	21.00
Eucalyptus	48.3	5.9	0.15	0.01	45.13	0.4	19.35
Olive husk	50.0	6.2	1.60	0.00	42.20	3.6	19.00
Hazelnut shell	52.9	5.6	1.40	0.00	42.70	1.4	19.30
Hazelnut seed coat	51.00	5.4	1.30	0.00	42.30	1.3	19.30
Beech	51.6	6.3	0.00	0.00	41.50	0.6	20.30
Sugarcane bagasse	44.8	5.4	0.40	0.01	39.60	9.8	17.33
Wheat straw	43.2	5.0	0.60	0.10	39.40	11.4	17.51
Wood bark	53.1	6.1	0.20	0.00	40.60	1.6	20.50
Poplar wood	51.60	6.3	0.00	0.00	41.50	0.6	20.70
Corncob	49.00	5.4	0.40	0.00	44.60	1.0	18.40
Corn stover	45.10	6.0	0.90	0.00	43.10	4.9	17.40
Rice hulls	38.50	5.7	0.50	0.00	39.80	15.50	15.30
Rice straw	39.20	5.1	0.60	0.10	35.80	19.2	15.80
Water hyacinth	39.80	5.0	1.90	0.00	34.30	19.0	14.60
Tea waste	48.60	5.5	0.50	0.00	39.50	1.4	17.10

[a] Dry basis, weight percent.

2.3 Chemical structure of biomass

The main components of biomass include cellulose, hemicellulose, lignin, some extractives, lipids, proteins, simple sugars, water, hydrocarbons, ash and inorganic compound. The basic structure of all biomass composes of three polymers as cellulose, hemicellulose and lignin. However, the proportion of component in biomass is different corresponding with types of biomass. Because these components have

different chemical structures example hardwood or deciduous woods have a higher proportion of cellulose, hemicellulose and extractives than softwood whereas softwood has a higher proportion of lignin. Usually, hardwoods contain about 43-47% cellulose, 25-35% hemicellulose, 16-24% lignin and 2-8% extractives while softwoods contains about 40-44% cellulose, 25-29% hemicelluloses, 25-31% lignin and 1-5% extractives [30].

Corncob is the central core of maize. It is the part of the ear on which the kernels grow. The chemical properties and physical characteristics of corncob is a suitable for feedstock to generated energy. Table 2.5 shows summaries of main chemical composition of corncob by other research. Corncob contains 32.3-45.6% cellulose, 39.8% hemicellulose-mostly composed of pentose (C5-sugar) and 6.7-13.9% lignin. Current, technology processes are available to convert the energy in the corn cob molecular structure. Thermochemical conversion technologies such as gasification and combustion can utilize the molecular structure of the cellulose, hemicellulose, and lignin present in cobs to produce heat energy and/or synthesis gas. In combustion, corn cobs are completely combusted in an oxygen rich environment to produce heat energy. Direct combustion heating processes could either be fueled exclusively with corncobs or co-fueled with coal. The advantages of using corn cobs as a partial coal substitute include a potentially cleaner emissions stream and the reduction of undesirable emissions and waste ash [31].

Table 2.5 The summaries of main chemical composition of corncob

	Hemicellulose (wt%)	**Cellulose (wt%)**	**Lignin (wt%)**	**Extractive matter (wt%)**	**Reference**
Corncob	31.0	50.5	15.0	3.5	Demirbas (2004) [32]
Corncob	38	30	3	-	Akwasi A.(2011) [19]
Corncob	32.1	52.9	13.1	1.9	Funda A. (2009) [21]
Corncob	75.7[a]	-	19.0	2.8	Akeem (2010) [15]

[a] Holocellulose is cellulose and hemicellulose

2.3.1 Cellulose

Cellulose is a homopolysaccharide composed of β-(1,4)-glycosidic units linked together by (1→4) glycosidic bonds shows in Figure 2.1. The based repeating unit of the cellulose polymer consists of two glucose anhydride units with called a cellobiose unit and molecular formula is $(C_6H_{12}O_6)_n$. As forming intramolecular and intermolecular hydrogen bonds between OH groups within the same cellulose chain and the surrounding cellulose chains, the chains tend to be arranged in parallel in the longitudinal direction and form to microfibril in the cell wall of plants. Cellulose is a crystalline structure, insoluble in most solvents and low accessibility to acid and hydrolysis of enzyme [30].

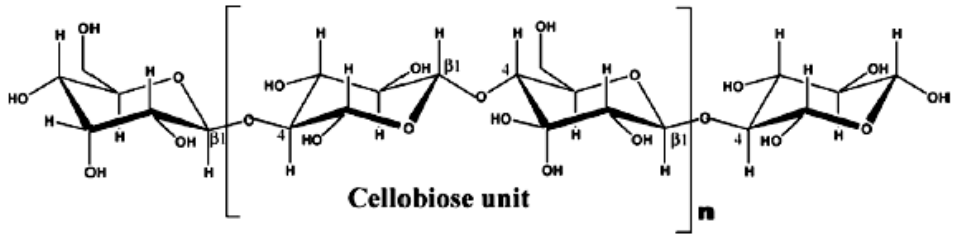

Figure 2.1 Chemical structure of cellulose.

2.3.2 Hemicellulose

Hemicellulose is a mixture of various polymerized 5-carbon or 6-carbon monosaccharaides such as glucose, mannose, galactose, xylose, arabinose, 4-*O*-methyl glucuronic acid and galacturonic acid residues [33]. Main chemical structure of the sugar units in hemicelluloses shows in Figure 2.2. The important sugar of the hemicelluloses component is xylose. The molecular formula is $(C_5H_8O_4)_n$. Due to the degree of polymerization n is 50 to 200, which is smaller than that of cellulose which these break down easily than cellulose, good soluble in alkali and more easily hydrolyzed. Hemicelluloses vary in amounts depending on tree species and the part of the plants.

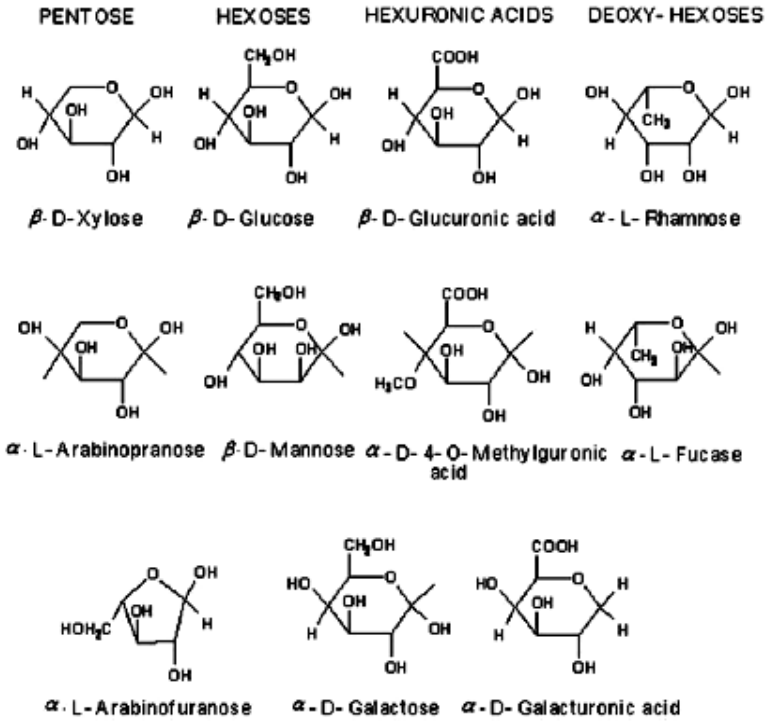

Figure 2.2 Chemical structures of the sugar units in hemicelluloses.

2.3.3 Lignin

Lignin is aromatic compound which consists of complex polymer based on phenyl propane monomeric units and three-dimensional structure shows in Figure 2.3. Linin is decomposed to monolignols unit which the primary chemical monolignols unit such as syringyl, guaiacyl, sinapyl alcohol and coniferyl alcohol shows in Figure 2.4. These chemical structures are bonded together by a linkage to form a very complex matrix. This matrix includes a variety of functional groups such as hydroxyl, methoxyl and carbonyl which impart a high polarity to the lignin macromolecule [34]. Lignin is covalently linked with xylans in the case of hardwood and with galactoglucomannans in softwood. Pyrolysis of lignin and combustion converted to chemical components with methoxy phenols group as characteristic of the chemical derives from lignin.

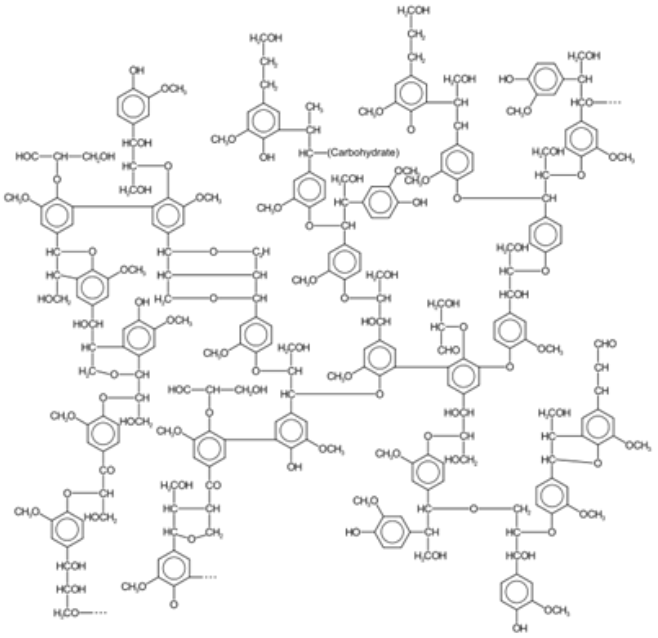

Figure 2.3 Chemical structure of lignin.

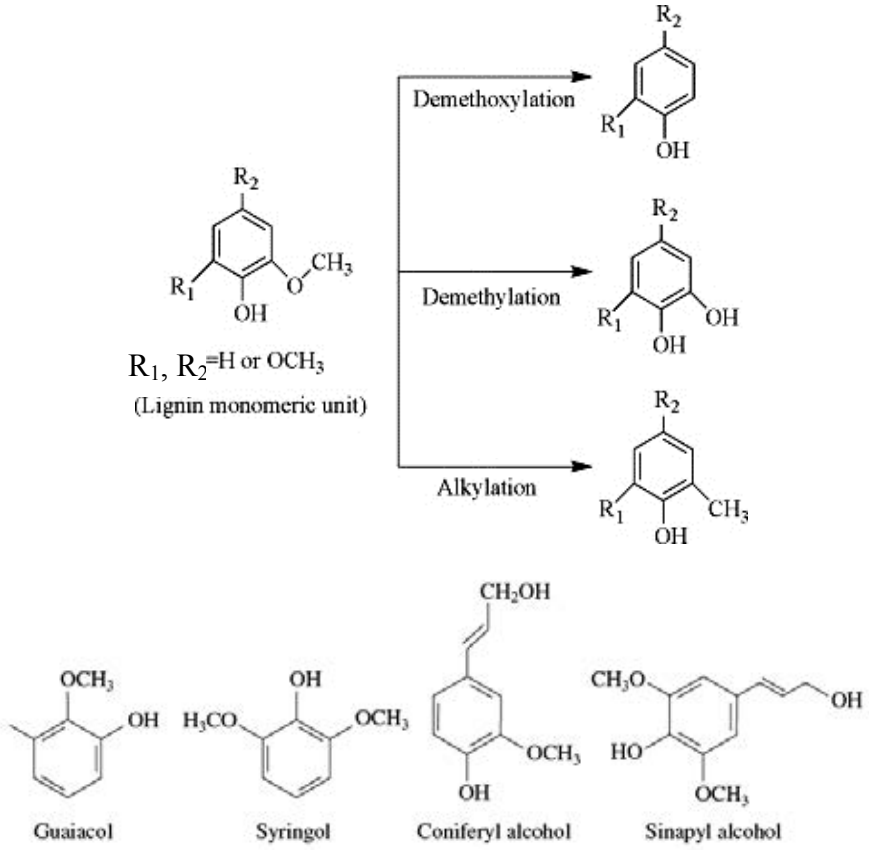

Figure 2.4 The primary chemical monolignol units in the lignin structure.

2.4 Thermochemical routes for biomass production

Biomass is used to respond a variety of energy need. Benefit of biomass energy including generating electricity, heat for industries facilities and fuel in vehicles. Main conversion routes of biomass to bioenergy and biofuels presents in Figure 2.5. The conversion technologies for the biomass energy production can be divided into three main routes consist of mechanical, thermo-chemical and biological route. The difference between biochemical and thermo-chemical processes is that biochemical processes are commonly slow processes (hours to weeks or years) which yield single or specific products such as methane and ethanol. But, thermo-chemical processes are rapid time (seconds to minutes) and obtained variety chemical product which these products are more compatible petroleum refining operations but the treatment process of gas product from undesirable contaminants compound is high cost [3].

The thermo-chemical conversion routes of biomass such as combustion, gasification, pyrolysis and liquefaction. Combustion is established commercial technology with application in most industries which the product of combustion biomass can be used to directly heat power and electricity. The disadvantage of combustion technology is environment problem. Gasification technology has been practiced for many years and pre-commercial technology. These processes generate to synthesis-gas which potentially more efficient than direct combustion of the original fuel because it can be combusted at higher temperatures and synthesis-gas may be burned directly in gas engines, used to produce methanol and hydrogen, or converted via the Fischer-Tropsch process into synthetic fuel or purified hydrogen gas as product. The pyrolysis and liquefaction technology produced high yield of liquid (bio-oil), gas and solid residues product compared with other technology. Liquid from pyrolysis technology was used to directly as a liquid fuel, added to petroleum refinery feedstock and catalytic upgraded to transport fuels [35].

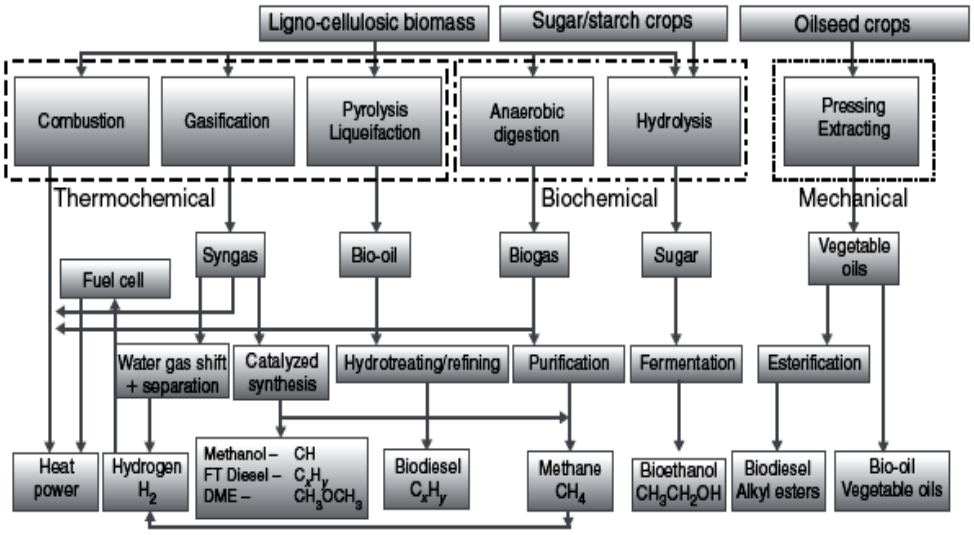

Figure 2.5 Main conversion routes of biomass.

2.4.1 Pyrolysis of biomass

Pyrolysis is a thermochemical process that converts biomass into non-condensable gases, liquid (bio-oil) and solid (charcoal), under absence of oxygen or less oxygen. The products were obtained from pyrolysis technologies are alternate energy sources which the applications of biomass pyrolysis products shows in Figure 2.6 [35].

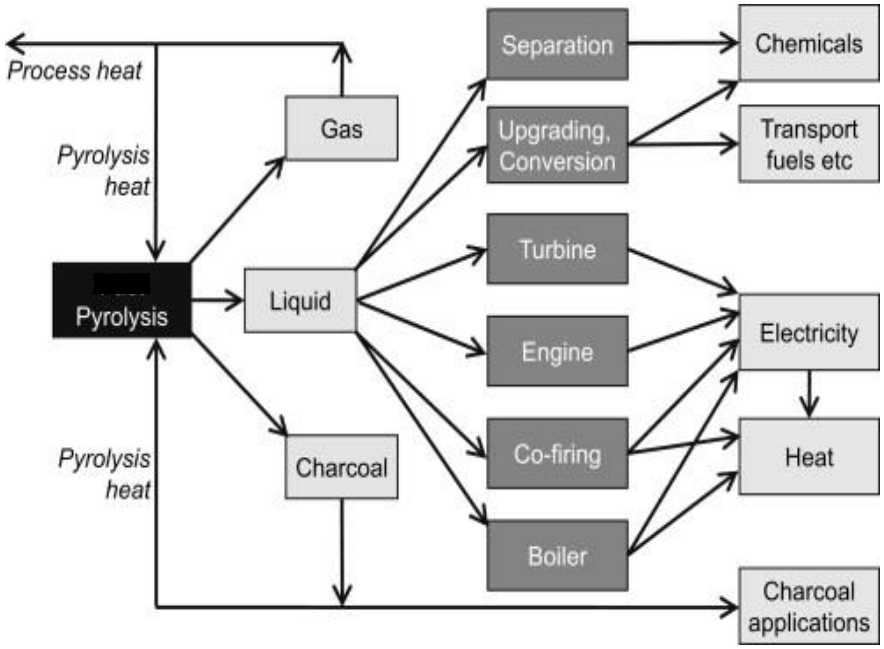

Figure 2.6 The applications of biomass pyrolysis products**.**

The composition of products depends on input component of biomass material, pretreatment, temperatures and heating reaction rates. The pyrolysis mode can be divided into three subclasses consist of conventional pyrolysis (carbonization), fast pyrolysis and flash pyrolysis. The main operating condition parameters for pyrolysis processes shows in Table 2.6

Table 2.6 The main operating condition factors for pyrolysis mode

	Conventional pyrolysis	**Fast pyrolysis**	**Flash pyrolysis**
Pyrolysis temperature (°C)	300-700	>550	400-600
Heating rate (°C /s)	0.1-2	10-200	>1000
Particle size (mm)	5-50	<1	<0.2
Solid residence time (s)	450-550	0.5-10	<0.5

2.4.2 Pyrolysis pathways and mechanisms [36]

The aim of pyrolysis is the optimization of high-value fuel products from biomass by thermal and catalytic process. Therefore, the biomass pyrolytic pathways and the subsequent products are influenced by various factors and the selectivity of products can be performed in different ways which the main reaction and the obtained product from biomass pyrolysis show in equations (1)-(2).

$$\text{Biomass} \xrightarrow{\text{heat}} \text{Char} + \text{Pyrolytic oil (high and moderate molecule weight organic liquid)} + \text{Condensable in oxygenate organic} + CO_2 + CO + H_2 + CH_4 + H_2O + \text{other} \quad (1)$$

$$\text{Organic liquid} \xrightarrow{\text{heat}} \text{Aromatic organic} + \text{low molecule weight organic liquid} + \text{Char} + CO_2 + CO + H_2 + CH_4 + H_2O + \text{other} \quad (2)$$

2.4.2.1 Cellulose pyrolysis

Cellulose is the main component of biomass and located in the cell wall of plant. The initially step of cellulose pyrolysis occurs at low temperature about 150°C. Generally, cellulose decomposes to form activated cellulose and then decomposed two pathways mechanism consist of depolymerization and ring scission at different temperature. The major two pathways during pyrolysis of cellulose are shows in Figure 2.7. At temperature lower than 300°C, pyrolysis of cellulose mainly involves the reduction in degree of polymerization, elimination of water, formation of carbonyl, carboxyl and hydro peroxide groups, and evolution of carbon monoxide (CO) and carbon dioxide (CO_2) and char residue. At low temperature pyrolysis produces very low organic liquid products yield. Whereas, at temperature higher than 300°C, the pyrolysis of cellulose involves ring scission reactions and leading to liquid product with the high yield about 87%.

The mainly products from depolymerization of cellulose convert to forms anhydro-oligosaccharides, levoglucosan (LA) and other monomeric anhydrosugars, furans, cyclopentanones and other related derivatives. The ring scission process mainly obtained hydroxyacetaldehyde (HAA), acetol (HA), other linear carbonyls, linear alcohols and esters.

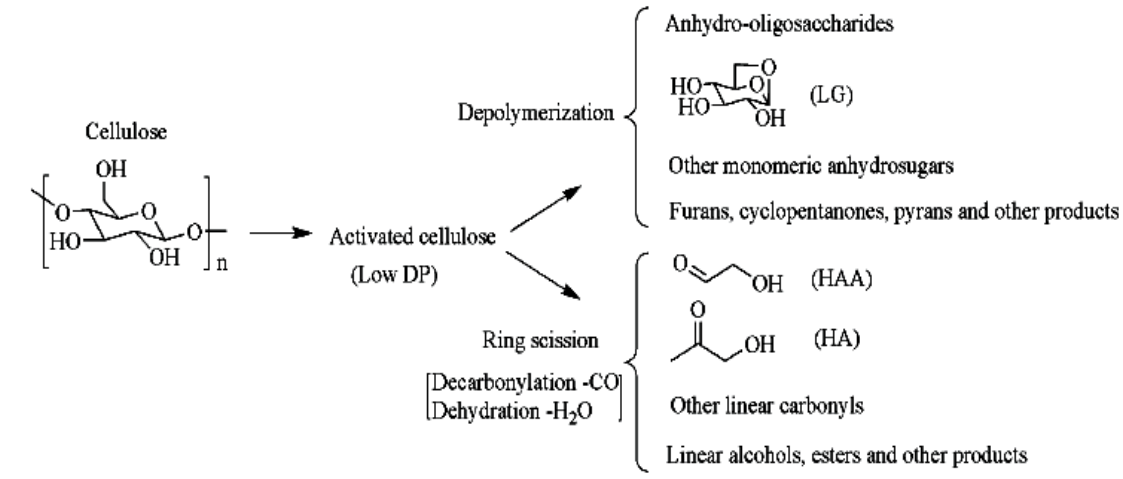

Figure 2.7 The major two pyrolytic pathways during pyrolysis of cellulose.

2.4.2.2 Hemicellulose pyrolysis

Hemicelluloses are less thermally stable than cellulose, due to the lack of crystallinity and pyrolysis pathway is generally thought to be similar to cellulose in the reaction mechanisms. The glucoronoxylans (refers to as xylan) are the predominant hemicellulose of hardwoods and glucomannan is most important hemicellulose of softwoods. Generally, xylan pyrolysis convert to higher char product than pyrolysis from cellulose and not form a typical depolymerization product which differ to the levoglucosan pyrolysis from cellulose. Decomposition of hemicellulose under pyrolysis conditions occurs in two steps. First step is the breakdown of the polymer into water soluble fragments followed by conversion to monomeric units and second step is decomposition of the monomeric units to volatiles. Hemicelluloses pyrolysis produced more gases and less solid residue than cellulose [31].

2.4.2.3 Lignin pyrolysis

Lignin is the amorphous material that surrounds cellulose fibers and highly linked three-dimensional them together. Lignin is the most complicated, least understood and most thermally stable component of biomass. The primary pyrolysis of lignin starts with thermal at temperature around 280-500°C whereas the complete decomposition of lignin occurs at higher temperatures compared with the decomposition of cellulose. The degradation and conversion of lignin can be achieved by thermo-chemical technology shows in Figure 2.8. Pyrolysis converts lignin to solid, liquid oil and gases with different temperature and heating rate. The composition of product and yield of individual compounds are strong functions of the lignin source and the isolation methods. The softwood of lignin shows a dominance of guaiacyl units whereas hardwood lignin shows similar amounts of both guaiacyl and syringly units. The pyrolysis of lignin obtains higher solid yield and lower liquid yield than holocellulose and the liquid product can be classified into three groups including the large molecular oligomers (pyrolytic lignins), the monomeric phenolic compounds and the light compounds (such as methanol, hydroxyacetaldehyde, acetic acid) [34].

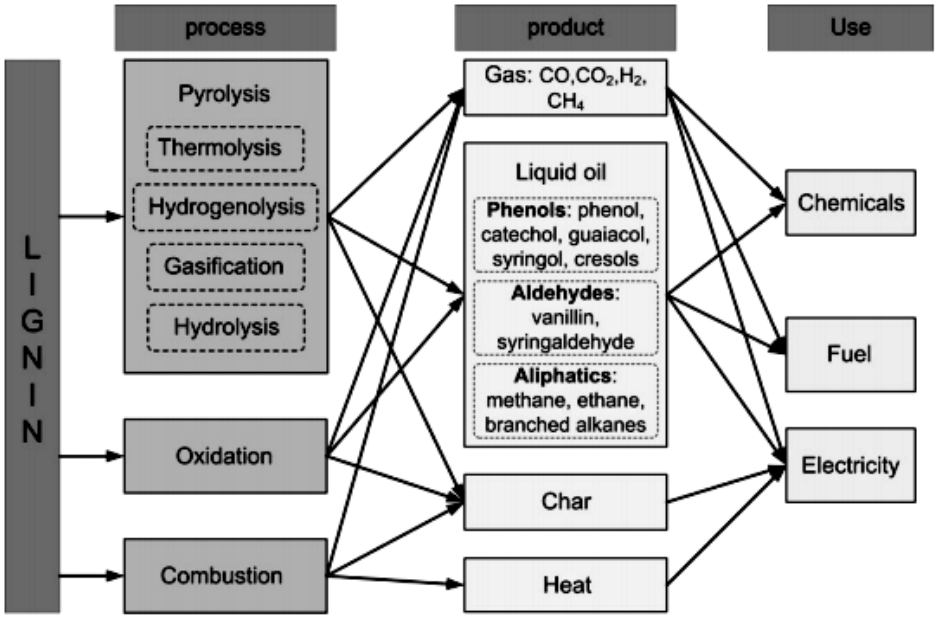

Figure 2.8 Major thermo-chemical lignin conversion processes and products.

2.5 Factors affecting to biomass pyrolysis [36]

Beside, effects of mechanisms and kinetics of pyrolytic reaction. The composition of biomass feedstock, heating rate, reactor temperature, reactor pressure, ambient atmosphere and existence of catalysts are affecting to yield and composition of products.

Composition of biomass

Biomass is complex and heterogeneous raw materials derived from different types of plant. Mainly compositions of biomass are 30-40% cellulose, 25-30% hemicellulose and 12-30% lignin. These compounds are responsible for the variety and complexity of products formed during the pyrolysis of biomass. At temperature higher than 300°C, cellulose and hemicellulose break down to liquid oil containing low sugar derivatives and less char whereas lignin is condensed to carbonaceous char and gives smaller amounts of liquid oil containing phenolic compounds.

Temperature

The components of biomass exhibit different thermal behaviors. The effects of temperature on pyrolysis products from lignocellulosic biomass are difference yields and distribution of chemical products. For example, at temperature range of 300-550°C occurred depolymerization of sugar cellulose whereas levoglucosan and other low molecule volatiles decomposed at temperature above 600°C. However, at higher temperatures above 700°C give the gas products such as CO, CO_2, CH_4 and H_2.

Heating rate

The heating rates affected to pyrolytic reactions, the sequence of reactions, and composition of the obtained products. The long heating rate periods permits the secondary reactions and converted to gas product whereas the rapid heating rate permits reduce these secondary reactions and converted to liquid products.

Atmosphere

The ambient atmosphere affects the heat transfer and nature of the secondary reactions. The atmosphere may be a vacuum or an inert or reactive surrounding. In a vacuum, primary products are rapidly reduced in the gas phase product thus are not available for further decomposition and reaction.

Pressure

Pressure is a significant influence on pyrolysis of biomass. The effects of pressure on the pyrolysis products can be interpreted by the effect of residence time of the volatile products.

Catalyst

Catalytic pyrolysis is respected to the most attractive way of decreasing the problems of the liquid pyrolysis products including polymerization, high viscosity, and corrosion. The advantages of catalyst in pyrolysis process are handling and treatment raw material during pyrolysis process that resulted to the improvement obtained bio-oil product.

2.6 Porous molecular sieves

Molecular sieves are porous materials that exhibit selective adsorption properties which can be classified on the IUPAC definitions into three main types depending on their pore sizes that are microporous materials, mesoporous materials, and macroporous materials. Properties and examples of these materials are shown in Table 2.7.

Table 2.7 IUPAC classification of porous materials

Type of porous molecular sieve	Pore size (Å)	Examples
Microporous materials	< 20	Zeolites, Activated carbon
Mesoporous materials	20-500	SBA-15, Pillared clays, FSM-16
Macroporous materials	> 500	Glasses

2.6.1 Zeolites

Zeolites are microporous crystalline aluminosilicates that has been studied by mineralogist for more than 200 years. They are comprised of channel and cavities of molecular dimensions ranging from 3 to 10 Å on diameter. The general formula for the composition of zeolite in the hydrated form is:

$$M_{x/n}\,[(AlO_2)_x\,(SiO_2)_y].\ w\ H2O$$

Where M is an extra framework cation that balances the anionic charge of the framework, n is the cation valence for M, x and y are the total number of aluminates and silicates per unit cell and z is the number of water molecules per unit cell. Typical cation include alkali metals, e.g. Na^+, K^+, alkaline earth metals, e.g. Ca^{2+}, Ba^{2+} and other cation as NH_4^+ and H^+ [37].

The application of natural zeolite can be broadly classified as building materials, agricultural, ion exchange, adsorbent and others. The adsorption and ion exchange properties of natural zeolites are exploited in application such as odor removal, fertilizer acid, soil amendment, animal feed supplement, water treatment, aquaculture, removal of radioactive species and heavy metals from waste streams.

2.6.1.1 Zeolites structure

Zeolite structures are composed of an infinitely extending three dimensional network of SiO_4 and AlO_4 tetrahedra. The tetrahedral are cross linked by the sharing of oxygen ions resulting in the empirical formula of $[SiO_2]$ and $[AlO_2]^-$ [38]. These tetrahedral refer to the primary building units (PBU) are shown in Figure 2.9 and the PBUs are assembled into the secondary building unit (SBUs) are shown in Figure 2.10, which are themselves assembled to form the zeolite structure framework. The PBUs of zeolite structure is a tetrahedral unit is composed of a central Si or Al atom surrounded by four oxygen atoms, namely $[SiO_2]$ and $[AlO_2]^-$ [39]. These tetrahedral are linked through the oxygen atoms to form channels and cages of discrete size with no two aluminum can share the same oxygen.

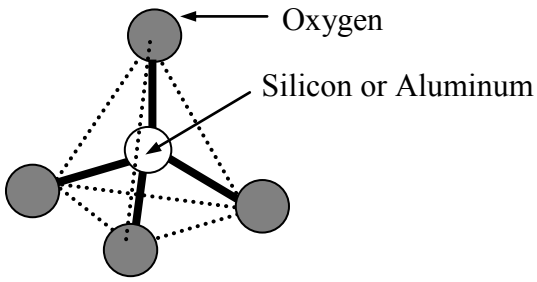

Figure 2.9 A primary building unit of porous materials (PBU).

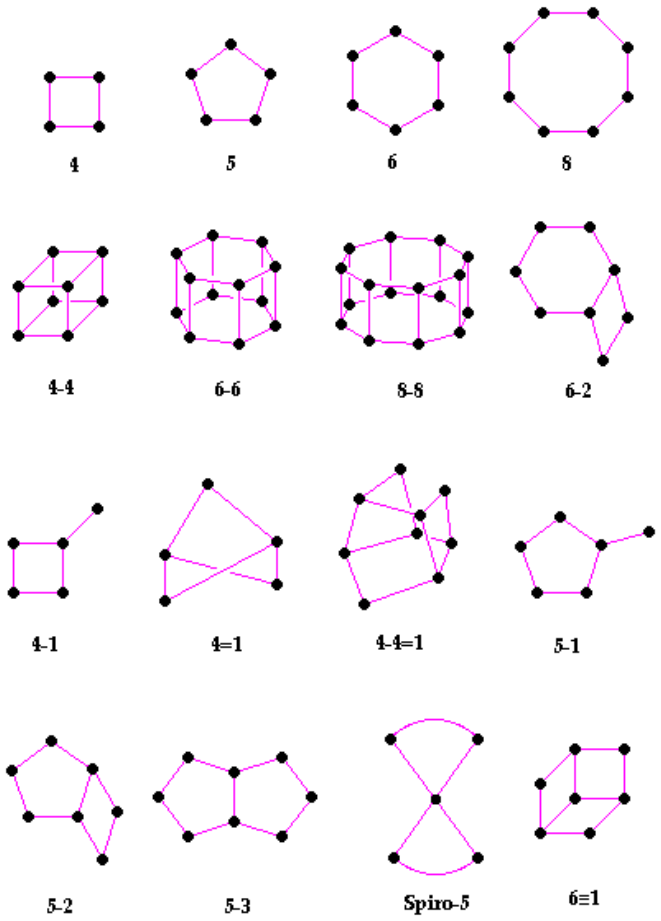

Figure 2.10 Secondary building units (SBU) in zeolite framework [38].

As a result of the negative charge from the framework charge of zeolite is negative and hence must be balanced by cations, typically from the alkali or alkaline earth metal cations. These cations can be exchanged by various types of cations, particularity +1 to +3 species. The position, size and number of cations can significantly alter the properties of zeolites. Figure 2.11 depicts schematically the building of zeolite framework [39]. Several tetrahedral units are joined so that each of four oxygen atoms is shared with another tetrahedral silica or alumina to form a wide range of small SBUs as shown in Figure 2.11(b). These SBUs are interconnected to produce a wide range of tertiary building units or polyhedral which in turn are arranged in three dimensional pattern to form extended characteristic framework of various crystal structures (Figure 2.11(c)). In these structures the corners of polyhedral represent Si or Al atoms and the connecting line are the distance between the centers

of neighboring tetrahedral units while oxygen atoms an omitted for the ease of structure demonstrated.

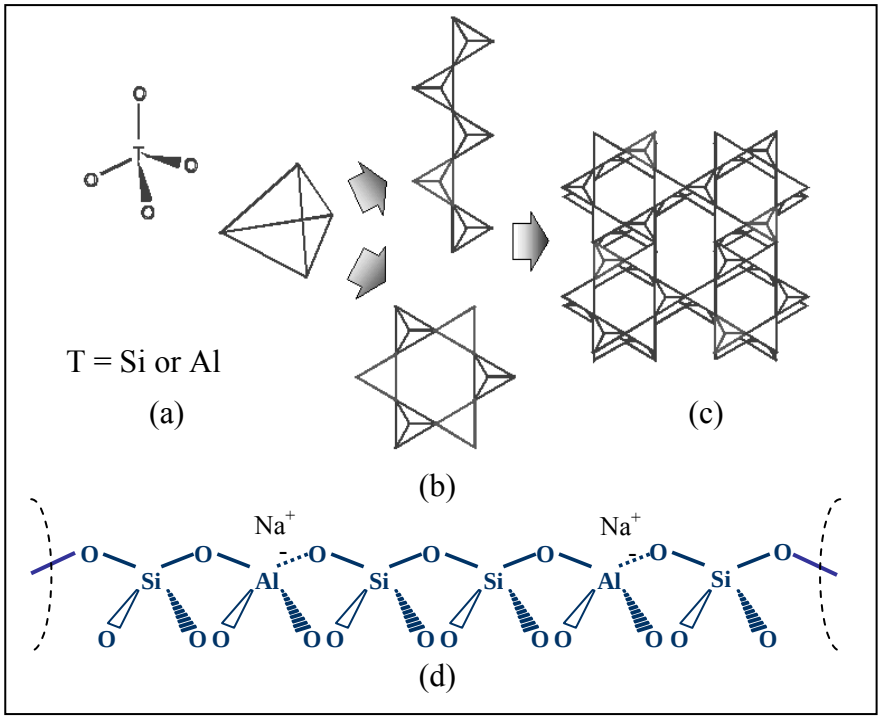

Figure 2.11 (a) A primary building unit, (b) secondary building unit, (c) framework of a porous materials, and (d) metal ions balancing the framework charges of a zeolite framework.

Zeolite pore consists of 8, 10 and 12 membered oxygen ring systems to form channels and pores which are interrelated to each other on zeolite framework. The channels may one, two or three dimension with different sizes. Zeolites can be classified according to their diameter of pore size; small pre which consist of 8-membered of oxygen ring systems with pore size < 4 Å such as zeolite A, chabazite and erionite; medium pore zeolite which consist of 10-membered of oxygen ring systems within 4.5 Å < pore size < 6.5 Å such as ZSM-5, ferierite and TS-1 and large pore zeolite with 12-membered oxygen systems with pore size > 6.5 Å such as mordenite, faujasite and zeolite beta [38]. Pore size of zeolite is around 3.5 Å to 8.0 Å which can separate the selective organic molecules based on their size.

2.6.1.2 Acid sites of zeolites

Acidity is one of the most important characteristics of zeolites and is very useful in acid catalysis. A good understanding of the nature and number of acid sites in a zeolite in needed in developing improved and novel catalysts for applications in the chemical structure. The activity of zeolites as acid catalysts is related to the acidity of active sites on their surface [40-41]. This means that the activity required is based upon the production of Brønsted acid sites arising from the creating „hydroxyls" within the pore structure. These hydroxyls are formed by ammonium exchange followed by a calcination step. Zeolites as usually synthesized normally have Na^+ balancing the framework charges, but these can be readily exchanged for protons by direct reaction with an acid, giving hydroxyl groups, the Brønsted acid sites. Alternatively, if the zeolite is not stable in acid solution, it is common to use the ammonium, NH_4^+, salt, and then heat it so that ammonia is driven off, leaving a proton. Further heating removes water from Brønsted site, exposing a tricoordinated Al ion, which has electron-pair acceptor properties; this is identified as a Lewis acid site. A scheme for the formation of these sites is shown in Figure 2.12. The surfaces of zeolite can thus display either Brønsted or Lewis acid sites, or both, depending on how the zeolite is prepared. Brønsted sites are converted into Lewis sites as the temperature is increased above 500°C, and water is driven off.

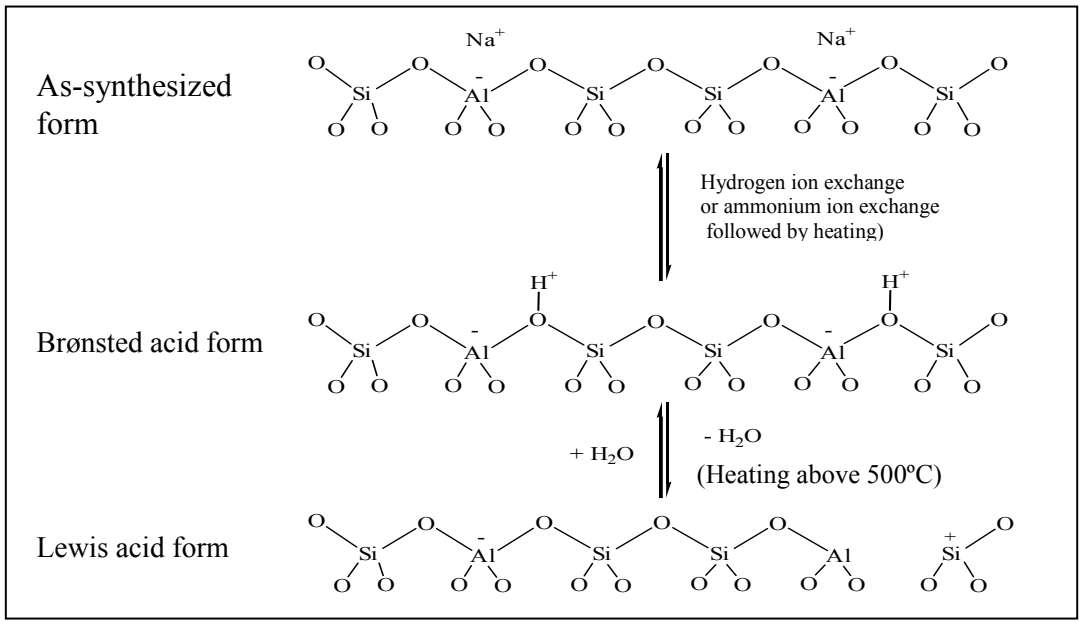

Figure 2.12 The generation of Brønsted and Lewis acid sites in zeolites [42].

2.6.1.3 Shape and size selectivity of zeolite

Shape and size selectivity presents a very important role in catalysis. Highly crystalline and regular channel structures are among the principal features that porous material used as catalysts offer over other materials. Shape selectivity is divided into 3 types: reactant shape selectivity, product shape selectivity and transition-state shape selectivity. These types of selectivity are shown in Figure 2.13. Reactant shape selectivity results from the limited diffusivity of some reactants, which cannot effectively enter and diffuse inside the porous materials. Product shape selectivity occurs when diffusing product molecules cannot rapidly escape from the crystal, and undergo secondary reactions. Restricted transition-state shape selectivity is a kinetic effect arising from the local environment around the active site: the rate steady for a certain reaction mechanism is reduced if the necessary transition state is too bulky to form readily [40-41].

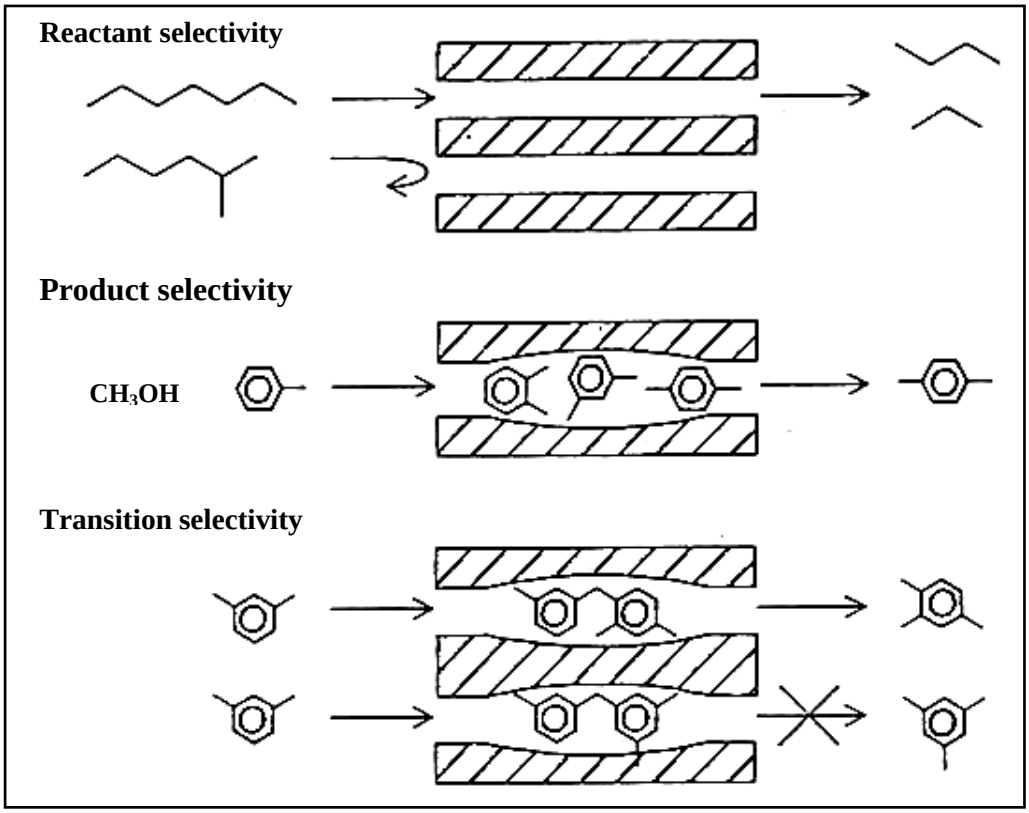

Figure 2.13 Three types of selectivity in porous materials: reactant, product and transition-state shape selectivity [43].

2.7 Beta zeolite

Beta zeolite is a large pore zeolite. It is known that the crystal size of zeolite catalyst can influence the reaction activity and selectivity [44]. Beta zeolite has been used as a cracking catalyst for higher production of olefins, as well as in the catalyst stability by increasing the crystallite size.

2.7.1 Structure and properties of beta zeolite

In 1967, beta zeolite with high silica (Si/Al>5) was first synthesized by Wadlinger *et al.* [45] and using tetraethylammonium hydroxide as the organic template. The use of organic bases has a significant impact on development of high silica zeolite but the structure is very complex. The unit cell composition of beta zeolite is:

$$(TEA, Na)_n[(AlO_2)_n(SiO_2)_{64-n}]$$

Beta zeolite exhibits characteristic properties of the 12-membered ring, shown in Figure 2.14, connecting together in three dimensional channel systems. There are two different types of channels: straight channel (100) and sinusoidal channel (001) [46]. These are shown in Figure 2.15.

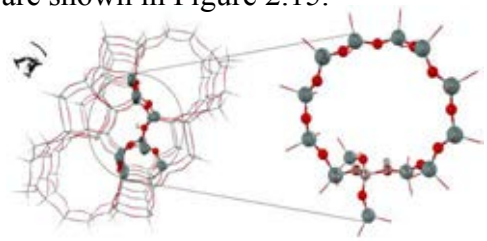

Figure 2.14 The ball-and-stick graphics represent the active region 14T including the main gateway to the intersection of beta zeolite (12-membered-ring) [47].

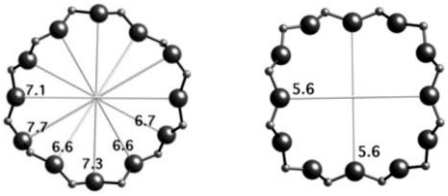

(a) (b)

Figure 2.15 The 12-ring viewed along (a) (100) plane and (b) (001) planes [48].

Their structures consist of intergrowth hybrid of two distinct structures termed Polymorphs A and B. These polymorphs grow in two dimensional sheets which randomly alternate in their structures. The smaller building units are double six-ring units connected by two four-ring and four, five-ring units. These are connected to form chains along the [001] direction, shown in Figure 2.16 [49]. The two polymorphs of beta zeolite, demonstrated in Figure 2.17, show only the T-atom positions (for simplicity). The oxygen atoms have been omitted for clarity.

1. Polymorph A: tetragonal crystal system, two different pore opening dimensions: 0.60x0.56 nm and 0.68x0.73 nm, there is arranged in an ABABAB. . . type configuration.

2. Polymorph B: monoclinic crystal system, two different pore opening dimensions: 0.68x0.55 nm and 0.68x0.73 nm, there is arranged in an ABCABC. . . type configuration

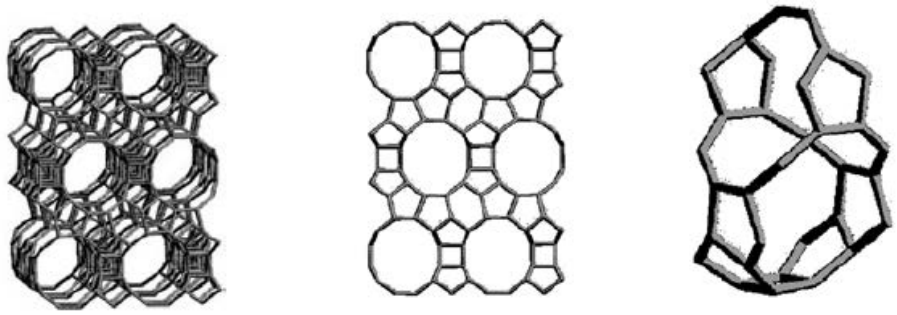

Figure 2.16 The framework of beta zeolite (a) view along [100] direction (b) projection viewed along [100] direction and (c) channel intersection viewed normal to [001] direction.

Beta zeolite was suggested as an active catalyst and a useful sorbent [50] because of its strong acidic property and pore system. The great potentials have taken for the catalytic cracking of aromatic, isobutane alkylation with n-butene, disproportionation of hydrocarbons, and isomerization [51]. Since beta zeolite

combines three important characteristics: large pore (12 oxygen member rings), high silica to alumina ratio and three dimension network or pores, it can give a certain level of shape selectivity, high thermal and chemical stability.

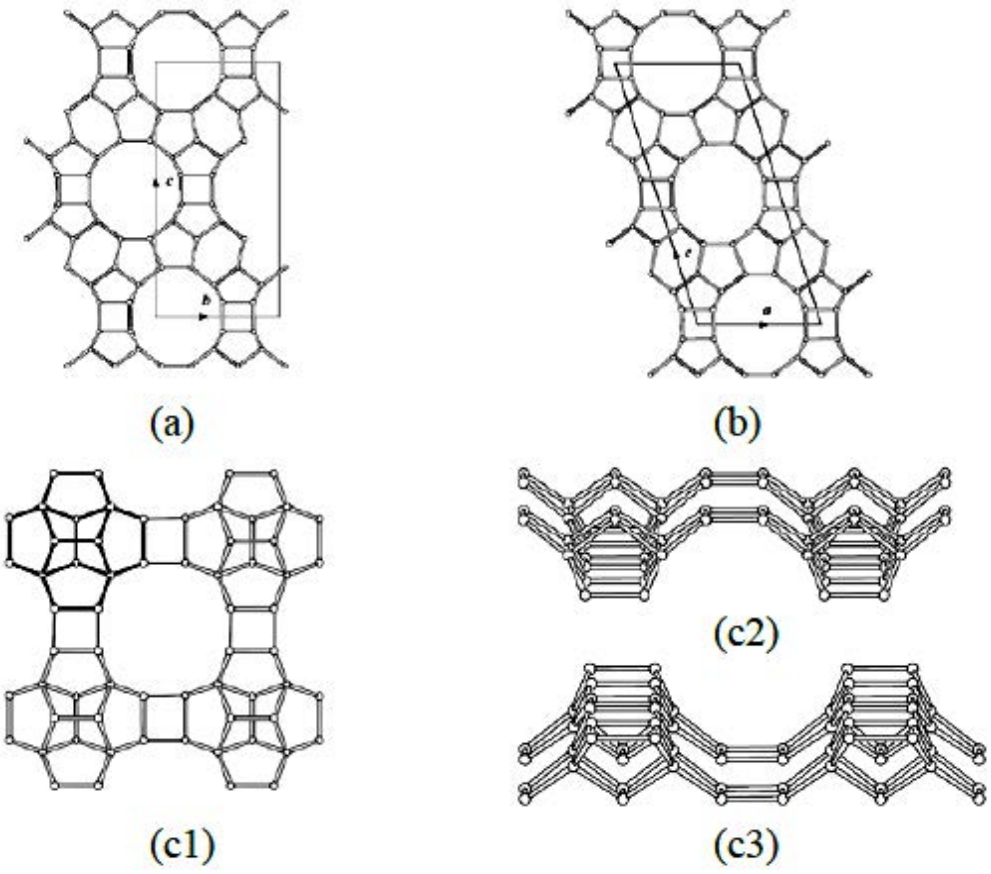

Figure 2.17 Frameworks of (a) polymorph A, (b) polymorph B of beta zeolite and (c1) a layer or periodic building unit (PBU) of the beta family of structure types, the tetragonal beta layer, is composed of T16 units (in bold). The layers depicted in parallel projection (c2) and in perspective view (c3).

2.8 Mesoporous materials [52-54]

Two classes of materials that are extensively used as heterogeneous catalyst and adsorption media are microporous and mesoporous materials. The members of the

microporous class are zeolites, which provide excellent catalytic properties by the virtue of their crystalline aluminosilicate framework. However, their applications are limited by the relatively small pore openings. Many attempts to synthesize zeolites with larger pores have been made, but they were unsuccessful. Larger pores are present in porous glasses and porous gels, which were known as mesoporous materials.

Mesoporous materials are a type of molecular sieves, such as silica or transitional alumina or modified layered materials such as pillared clays and silicates. Mesoporous silica has uniform pore sizes from 2 to 50 nm and has found great utility as catalysts and sorption media because of the regular arrays of uniform channels. Larger surface area is desired for enhancing of the reactions.

2.8.1 Classification of mesoporous materials

Mesoporous materials can be classified by different synthetic methods. By varying different types of templates used and pH of gel for synthesizing hexagonal mesoporous materials new hexagonal materials can be obtained. The interaction of various types of template with inorganic species for assembling these materials are different as summarized in Table 2.8, together with the condition typically employed for a synthesis.

Table 2.8 Various synthesis conditions of hexagonal mesoporous materials and the types of interaction between templates and inorganic species

Materials	Template	Assembly	Solution
MCM-41	Quaternary ammonium salt	Electrostatic	base or acid
FSM-16	Quaternary ammonium salt	Electrostatic	base
SBA-15	Amphiphilic triblock copolymer	H- bonding	acid (pH<2)
HMS	Primary amine	H- bonding	neutral

MCM-41 and FSM-16 can be synthesized using quaternary ammonium salt as a template. In case of SBA-15, amphiphilic tribock copolymer can be modified as a template and must be synthesized in acid condition of hydrochloric acid. On the other hand, HMS can be prepared in neutral and environmentally benign condition using primary amine as a template. Although these materials have the same hexagonal structure, some properties are different as shown in Table 2.9.

Table 2.9 Properties of some hexagonal mesoporous materials [55]

Material	**Pore size (Å)**	**Wall thickness (nm)**	**BET specific surface area (m^2/g)**	**Framework structure**
MCM-41	15-100	1	>1000	Honey comb
FSM-16	15-32	-	680-1000	Folded sheet
SBA-15	46-300	3-6	630-1000	Rope-like
HMS	29-41	1-2	640-1000	Wormhole

2.8.2 Synthesis schemes of mesoporous materials

Crystalline molecular sieves are generally obtained by hydrothermal crystallization. The reaction gel, usually, contains cations (e.g. Si^{4+} for silicate materials, Al^{3+} for aluminate materials) to form the framework; anionic species (e.g. OH^- and F^-); organic template and solvent (generally water). Typically, the nature of template can be considered into two parts that are hydrophobic tail on the alkyl chain side and hydrophilic head on the other side. The examples of templates used are primary, secondary tertiary and quaternary amines, alcohols, crown or linear ethers, and as well as polymers. An understanding of how organic molecules interact with each other and with the inorganic frameworks would increase the ability to design rational routes to molecular sieve materials. The organic templates are frequently occluded in the pores of the synthesized material, contributing to the stability of mineral backbone.

2.8.3 Interactions between inorganic species and surfactant micelles

A number of models have been proposed to explain the formation of mesoporous materials and to provide a rational basis for synthesis routes [54]. In general, these models are predicted upon the presence of surfactants in a solution to direct the formation of inorganic mesostructure from stabilized inorganic precursors. The type of interaction between the surfactant and the inorganic species was significantly different depending on the various synthesis routes as shown in Table 2.10.

Table 2.10 Example routes for interactions between the surfactants and the inorganic soluble species

Surfactant type	Inorganic type	Interaction type	Example materials
Cationic (S^+)	I^-	S^+I^-	MCM-41, MCM-48
	I^+X^-	$S^+X^-I^+$	SBA-1, SBA-2, zinc phosphate
	I^0F^-	$S^+F^-I^0$	silica
Anionic (S^-)	I^+	S^-I^+	Al, Mg, Mn, Ga
	I^-M^+	$S^-M^+ I^-$	alumina, zinc oxide
Neutral S^0 or N^0	I^0	S^0I^0 or N^0I^0	HMS, MSU-X, aluminum oxide
	I^+X^-	$S^0X^-I^+$	SBA-15

Where; S^x or N^x : surfactant with charge of X

I^x : inorganic species with charge of X

X^- : halogenide anions

F^- : fluoride anion

M^{n+} : with charge of X

Using ionic surfactant (S^+ and S^-), the hydrophilic head mainly binds with inorganic species through electrostatic interactions. There are two possible formation routes. Firstly, direct pathway: surfactant and inorganic species of which charges are

opposite interact together directly (S^+I^- and S^-I^+). Another is the indirect pathway, occurring when the charges of surfactant and inorganic species are the same, so the counter ions in solution get involved as charge compensating species for example the $S^+X^-I^+$ path takes place under acidic conditions, in the present of halogenide anions (X^- = Cl^- or Br^-) and the S^-M^+ I^- route is the characteristic of basic media, in the existence of alkaline cation (M^+ = Na^+ or K^+). Figure 2.17 shows the possible hybrid inorganic-organic interfaces.

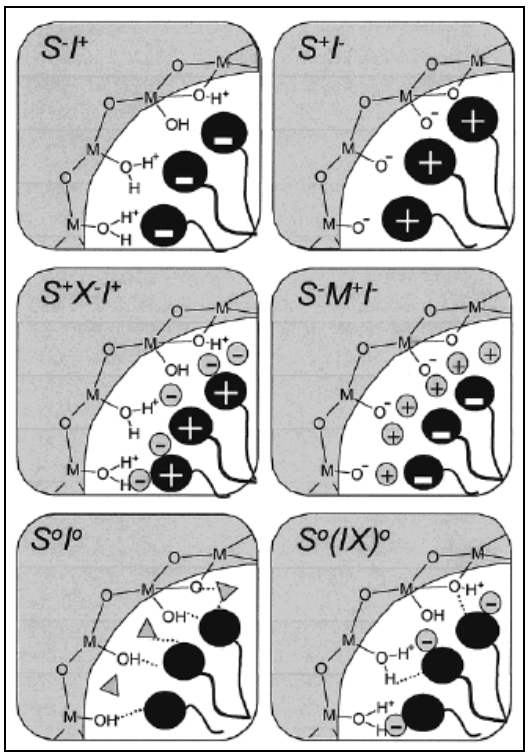

Figure 2.18 Schematic representation of the different types of silica-surfactant interfaces. Dashed line corresponded to H-bonding interactions [56].

In case of non-ionic surfactant (S^0 or N^0), the main interaction between template and inorganic species is hydrogen bonding or dipolar, which is called neutral path i.e. S^0I^0 and $S^0F^-I^+$. Nowadays, non-ionic surfactants give important commercial advantages in comparison to ionic surfactants because they are easily separable, nontoxic, biodegradable and relatively cheap.

The pore diameter of these materials was controlled by alkyl chain length of surfactant. Mechanism of mesoporous formation was different depending on synthesis route for each material.

2.8.4 Formation mechanism of mesoporous materials

2.8.4.1 Liquid crystal templating mechanism

A liquid crystal templating (LCT) mechanism was proposed by the Mobil"s researchers that firstly reported for M41S material. The variation of surfactant concentration plays a significant role to control the structure. Figure 2.19 shows two possible way of the LCT mechanism for hexagonal MCM-41.

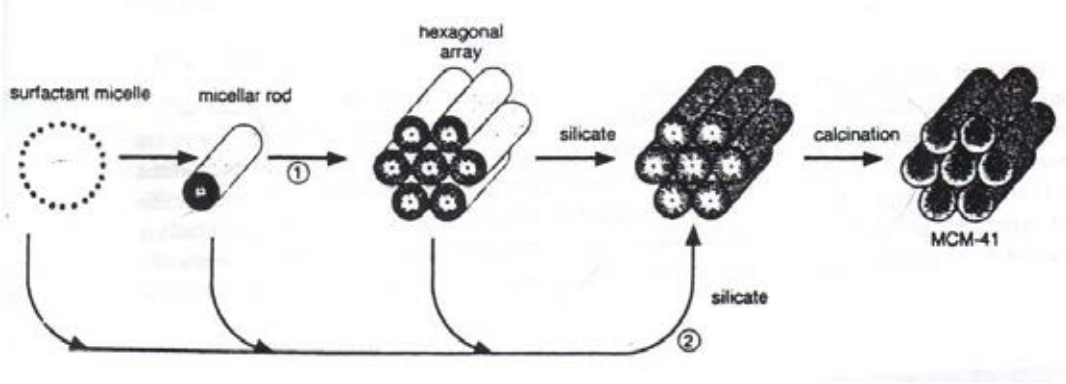

Figure 2.19 Two possible ways for the LCT mechanism [56].

There are two main pathways, in which either the liquid-crystal phase was intact before the silicate species were added (pathway 1), or the addition of the silicate results in the ordering of the subsequent silicate-encased surfactant micelles (pathway 2).

2.8.4.2 Folding sheet formation

The intercalation of ammonium surfactant into hydrated sodium silicate, which composed of singled-layered silica sheet called kanemite, produces the lamellar-to-hexagonal phase in FSM-16. After surfactants were ion-exchanged into

the layered structure, the silicate sheets were folded around the surfactants and condensed into hexagonal mesostructure. The final product was claimed to be very similar to MCM-41. However, Vartuli *et al*. [55] found that the layered structures were still retained in the kanemite-derived mesoporous materials. Folding sheet formation is illustrated in Figure 2.20.

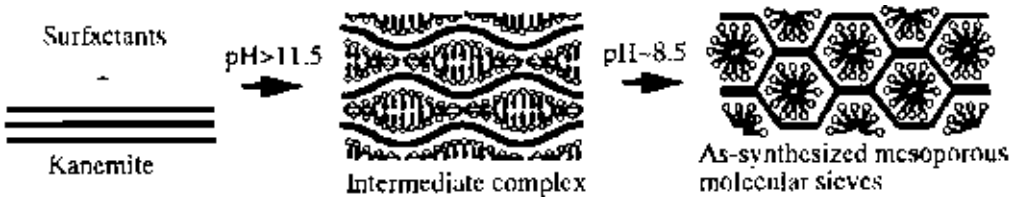

Figure 2.20 Schematic models representing "folding sheets" mechanism [56].

2.8.4.3 Hydrogen bonding interaction

Tanev *et al.* [57] showed that mesoporous silica could be prepared by the hydrogen-bonding interaction of alkylamine (S°) head group and hydroxylated tetraethyl orthosilicate (I^{o}) as shown in Figure 2.21. The materials lacked long-range order of pore, but had higher amounts of interparticle of mesoporosity, because the long-range effects of the electrostatic interaction that would normally control the packering of micellar rods were absent. This neutral templating synthesis route produced mesoporous silicates with thicker walls and higher thermal stability compared to the LCT-derived silicates. The silicate framework in the resulting mesophase was neutrally charged. From this reason, the surfactant can be easily removed by solvent extraction.

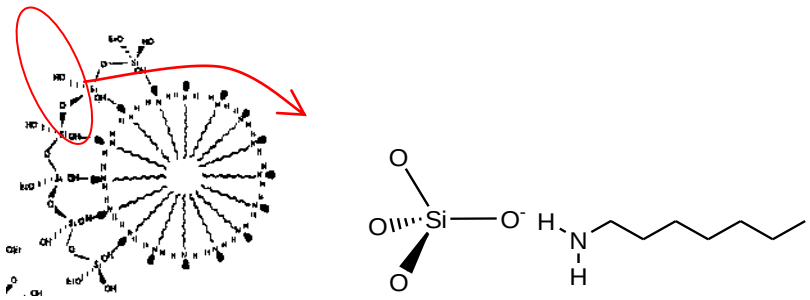

Figure 2.21 Schematic representation of the S^{o} I^{o} templating mechanism of formation of HMS [54].

2.8.4.4 Synthesis strategy of mesoporous material using block-copolymer as structure directing agent

The synthesis of mesoporous materials such as MCM-41, FSM-16 ionic surfactant i.e. the cationic, alkyltrimethyl ammonium (C_nTA^+, $8<n<18$), and anionic surfactant, tertiary amine ($C_nH_{2n+1}N^+(CH_3)_3$) are used as template, respectively. These syntheses were done in extreme (alkaline) pH condition and the obtained materials having pore size in the range of 15 to 100 Å only. However, by this mean, two limitations occurred:

(1) The lower stability of the obtained materials: due to the thinner pore wall of materials (8-13 Å).

(2) Difficult to expanding the pore size: the ionic surfactants give a limited pore size. The only way to expand the pore size is in employing swelling agents such as 1,3,5-trimethyl benzene, involving complicate synthesis.

Thus, the block copolymer has been used to solve these problems. Generally, amphiphilic block copolymer has been used in the field of surfactants, detergent manufacturing, emulsifying, coating, etc. The properties of block copolymer can be continuously tuned by adjusting solvent composition, molecular weight, or type of polymers. Figure 2.22 shows typical block copolymer used as templates.

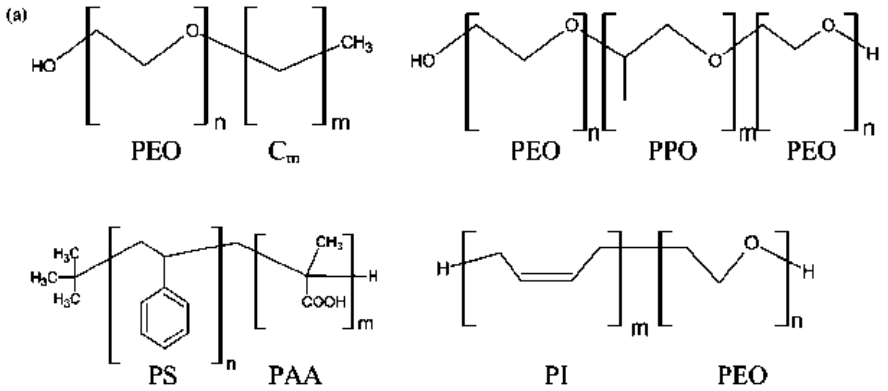

Figure 2.22 Block copolymer used in mesostructured generation [58].

Some advantages of using these block copolymer are:

(1) *The thicker wall thickness* (about 15-40 Å), enhancing hydrothermal and thermal stability of materials.

(2) *Pore diameter can be tuned easier* by varying type or concentration of polymer.

(3) *Easier to remove from mineral framework* by thermal treatment or solvent extraction. Due to the hydrogen bonding interaction between template and inorganic framework, therefore, it should be easier to dissociate as compared to ionic templates (electrostatic interaction).

Interaction between block copolymer template and inorganic species, called hybrid interphase (HI), is particularly important, especially in PEO-PPO based one. Different possible interactions taking place at the HI are schematized in Figure 2.23. Most of the fine HI characterization has been performed on PEO-based (di or triblock) templates. Melosh *et al*. [58] determined that in F127-templated silica monoliths, organization arose for polymer weight fractions higher than 40%. For lower polymeric silica ratios, non-ordered gels were formed. This lack of order was due to a relatively strong interaction (probably of H-bonding type) of the (Si-–O–Si) polymers forming the inorganic skeleton with both PEO and PPO blocks.

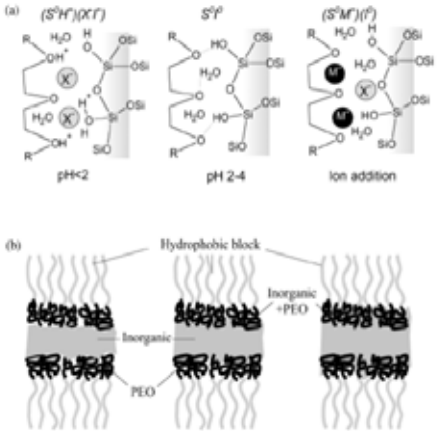

Figure 2.23 (a) Schematic view of the $(S^0H^+)(X^-\ I^-)$, S^0I^0, and $(S^0\ M^+)(X^-I^0)$ hybrid interphases (HIs) (b) Three possible structures of a HI composed by a nonionic polymer and an inorganic framework [59].

2.9 SBA-15

2.9.1 Structure and properties of SBA-15

SBA-15 mesoporous material has been synthesized under acidic condition using triblock copolymer as a structure directing agent. This mesoporous material has shown higher hydrothermal stability as compared to MCM-41 due to its thicker pore walls. They also pores uniform and hexagonal-structured channel similar to MCM-41 with larger pore size which make them more desirable to deal with bulky molecule. Some properties of MCM-41 and SBA-15, two well-known materials, are compared as described in Table 2.11. SBA-15 shows a better performance than MCM-41 in almost of properties.

Table 2.11 Comparison of two well-known mesoporous materials, MCM-41 and SBA-15 in their characteristic properties [60, 61]

Properties	MCM-41	SBA-15
Pore size (Å)	20-100	46-300
Pore volume (mL/g)	>0.7	0.8-1.23
Surface area (m^2/g)	>1000	690-1040
Wall thickness (Å)	10-15	31-64

2.9.2 Synthesis of SBA-15 and formation mechanism

For SBA-15 materials, aging time and temperature are particularly important. Some research found that mesoporous SBA-15 prepared from calcination of an „as-prepared" hybrid precursor contained a significant fraction of microporosity; further aging of the precursor in the mother liquors leads to an improvement on the pore size distribution (Figure 2.24), in agreement with the first work by Stucky *et al*. [10].

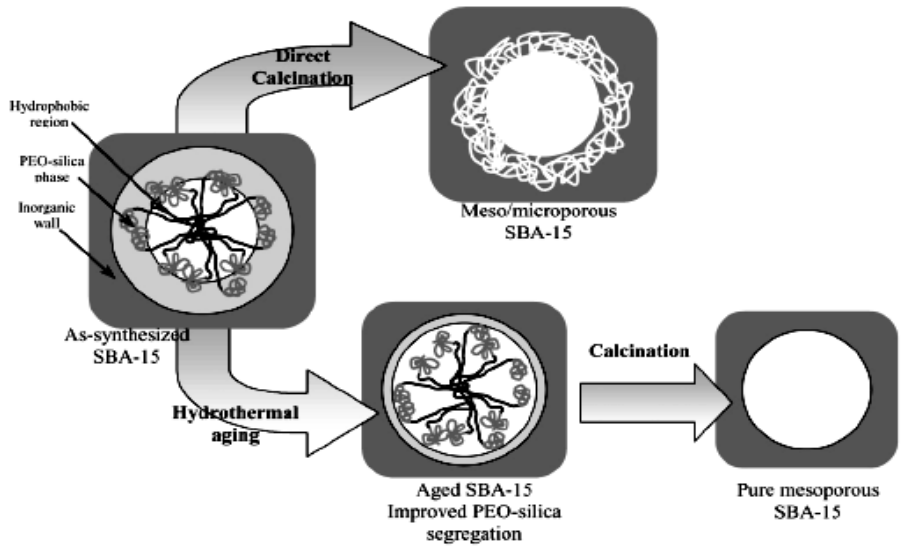

Figure 2.24 Pore evolution upon thermal treatment, depending on pre-treatment and aging [59].

Aging of an as-prepared precipitate at 80–100°C seems to help segregation of the PEO blocks and the inorganic framework, by promoting condensation of the latter. High temperatures also change the polymer behavior. It is known that for T >60°C, PEO blocks become less hydrophilic and expel water similar to PPO blocks when the temperature is higher than 40°C [59]. For a mechanism, firstly alkoxysilane species (TMOS or TEOS) are hydrolyzed as:

$$Si(OEt)_4 + nH_3O^+ \xrightarrow[pH<2]{\text{hydrolysis}} Si(OEt)_{4-n}(H_2O^+)_n + n\ EtOH$$

This is followed by partial oligomerization at the silica. Furthermore, at this condition, the PEO parts of surfactant associate with hydronium ions as followed:

$$-PEO_m- + yHX \xrightarrow{H_2O} -PEO_{m-y}[(EO)\cdot 3H_2O^+]_y\ ---X_y^-$$

Next, coordination sphere expansion around the silicon atom by anion coordination of the form $X^-SiO_2^+$ may play an important role. The hydrophilic PEO blocks are expected to interact with the protonated silica and thus be closely associated with the inorganic wall. During the hydrolysis and condensation of the silica species, intermediate mesophase is sometimes observed and further condensation of silica species and

organization of the surfactant and inorganic species result in the formation of the lowest energy silica-surfactant mesophase structure allowed by solidifying network.

2.10 Modification of catalysts

2.10.1 Incorporation of aluminum into SBA-15

In the metal-substituted mesoporous materials, aluminum-incorporated mesoporous materials have the great potential in moderating acid-catalyzed reactions for large molecules. However, it is very difficult to introduce the metal ions directly into SBA-15 due to the easy dissociation of metal-O-Si bonds under strong acidic conditions.

To date, only a few studies on the direct synthesis of Al-SBA-15 have been reported [61-62]. The comparison of direct and post syntheses of Al-SBA-15 is described in Table 2.12.

Table 2.12 Comparison of direct synthesis and post synthesis methods of Al-SBA-15

	Direct synthesis method	**Post synthesis method**
Synthesis condition	Require complicated procedure	Simple method
Aluminum form in materials	Most of samples have both tetrahedral and octahedral aluminum	Most of samples have only tetrahedral aluminum
Catalyst activity	Lower activity due to extra-framework aluminum	Higher activity due to aluminum in framework

The direct synthesize Al-SBA-15 is difficult and often not stoichiometric. From this viewpoint, therefore, the development of a simple post synthesis method for the alumination of the mesoporous silicas that are synthesized under strongly acidic conditions becomes an appealing alternate choice.

Nowadays, several post synthesis method where aluminum was grafted onto the mesoporous wall with various aluminum sources such as $Al(CH_3)_3$, $AlCl_3$ have been developed without the mesoporous structure seriously destroyed [63]. In the case of zeolites, the introduction of Al into their framework will lead to the formation of bridging hydroxyl groups (Brønsted acid sites). However, whether the similar situation occurs in mesoporous materials still keeps argument. Some researchers assigned the hydroxyl vibration at about 3606 cm^{-1} in IR spectrum to the acidic bridging hydroxyl groups, while others disagreed with the assignment. For example, Trombetta *et al.* argued that the Brønsted acid sites in mesoporous materials or aluminosilicates resulted from terminal silanol groups in the vicinity of aluminum atoms [64]. After the adsorption of a basic probe, such as pivalonitrile, the terminal silanol groups were induced to form the bridging hydroxyl groups (SiOHAl, shown in Figure 2.25).

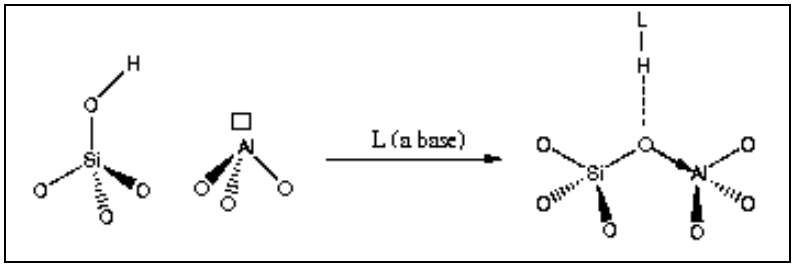

Figure 2.25 Aluminosilicates material using basic probe (L) inducing to form the bridging hydroxyl group [64].

2.10.2 Impregnation [62, 65]

Supported metal catalysts may be prepared by three distinct methods (*i*) deposition, (*ii*) co-precipitation and (*iii*) impregnation. All of these, the last mentioned is the most important. It consists of soaking the carrier with a solution of a suitable metal salt, followed by evaporation to dryness. The supported salt is then either reduced or, in certain case, calcined in air to convert the salt to the oxide which is then reduced to the metal. The main functions of carrier are to provide a structural framework for the catalytic component and increase the surface area per unit weight of metal. Other desirable effects may include such factors as increased stability due to small crystallites of metal being sufficiently separated to prevent sintering and a

greater resistance to poisoning. The choice of carrier depends to a large extent upon the purpose for which the catalyst is required.

-Impregnation of metal on SBA-15 [62]

SBA-15 is a mesoporous ordered silica with promising properties as a catalyst support, for examples, high surface area, large mesoporous and low acidity. These benefits to the increase in dispersion of the active species, the internal diffusion of the reactant and product where functionalization of the siliceous carrier with an active component can be achieved through a number of methods. The properties of SBA-15 materials modified by the wet impregnation of metal such as nickel, platinum, palladium and ruthenium the active metal precursor is dissolved in an aqueous or organic solvent. Then the metal-containing solution is added to a SBA-15 support containing the same pore volume as the volume of solution that was added. Capillary action draws the solution into the pores. The catalyst can be dried and calcined to drive off the volatile components within the solution, depositing the metal on the catalyst surface.

2.11 Characterization of mesoporous hexagonal structure

2.11.1 Powder x-ray diffraction (XRD) [63]

X-ray powder diffraction (XRD) is an instrumental technique used to identify minerals, as well as other crystalline materials. XRD is a technique in which a collimated beams of nearly monochromatic. X-rays is directed onto the flat surface of a relatively thin layer of finely ground material. XRD can provide additional information beyond basic identification. If the sample is a mixture, XRD data can be analyzed to determine the proportion of the different minerals present. Other information obtained can include the degree of crystallinity of the minerals present, possible deviations of the minerals from their ideal compositions, the structural state of the minerals and the degree of hydration for minerals that contain water in their structure.

XRD is a reliable technique that can be used to identify hexagonal mesoporous structure which performs five well-resolved peaks corresponding to lattice planes of Miller indices (100), (110), (200), (210), and (300). These XRD peaks appear at low angle (2θ angle between 0.5 and 3 degree) due to the materials are not crystalline at atomic level, diffraction at higher angles are not observed. Figure 2.26 shows a monochromatic beam of X-ray incident on the surface of crystal at an angle 2θ. The scattered intensity can be measured as a function of scattering angle 2θ. The resulting XRD pattern efficiently determines the different phases present in the sample.

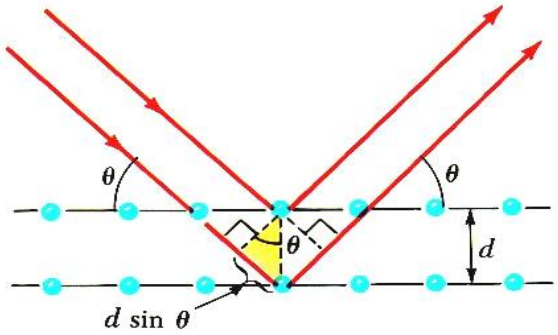

Figure 2.26 Diffraction of x-ray by regular planes of atoms [64].

Using this method, Braggs‟ law is able to determine the interplanar spacing of the samples, from diffraction peak according to Bragg angle.

$$n\lambda = 2\,d\sin\theta$$

Where the integer *n* is the order of the diffracted beam, λ is the wavelength; *d* is the distance between adjacent planes of atoms (the *d*-spacings) and θ is the angle between the incident beam and these planes.

2.11.2 Nitrogen adsorption-desorption technique [65-66]

The N_2 adsorption-desorption technique is used to determine the physical properties of mesoporous molecular sieves, that are surface area, pore volume, pore diameter and pore-size distribution of solid catalysts. Adsorption of gas by a porous material is described by an adsorption isotherm, the amount of adsorbed gas by the

material at a fixed temperature as a function of pressure. Porous materials are frequently characterized in terms of pore sizes derived from gas sorption data. The IUPAC classification of adsorption isotherms is illustrated in Figure 2.27.

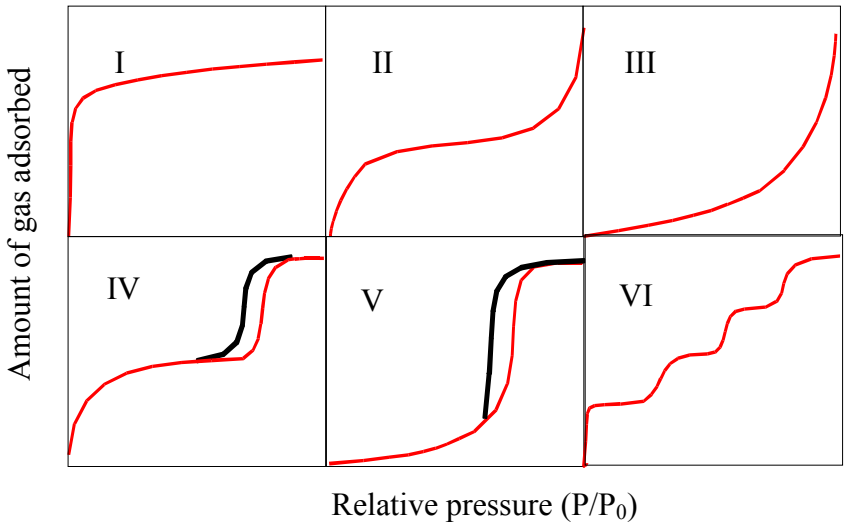

Figure 2.27 The IUPAC classification of adsorption isotherm [65].

Adsorption isotherms are described as shown in Table 2.13 based on the strength of the interaction between the sample surface and adsorptive. Pore size distribution is measured by the use of nitrogen adsorption/desorption isotherm at liquid nitrogen temperature and relative pressures (P/P_o) ranging from 0.05-0.1. The large uptake of nitrogen at low P/P_o indicates filling of the micropores (<20 Å) in the adsorbent. The linear portion of the curve represents multilayer adsorption of nitrogen on the surface of the sample, and the concave upward portion of the curve represents filling of mesoporous and macropores. The multipoint Brunauer, Emmett and Teller (BET) method is commonly used to measure total surface area.

$$\frac{1}{W[(P_o/P)-1]} = \frac{1}{W_mC} + \frac{C-1}{W_mC}(P/P_o)$$

Where W is the weight of nitrogen adsorbed at a given P/P_o, and W_m is the weight of gas to give monolayer coverage, and C is a constant that is related to the heat of adsorption. A slope and intercept are used to determine the quantity of

nitrogen adsorbed in the monolayer and calculate the surface area. For a single point method, the intercept is taken as zero or a small positive value, and the slope from the BET plot is used to calculate the surface area. The surface area reported depend upon the method used, as well as the partial pressures at which the data are collected.

Table 2.13 Features of adsorption isotherms

Type	**Interaction between sample surface and gas adsorbate**	**Porosity**	**Example of sample-adsorbate**
I	relatively strong	Micropores	activated carbon-N_2
II	relatively strong	Non porous	oxide-N_2
III	weak	Non porous	carbon-water vapor
IV	relatively strong	Mesopore	silica-N_2
V	weak	Micropores	
		Mesopore	activated carbon-water vapor
VI	relatively strong sample surface has an even distribution of energy	Nonporous	graphite-Kr

2.11.3 Solid state ^{27}Al-magic angle spinning-nuclear magnetic resonance (^{27}Al-MAS-NMR) [67]

Another important characterization technique for microporous materials is solid state NMR. ^{27}Al-MAS-NMR spectroscopy has been employed to distinguish between tetrahedrally and octahedrally coordinated aluminum in the framework at approximately 50 and 0 ppm, respectively. Therefore, the amount of framework aluminum can be determined.

2.11.4 Scanning electron microscope (SEM) [68]

The scanning electron microscope (SEM) has unique capabilities for analyzing surfaces and morphology of materials. It is analogous to the reflected light microscope, although different radiation sources serve to produce the required illumination. Whereas the reflected light microscope forms an image from light reflected from a sample surface, the SEM uses electrons for image formation. The different wavelength of these radiation sources result in different resolution levels: electron have much shorter wavelength than light photons, and shorter wavelength are capable of generating the higher resolution information. Enhanced resolution in turn permits higher magnification without loss of detail. The maximum magnification of the light microscope is about 2,000 times; beyond this level is "empty magnification", or the point where increased magnification does not provide additional information. This upper magnification limit is a function of the wavelength of visible light, 2000 Å, which equal the theoretical maximum resolution of conventional light microscope. In comparison, the wavelength of electron is less than 0.5 Å, and theoretically the maximum magnification of electron beam instrument is beyond 800,000 times. Because of instrumental parameters, practical magnification and resolution limits are about 75,000 times and 40 Å in a conventional SEM. The SEM consists basically of four systems:

1. The *illuminating/imaging system* produces the electron beam and directs it onto the sample.

2. The *information system* includes the data released by the sample during electron bombardment and detectors which discriminate among analyze these information signals.

3. The *display system* consists of one or two cathode-ray tubes for observing and photographing the surface of interest.

4. The *vacuum system* removes gases from the microscope column which increase the mean free path of electron, hence the better image quality.

2.11.5 Transmission electron microscope (TEM) [68]

TEM is a microscopy technique used for studying the size, size distribution and morphology of particles. TEM involves a beam of accelerated electron, 50-200 keV, emitted by a tungsten filament cathode in vacuum. These electrons are deflected in small angles by atoms in sample and transmitted through a thin sample. Then, these electrons are magnified by magnetic lenses and hitting a fluorescent screen coated with a phosphor to generate the bright field image. A schematic diagram of transmission electron microscope is shown in Figure 2.28. The images from electron microscopes indicate the shape of a sample crystallite which can be used to determine size and morphology of solid nanoparticles.

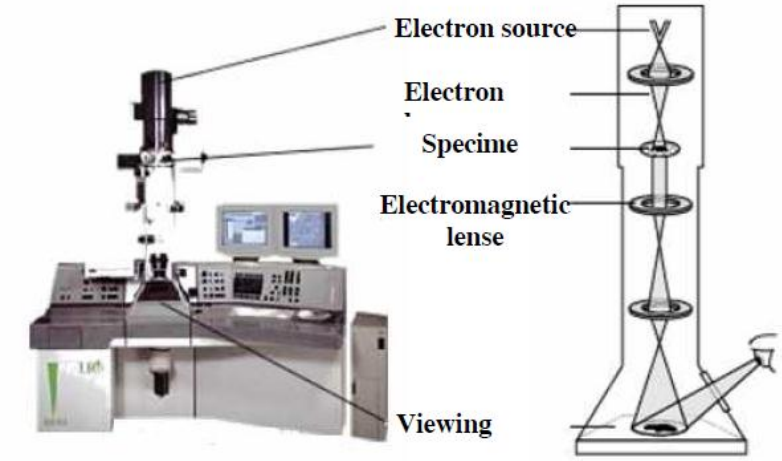

Figure 2.28 Schematic diagram of transmission electron microscope.

CHAPTER III

EXPERIMENTAL

3.1 Instruments, Apparatus and Analytical Techniques

Oven and furnace

Memmert UM-500 oven was used for hydrothermal process of SBA-15 at crystallization at temperature 100°C. It was also used for drying the catalysts. Carbolite RHF 1600 muffle furnace was used for calcination to remove moisture and organic template from the catalyst. As-synthesized SBA-15, Al-SBA-15 and beta zeolite were heated to 100°C with a heating rate of 1°C/min and dwelled at 100°C for an hour. After that the temperature was raised up 550°C with the same heating rate and dwelled at that temperature for 5 h. Metal-SBA-15 and metal-beta zeolite were calcined at 100°C for 1 h and 500°C for 4 h with the heating rate of 1°C/min. After calcination, as-synthesized SBA-15 and beta zeolite have new name as calcined SBA-15 and calcined beta zeolite. The heating program of SBA-15, Al-SBA-15 and beta zeolite was showed in Schemes 3.1 and metal-SBA-15 and metal-beta zeolite was showed in Schemes 3.2.

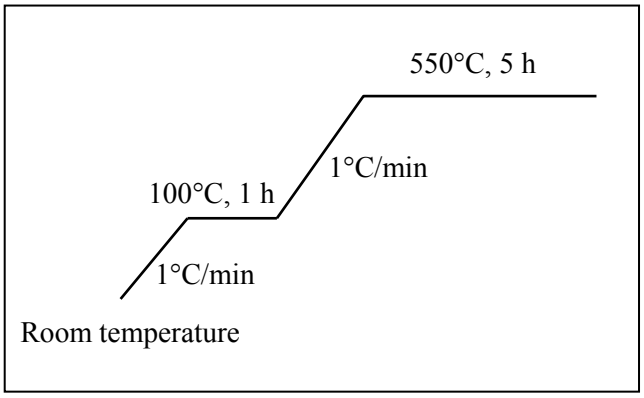

Scheme 3.1 The heating program of SBA-15, Al-SBA-15 and beta zeolite.

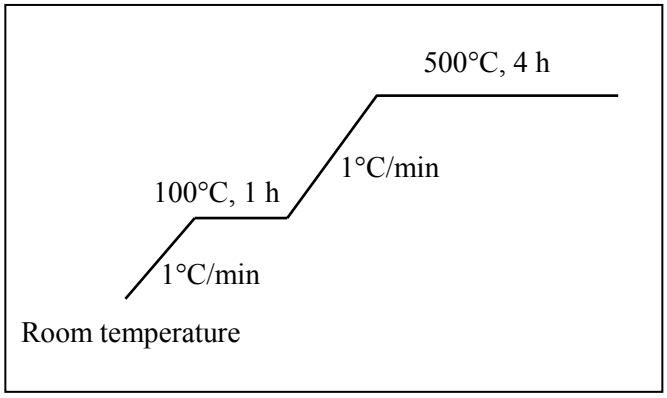

Scheme 3.2 The heating program of Metal-SBA-15 and Metal-beta zeolite.

Powder x-ray diffraction (XRD)

The x-ray diffraction patterns of powder catalysts were determined by a Rigaku, Dmax 2200/Ultima^{+} diffractometer using a monochromator with Cu Kα radiation operated at 40 kV and 30 mA. The low-angle XRD patterns were collected in the 2θ range from 0.5 to 3.0 degree for SBA-15, Al-SBA-15 and metal-SBA-15 whereas the wide-angle XRD patterns were collected in the 2θ range from 10 to 80 degree with scan speed of 1.0 degree min^{-1}. For XRD patterns of beta zeolite and metal-beta zeolite, they were collected in the 2θ range from 5 to 80 degree with scan speed of 5.0 degree min^{-1}, the scattering slit, divergent slit, and receiving slit, were fixed at 0.5 degree, 0.5 degree, and 0.15 mm, respectively. The XRD phase identification was made by comparison to the Joint Committee on Powder Diffraction Standards (JCPDSs).

Nitrogen adsorption-desorption isoterm analyzer

Nitrogen adsorption-desorption isotherm analyzer were carried out using a BEL Japan BELSORP-mini 28SP instrument for characterization of catalyst porosity in terms of nitrogen adsorption-desorption isotherms, specific surface area, external surface area and pore size distribution of catalysts. Before analysis, calcined sample was weighed constant 40 mg and pretreated at 400°C for 2-3 h under vacuum. Adsorption isotherms were measured at 77 K (liquid nitrogen) using nitrogen of 99.999% purity as an adsorbate.

Scanning electron microscopy (SEM)

The morphology and particles size of calcined SBA-15, Al-SBA-15, beta zeolite, metal-SBA-15 and metal-beta zeolite samples were analyzed by JSM-5410 LV scanning electron microscope with 15 kV of acceleration voltage. All samples were coated with sputtering gold under vacuum for conductivity. The loading metal in supported catalyst was measured by Hitachi/S-4800 scanning electron microscope and energy dispersive X-ray spectrometer (SEM-EDX).

^{27}Al MAS nuclear magnetic resonance spectroscopy

The spectra of aluminum tetrahedral in catalysts were analyzed by ^{27}Al-magnetic angle spinning nuclear magnetic resonance using ^{7}Al MAS NMR, Bruker advance DPX-300 spectroscopy operating at 78 MHz.

Gas chromatography

Hydrocarbon gas products from pyrolysis processes were analyzed by a Varian CP-3800 model gas chromatograph equipped with a 0.53 mm inner diameter and 50 m length of KCl/Al_2O_3-PLOT column. The column temperature was started at 35°C and maintained for 5 min. Then the temperature was increased to 140°C at a rate of 3°C/min and maintained for 10 min. The total time was 50 min, whereas the permanent gas analyzed by equipped with a 1 mm inner diameter and 2 m length of ShinCarbon ST 100/120-Micropacked column. The column temperature was started at 35°C and maintained for 8 min. Then the temperature was increased to 180°C at a rate of 30°C/min and maintained for 10 min. The total time was 23 min. Liquid products were identified using the similar instrument as the gases products but equipped with a 0.25 mm inner diameter and 30 m length of CP-sil5 column (equivalent to VF-1ms column). The column temperature was started at 30°C and maintained for 1 min. and temperature was increased to 35°C at a rate of 0.5°C/min, for 1 min. and temperature was increased to 40°C at a rate of 0.5°C/min, for 1 min. Then temperature increased to 185°C at a rate of 0.5°C/min, for 1 min. The total time was 48 min. The volumes of each sample injections are 3.0 µl, 300 µl and 1.0 µl for hydrocarbon gas, permanent gas and liquid, respectively. Detector of hydrocarbon gas and liquid samples was flame ionization detector (FID) using carrier gas as N_2, while permanent gas detector

was thermal conductivity detector (TCD) using carrier gas as He. The column heating programs of gas and liquid analysis are shown in Schemes 3.3, 3.4 and 3.5 respectively.

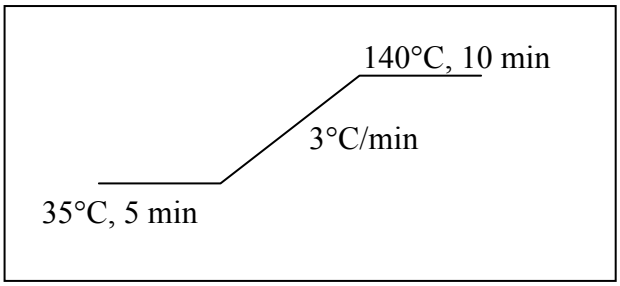

Scheme 3.3 The column heating program for hydrocarbon gas analysis.

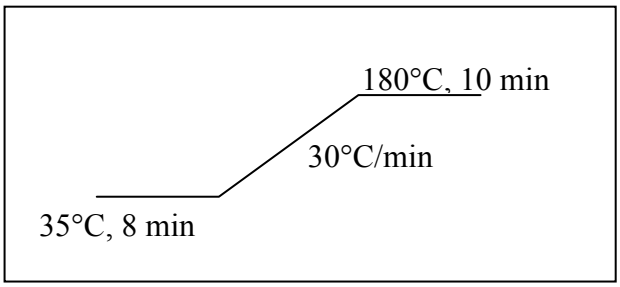

Scheme 3.4 The column heating program for permanent gas analysis.

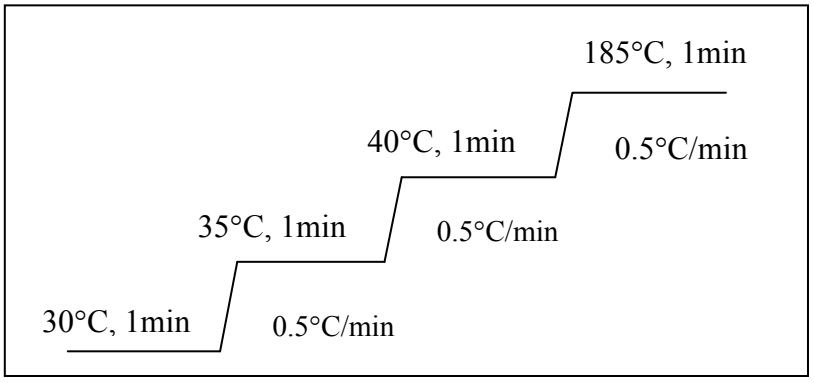

Scheme 3.5 The column heating program for liquid analysis.

Gas chromatography-mass spectrometer

Qualitative analysis of liquid product was identified with GC-MS technique. GC system network of Varain CP-3800, mass selective detector of GC-MS Saturn 2200 equipped with a 0.25 mm inner diameter and 30 m length of VF-1ms capillary column. The identification of the peaks was based on computer matching of the mass spectra with the National Institute of Standards and Technology (NIST) library, USA.

Transmission electron microscope (TEM)

The microstructure of metal supported on SBA-15 and metal supported on beta zeolite were performed on a JEOL; JEM-2100 electron microscope with an acceleration voltage of 200 kV.

Simultaneous thermal analyzer (TGA)

Thermal decomposition and weight loss as a function of temperature (or time) for corncob were analyzed using TGA Netzsch; STA490C. The operation following temperature profile: the heat was started at 30°C with rate of 10°C min^{-1} and hold constant at 100°C for 20 min. Then, with a rate 20 °C min^{-1}, the temperature was increased up to 600°C and stabilization for 20 min and the final temperature of 900°C with a rate 20°C min. The sample was heating in air.

Elemental analyzer (CHN/O analyzer)

The ultimate analysis of corncob were analyzed the elemental carbon (C), hydrogen (H), nitrogen (N) and oxygen (O) composition using CHN/O analyzer; Perkin Elmer-PE2400 Series II at Scientific and Technological Research Equipment Centre of Chulalongkorn University.

Chemicals and Gases

1. Triblock copolymer Pluronic P123 (PEO_{20}-PPO_{70}-PEO_{20}, average molecular weight = 5800) (Aldrich)
2. Tetraethyl orthosillicate 98%, TEOS, $C_8H_{20}O_4Si$ (Fluka, reagent grade)
3. Sodium aluminate, $NaAlO_2$, (Riedel-de Haën, reagent grade)
4. Hydrochloric acid, HCl, (Fluka, 37wt%)
5. Palladium(II) chloride, $PdCl_2$ (Aldrich)
6. Nickel(II) nitrate hexahydrate, $Ni(NO_3)_2.6H_2O$ (Merck)
7. Standard gas mixture for GC analysis was kindly obtained from PTT Chemical Public Company Limited.
8. Nitrogen gas, N_2, (Thai Industrial Gases, highly pure grade)
9. Beta zeolite and ZSM-5 commercial catalysts, SiO_2/Al_2O_3 = 30 (ZEOCHEM)

3.2 Preparation of corncob biomass

The corncob biomass materials as raw material which was used in pyrolysis cracking process were collected from Nakhon Sawan Field Crop Research Center in Thailand. Prior to experiments, the corncob was ground and sieved less than 1.4 mm. After that the corncob was dried in oven at 130°C. The component composition of the corncob was followed by Dietrich Meier *et al.* and Sineenat *et al.* [15], [24].

3.3 Preparation of the catalysts

3.3.1 Synthesis of pure SBA-15 (SBA-15)

SBA-15 synthesis was performed by hydrothermal method reported by Stucky *et al.* [10]. The gel mole composition of 1TEOS: 0.017P123: 80.56HCl: 40.85H_2O was prepared by dissolving 4 g triblock copolymer pluronic P123 ($EO_{20}PO_{70}EO_{20}$) as a directing agent, with stirring in 120 g of hydrochloric acid (HCl, 2M) and added 30 g of deionized water (H_2O). The mixture was stirred for 30 min or until it became a homogeneous solution, called template-solution. Then 8.5 g of tetraethyl orthosilicate (TEOS) was added to the template solution in sequence under vigorous stirring for 1 h and then ageing for 24 h at 40°C with stirring. The white gel solution was transferred into a Teflon-PARR autoclave for crystallization for 48 h at 100°C. The obtained white solid was filtered and washed several times with distilled water to neutral pH value, and dried in air for a day. As-synthesized SBA-15 was obtained. The template was removed by calcination of the as-synthesized sample at the temperature of 550°C for 5 h as the calcined SBA-15. The synthesis procedure of SBA-15 was shown in Scheme 3.6.

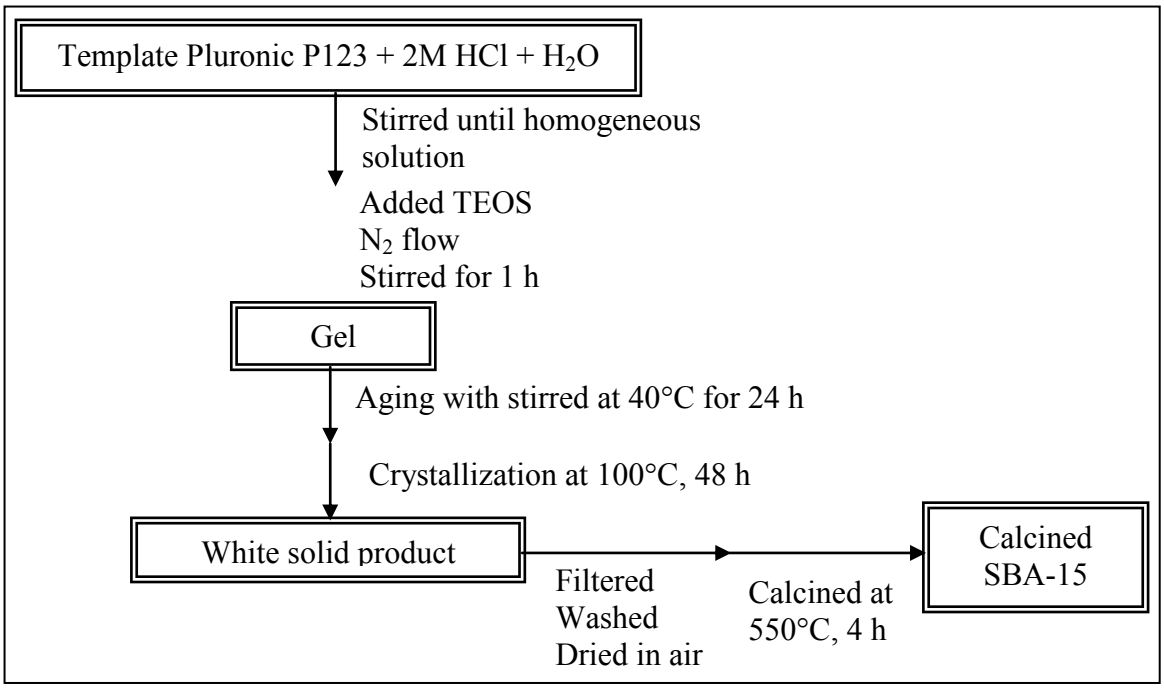

Scheme 3.6 Diagram of the SBA-15 synthesis.

3.3.2 Synthesis of Al-SBA-15

The Al-containing SBA-15 type materials with different SiO_2/Al_2O_3 mole ratio in gel of 60, 30 and 20 were prepared by post-synthesis procedure. Alumination of calcined SBA-15 was conducted by stirring 50 mL of water containing exactly amount of sodium aluminate at room temperature for 12 h which the composition of sodium aluminate used were shown in Table 3.1. The solid material was separated by filtration, washed with distillated water, and dried at 40°C, the obtained solid material named as-synthesized Al-SBA-15. As-synthesized Al-SBA-5 samples remained Na ion form was removed by ion exchange with 0.01M NH_4Cl [11]. After filtration, repeatedly washed with distillated water and calcined at 550°C for 5 h. The procedure was summarized in Scheme 3.7.

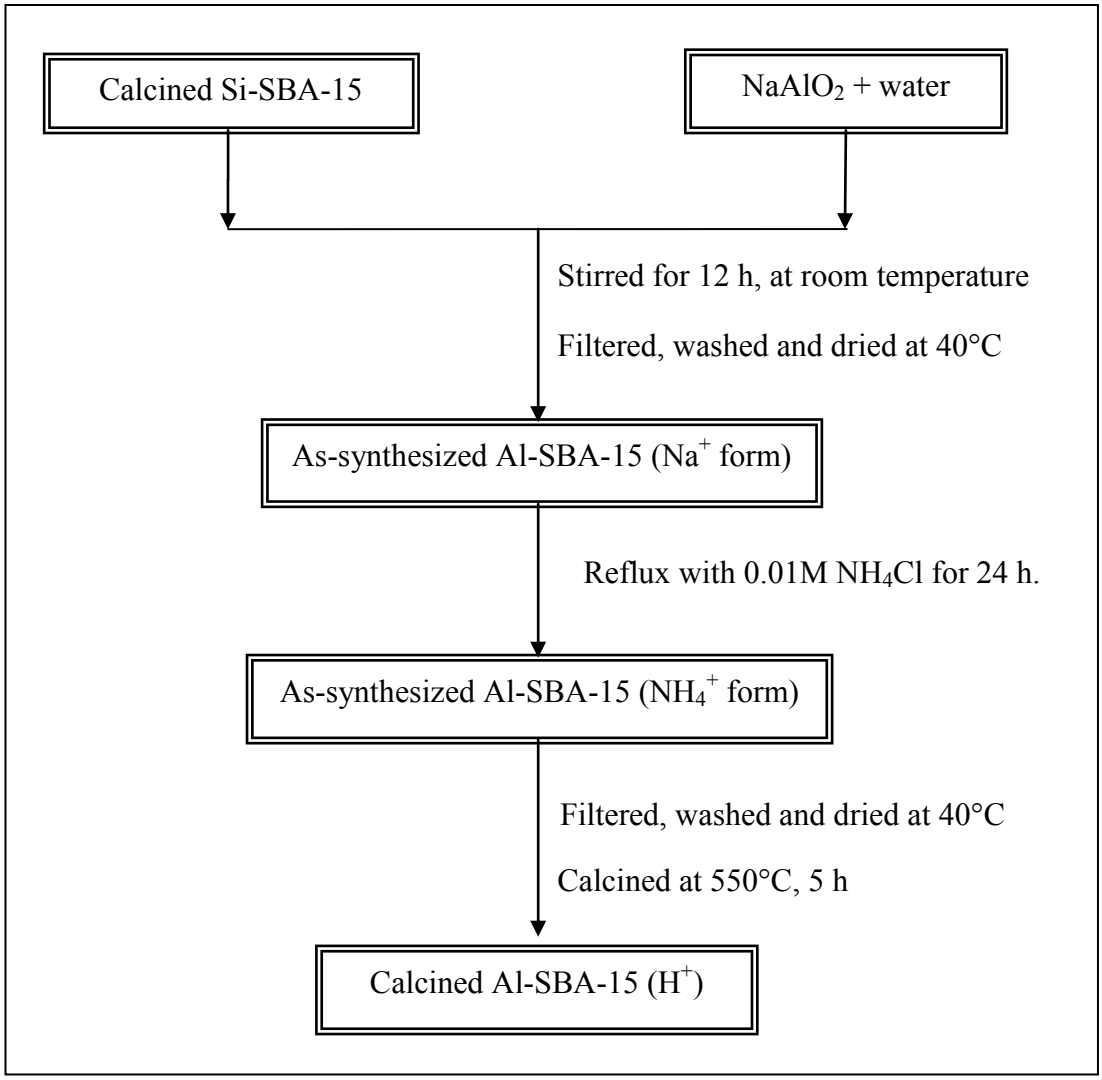

Scheme 3.7 Diagram of Al-SBA-15 by post-synthesis procedure.

Table 3.1 The composition of sodium aluminate in alumination of the Al-SBA-15 with various SiO_2/Al_2O_3 ratios

SiO_2/Al_2O_3 molar ratio in gel	**$NaAlO_2$ dissolved in 50.0 mL H_2O (g)**
20	1.6400
30	0.7288
60	0.1822

3.3.3 Preparation of metal supported on SBA-15 and beta zeolite (M-SBA-15 and M-BEA)

Supported metal catalysts were also prepared by impregnating of pure Si-SBA-15 and beta zeolite with an aqueous solution containing nickel(II) nitrate hexahydrate ($Ni(NO_3)_2.6H_2O$) and palladium(II) chloride ($PdCl_2$) under stirring at 60°C until dryness, and dried at 120°C overnight. The amount of metal loading was 5wt% of catalyst. $PdCl_2$ was dissolved in 1M HCl because $PdCl_2$ did not dissolve completely in water. All the catalysts were calcined at 500°C for 4 h. The catalysts have been denoted as M-SBA-15(X) and M-BEA(X) where X is the metal loading (wt%) [62].

3.4 Pyrolysis of Corncob

The pyrolysis cracking activity test of corncob was carried out under reaction temperature between 250 to 600°C using as catalyst compared with non-catalyst. This pyrolysis cracking was performed in a closed reactor, which is a stainless steel reactor with 4.4 cm. in diameter and 37 cm. in length, under atmospheric pressure. A total of 5 g of corncob and 0.5 g of catalyst were loaded into the reactor. For thermal cracking, only corncob was loaded into the reactor. Before a pyrolysis cracking process, the reactor was set up, and purged with N_2 gas at flow rate of 20 ml/min to remove air. The pyrolysis process was started with heating the tube reactor to the reaction temperature with heating rate of 20°C/min by a split-tube furnace equipped with a programmable temperature controller and a K-type thermocouple. Once the reaction temperature was reached the setting point, it was kept constant for 40 min. The product fraction was flowed from the reactor by the nitrogen gas through a condenser. While the gas fraction was passed through the condenser and collected into a Tedlar bag, the liquid product was condensed in a condenser at a temperature of cold water and collected into a graduated cylinder. The gas was collected since the start of heating. After the reaction was completed, the reactor was cooled down to room temperature and the product fractions were weighed. The values of %conversion and %yield fraction of products were calculated based on the equations as follows:

$$\%\text{Conversion} = \frac{(\text{mass of liquid fraction} + \text{mass of gas fraction})}{\text{mass of corncob}} \times 100$$

mass of gas fraction = mass of the reactor with biomass and catalyst before reaction – mass of the reactor with residue and used catalyst after reaction – mass of liquid fraction

$$\%\text{Yield product fraction} = \frac{\text{mass of product fraction}}{\text{mass of corncob}} \times 100$$

The products were classified into three fractions: gas fraction (products which were not condensed at temperature of cooling water), liquid fraction and residue. The gaseous product was estimated by subtracting the weight of liquid products and residues from the starting material. The liquid fraction obtained from the reaction was separated into two fractions distillated liquid and heavy liquid, by distillation at 120°C. The gas products and distillate oil products were analyzed by a gas chromatograph. The apparatus was shown in Figure 3.1 and process diagram is shown in Scheme 3.8.

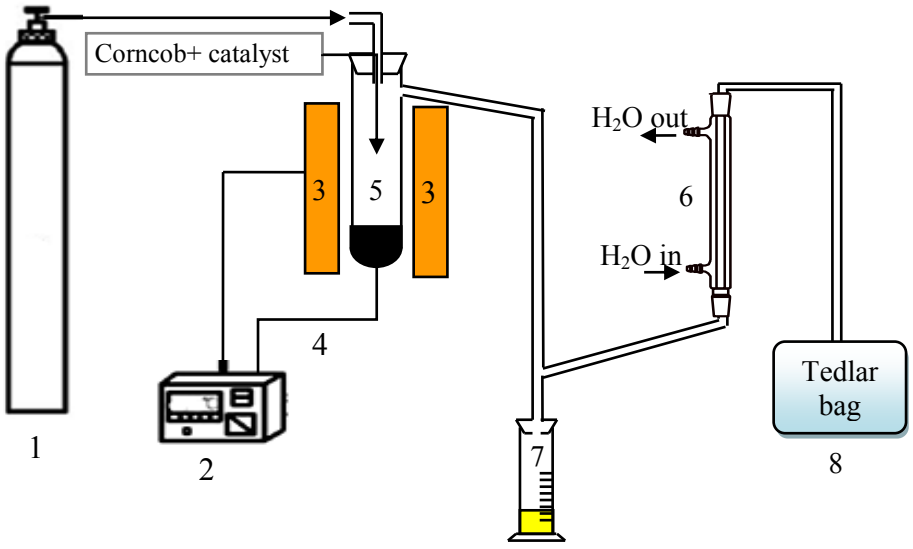

Figure 3.1 Pyrolysis cracking apparatus. 1. Nitrogen gas; 2.Temperature controller; 3.A split-tube furnace; 4.K-type thermocouple; 5.Furnance; 6.Condenser; 7.Graduated cylinder; 8.Tedlar bag.

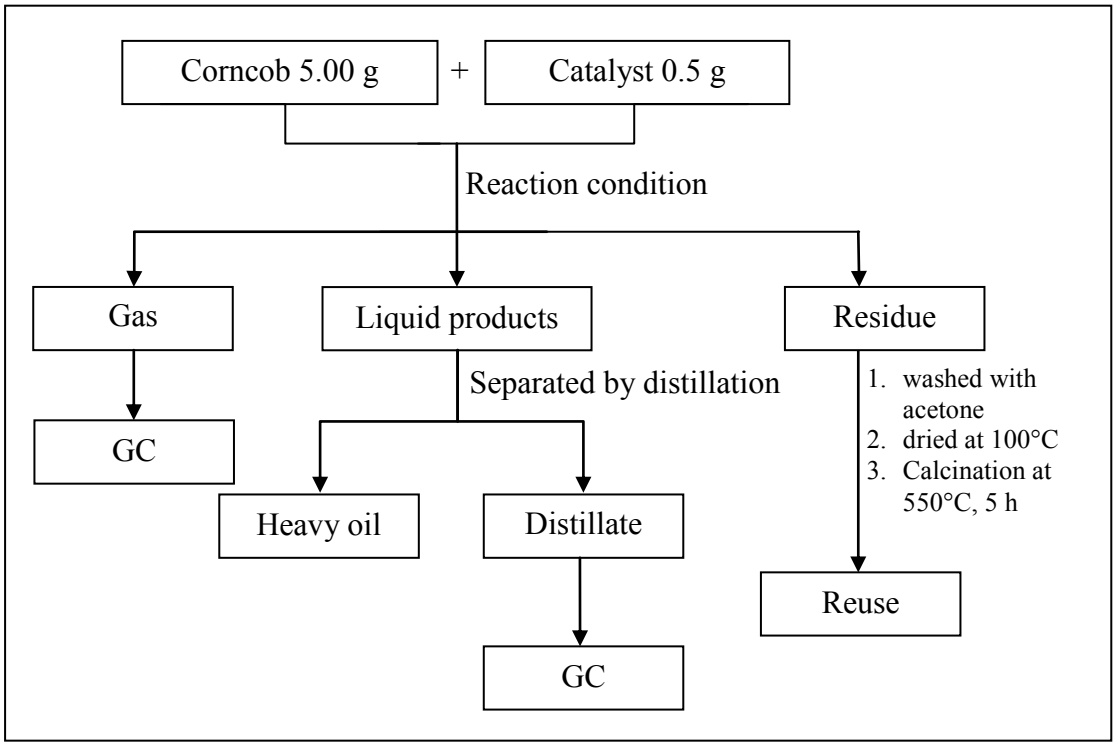

Scheme 3.8 Diagram of pyrolysis cracking process of corncob.

3.4.1 Effect of reaction temperature

The effect of reaction temperature on pyrolysis cracking of corncob was studied at 250, 300, 400, 500 and 600°C for 40 min, heating rate of 20°C/min and purged with N_2 gas at flow rate of 20 ml/min.

3.4.2 Effect of catalyst type

The effect of catalytic cracking of the pyrolysis from corncob was performed by using catalysts, including two microporous zeolites (HBEA and ZSM-5) and two mesoporous catalysts (SBA-15, Al-SBA-15). Moreover, catalytic pyrolysis was investigated metal-supported catalysts such as Ni and Pd. The catalytic pyrolysis was studied at 300°C for 40 min, heating rate of 20°C/min, 10wt% of catalyst to corncob, compared with thermal cracking.

3.4.3 Effect of corncob to catalyst Ratio

The effect of catalyst ratio was studied by catalytic cracking of the pyrolysis from corncob over Al-SBA-15 (SiO_2/Al_2O_3 = 20) at 300°C for 40 min, heating rate of 20°C/min and 5 wt% and 10 wt% of catalyst to corncob.

3.5 Reused catalyst

The spent Al-SBA-15 catalyst (SiO_2/Al_2O_3 ratio = 20) from pyrolysis of corncob at the reaction temperature of 300°C from each cycle was reused by washed with acetone and calcination in air at 550°C for 5 h. The reused catalyst was characterized by XRD, SEM, N_2 adsorption and tested for its activity by pyrolysis catalytic of corncob at the reaction temperature of 300°C for 40 min, heating rate of 20°C/min and 10wt% of catalyst to corncob.

CHAPTER IV

RESULTS AND DISCUSSION

The characteristic analysis of biomass material were included the composition of corncob by the proximate analysis, ultimate analysis and thermal stability using thermogravimetric analysis (TGA). Meanwhile, the prepared catalyst samples were characterized, the crystallinity by X-ray powder diffraction (XRD), the specific surface area by N_2 adsorption-desorption isotherms, the morphology by scanning electron microscopy (SEM) and the microstructure by transmission electron microscopy (TEM).

4.1 Biomass material characterization

4.1.1 Composition of corncob

The proximate and ultimate analysis were performed with the method ASTM-D3172-73(84) [69]. This method was used to determine a thermo-chemical behavior of material and elemental composition were performed in Table 3.1 [24]. The corncob contained high volatile matter about 80wt% which resulted in volatile matter compounds including volatile gases, hydrocarbons and solid char. Furthermore, corncob contained low ash content about 2wt%. The ash in biomass was important. The ash affects to efficiency of pyrolysis process under high temperature. The decomposition of ash may cause slag solid in pyrolysis reactor [70].

Table 4.1 Proximate and ultimate analysis of corncob

Proximate analysis[a] (wt%)		**Ultimate analysis[b] (wt%)**	
Moisture	3	C	46.26
Ash	2	H	6.46
Volatile matter	80	N	0.11
Fixed carbon	15	O (by difference)	47.17

[a] Determined according to the ASTM Standard Test Method D3172

[b] Determined according to the CHNO elemental analyzer

4.1.2 Thermogravimetric analysis of corncob (TGA)

The thermal stability of the corncob was studied by measuring weight loss of the sample as a function of temperature. The operation was performed by TGA analyzer shown in Figure 4.1 [71]. The result indicated that was found the thermal stability included three steps. The first step, 7.6 wt% of moisture evaporation was occurred at range 90-120°C. In the second step, cellulose, hemicellulose decomposed to light volatile and gases (H_2O, CO_2 and CO) about 53.4 wt% at the range 300-450°C. The third step occurred in the range of 500-900°C. That explained the heavier volatiles and char product were 18.1 wt%. The remained solid was ash about 2.7 wt% [13, 24].

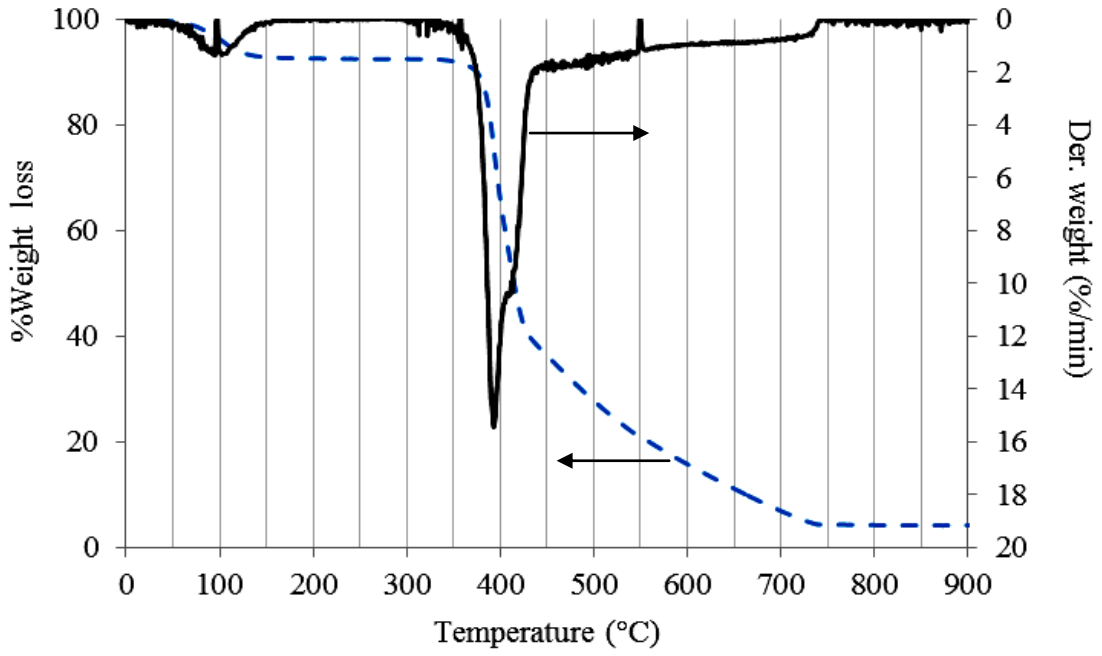

Figure 4.1 TGA and DTG curves for of corncob.

4.2 Characterization of catalysts

4.2.1 Pure SBA-15 (SBA-15)

4.2.1.1 Powder x-ray diffraction (XRD)

The powder XRD patterns of as-synthesized SBA-15 and calcined SBA-15 were shown in Figure 4.2. The SBA-15 exhibited planes of hexagonal mesoporous structure at (100), (110) and (200) [84]. After calcination in air at 550°C for 5 h, the peak intensity increased because template was removed from the channels of material and the hexagonal structure was not destroyed by calcination.

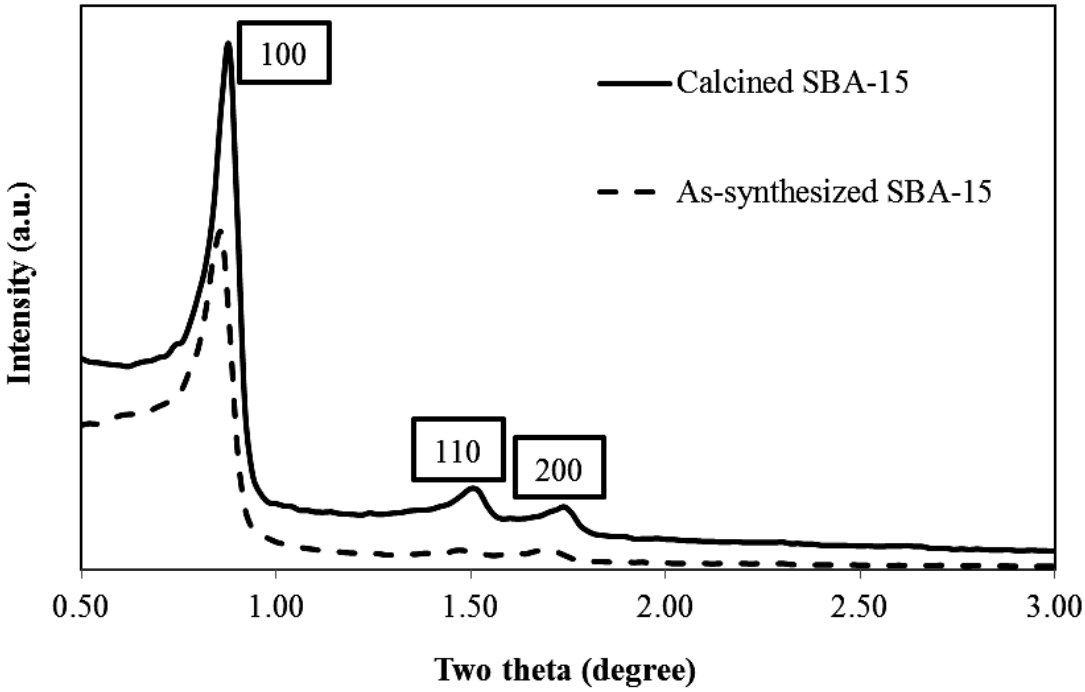

Figure 4.2 XRD patterns of as-synthesized SBA-15 and calcined SBA-15.

4.2.1.2 Nitrogen adsorption-desorption

The N_2 adsorption-desorption isotherm of calcined SBA-15 was shown in Figure 4.3 (a). The calcined SBA-15 exhibited the type IV isotherm with the hysteresis loop between relative intensity 0.6 to 0.8, which was the characteristic pattern of well-ordered mesoporous material.

The multipoint Brunauer, Emmett and Teller (BET) method was used in measuring the specific surface area of calcined SBA-15, which was found at

847.07 m^2/g. The value of the total mesopore volume calculated using BJH method was 1.0628 cm^3/g. The pore size distribution of calcined SBA-15 was shown in Figure 4.3(b) and to exhibited narrow pore size distribution was found in SBA-15 at pore diameter of 8.06 nm

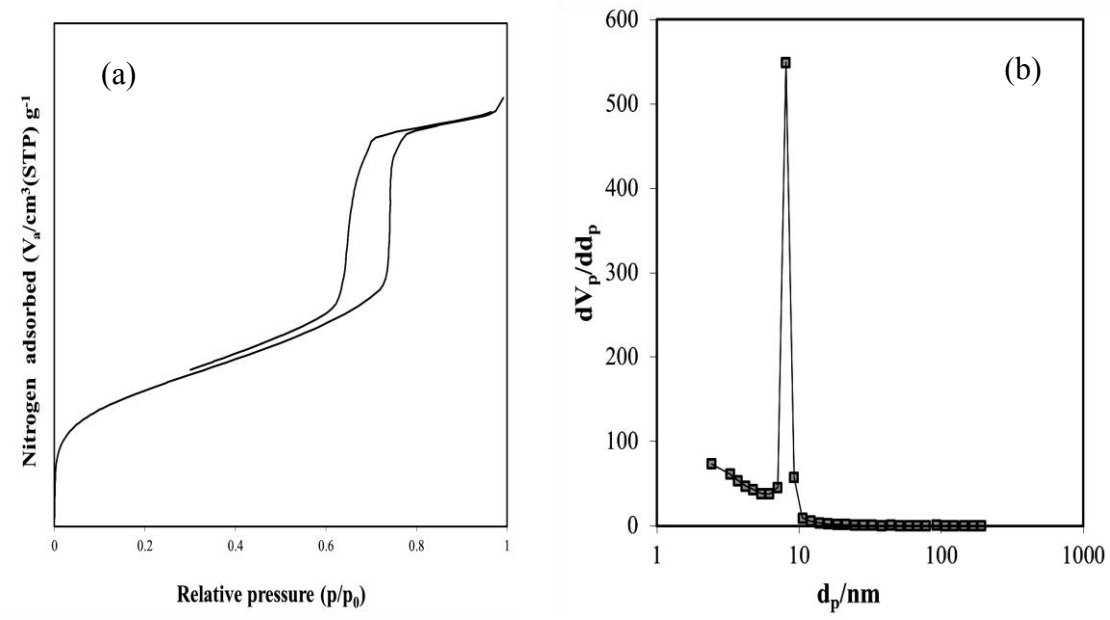

Figure 4.3 (a) Nitrogen adsorption-desorption isotherm and (b) the pore size distribution diagram of SBA-15.

4.2.1.3 Scanning electron microscope (SEM)

The SEM images of the calcined pure SBA-15 sample at different magnifications were shown in Figure 4.4. The SEM images revealed that the calcined SBA-15 consists of a bundle of rope-liked particles with uniform size and exhibited small rod particles about 1.0 × 1.2 μm. which agglomerated to rope-liked structure.

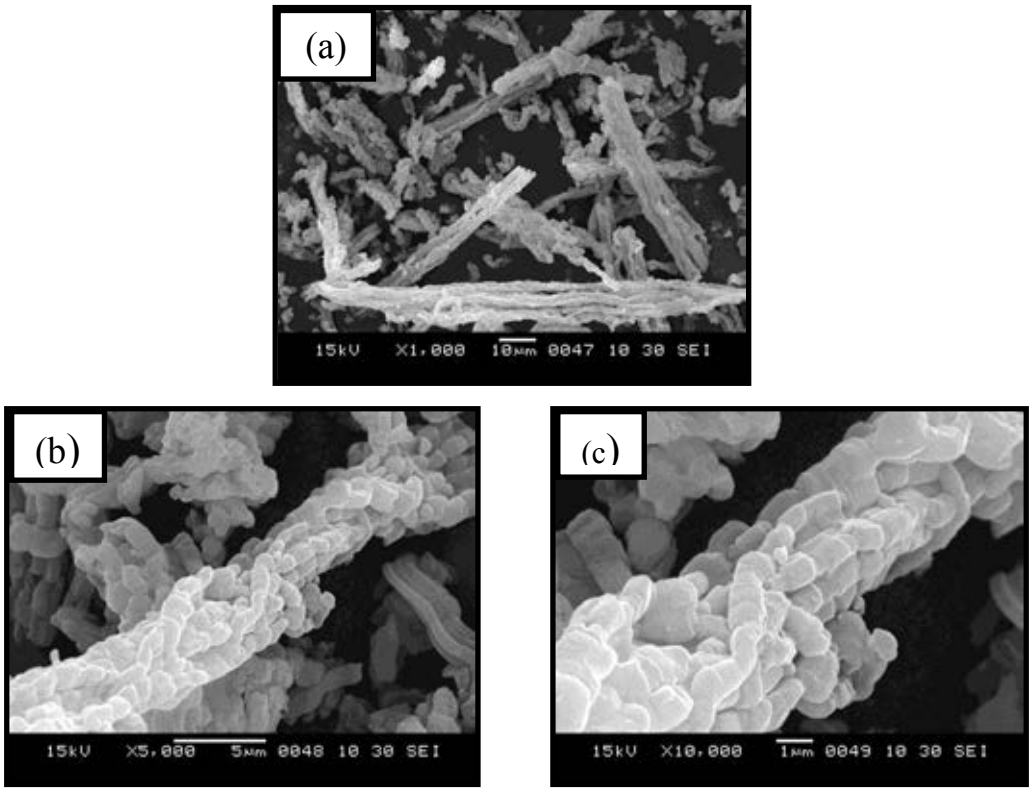

Figure 4.4 SEM images of calcined SBA-15 (a) ×1,000 (b) ×5,000 and (c) ×10,000.

4.2.1.4 Transmission electron microscope (TEM)

The microstructure of calcined SBA-15 powder was examined by TEM micrograph as shown in Figure 4.5. The TEM image presented the well-ordered hexagonal arrays of one-dimensional mesoporous channels of SBA-15.

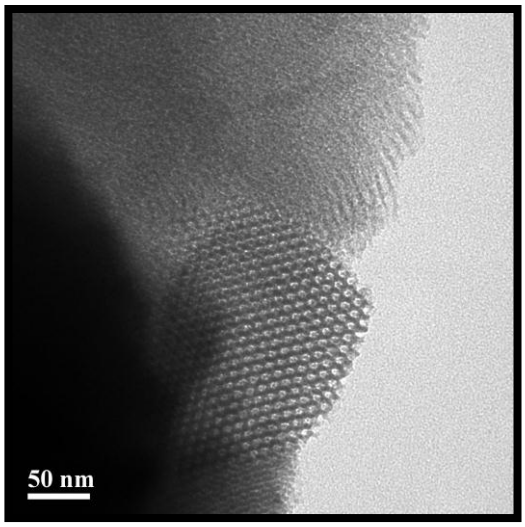

Figure 4.5 TEM image of calcined SBA-15.

4.2.2 Incorporation of aluminum into SBA-15 (Al-SBA-15)

4.2.2.1 Powder x-ray diffraction (XRD)

The powder XRD patterns of Al-SBA-15 with SiO_2/Al_2O_3 ratio in gel about 20, 30 and 60 were shown in Figure 4.6. After incorporated Al in the SBA-15 framework, the peaks of various SiO_2/Al_2O_3 ratios in Al-SBA-15 indicating the maintained the characteristic patterns of hexagonal mesoporous structure which could be indexed to (100), (110) and (200).The intensity of the (100) reflection increases when SiO_2/Al_2O_3 ratios in gel was increased. In addition, the XRD patterns of Al-SBA-15 at various SiO_2/Al_2O_3 ratios were shifted slightly to higher angle resulting from the shrinkage during the recalcination process or change in lattice parameters and d-spacing due to Al inclusion in crystal structure of SBA-15 [62].

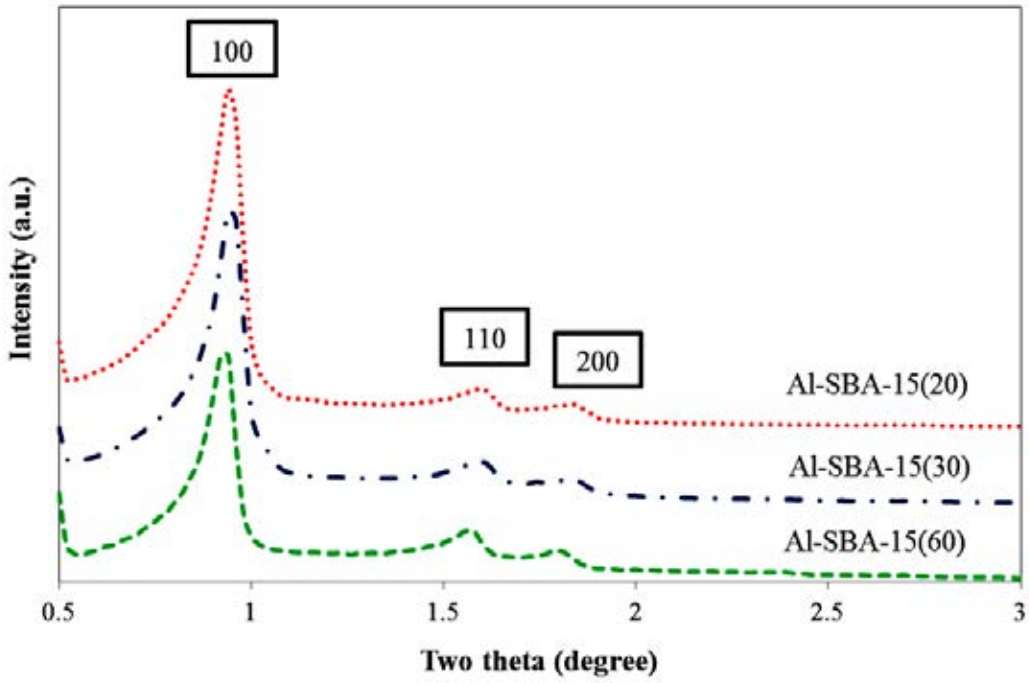

Figure 4.6 XRD patterns of Al-SBA-15 with SiO_2/Al_2O_3 ratios in gel about 60, 30 and 20.

4.2.2.2 Nitrogen adsorption-desorption

The N_2 adsorption-desorption isotherms of the Al-SBA-15 at three SiO_2/Al_2O_3 mole ratios were shown in Figure 4.7. All samples showed N_2 sorption isotherms of type IV with a H1 hysteresis loop, which is the characteristic of mesoporous material. A well-defined step occurred at relatively high pressure of 0.6-0.8, confirmed to capillary condensation of N_2, indicated of the uniformity of the pores [72]. The physical properties of the Al-SBA-15 with various SiO_2/Al_2O_3 ratios were listed in Table 4.2. It was clearly indicating the total specific surface areas and pore volumes reduced with the increasing of the aluminum loading. Incorporated Al in the SBA-15 framework led to a reduction in the amount of nitrogen up taken in SBA-15 depending on the quantities of aluminum due to the decreasing of mesoporous volume. Moreover, amount of aluminum was increased, the d-spacing was decreased indicating that the distance from each plane was reduced. Considering the effect of aluminum content in catalysts, wall thickness was calculated based on the equations (1)-(2). The result showed that the wall thickness reduced when the aluminum quantity in SBA-15 increased, corresponding to the decrease of d-spacing as $d_{(100)}$ in the equation. However, SBA-15 at low aluminum content SiO_2/Al_2O_3 = 60 did not significantly change in term of XRD result [73].

$$\text{Wall thickness} = a_0 - \text{pore size} \quad (1)$$

$$a_0 = 2 \times d_{(100)} / \sqrt{3} \quad (2)$$

a_0 = total specific surface area from BET method

$d_{(100)}$ = d-spacing of the (100) reflection plane from XRD method

Table 4.2 Physical properties of the calcined SBA-15 and Al-SBA-15

Sample	Total specific Surface Area (m^2/g)[a]	Mesopore volume (cm^3/g)[b]	Pore size distribution (nm)[b]	$d_{(100)}$[c] (nm)	Wall thickness[d] (nm)
SBA-15	847.07	1.0628	8.06	10.26	3.79
Al-SBA-15(60)	423.17	0.8646	8.06	10.01	3.50
Al-SBA-15(30)	408.33	0.7969	8.06	9.38	2.78
Al-SBA-15(20)	357.60	0.6636	8.06	9.18	2.54

[a] Determined by BET method,

[b] Determined by BJH-plot method,

[c] Determined by XRD, Jade 5.6,

[d] Determined as: a_0-pore size ($a_0 = 2\times d_{(100)} / \sqrt{3}$)

The pore size distributions were calculated by BJH method showed in Figure 4.8. All samples represented a narrow distribution with the pore size of 8.06 nm by comparing to pure SBA-15 in Figure 4.3 (b). The pore size of all Al-SBA-15 samples still remained unchanged, indicating the extreme stability of Al-SBA-15.

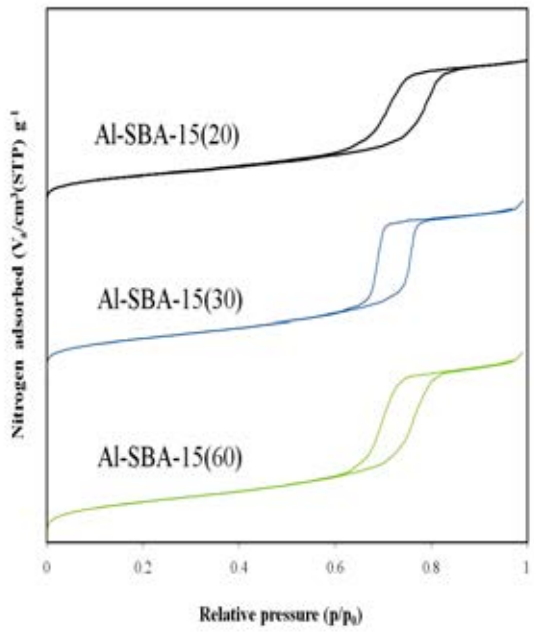

Figure 4.7 Nitrogen adsorption-desorption isotherms of Al-SBA-15 with SiO_2/Al_2O_3 ratios about 60, 30 and 20.

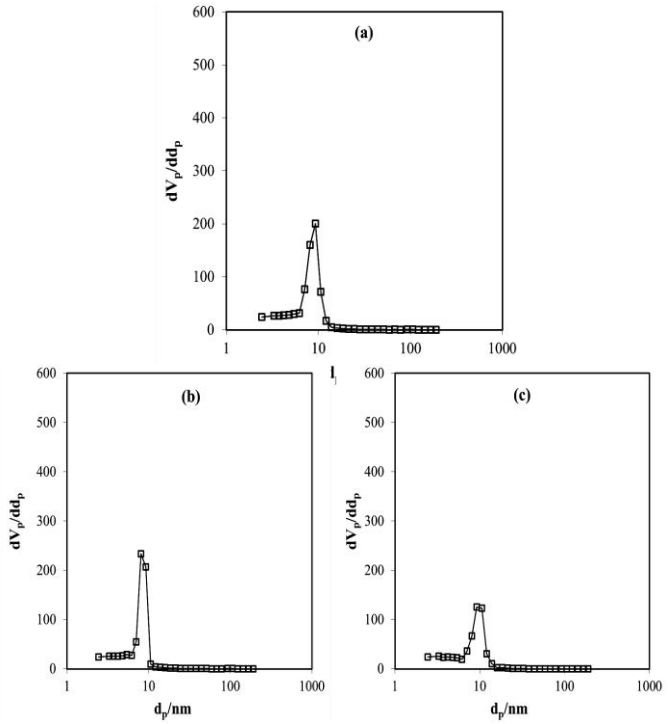

Figure 4.8 Pore size distributions of (a) Al-SBA-15(60), (b) Al-SBA-15(30) and (c) Al-SBA-15(20).

4.2.2.3 ^{27}Al-MAS-NMR spectra

The ^{27}Al-MAS-NMR spectra of Al-SBA-15 with various SiO_2/Al_2O_3 ratios samples were presented in Figure 4.9. Solid state ^{27}Al-MAS-NMR could provide the information of the aluminum atoms that they were located at the framework or non-framework site. All Al-SBA-15 catalysts showed two peaks. The first peak located at about 56 ppm, which could be assigned to tetrahedral (T_d) coordination framework aluminum formed in the mesoporous walls of the material [72, 74]. The second peak located to nearly at 0 ppm was assigned to octahedral (O_h) coordination non-framework site due to calcination lead to dealumination from tetrahedral site to extra-framework or octahedral site [9].

Table 4.3 showed the comparison of T_d/O_h ratios in the Al-SBA-15 with SiO_2/Al_2O_3 ratios about 60, 30 and 20. The result showed that the amount of aluminum increased with the increasing of aluminum into the tetrahedral framework.

Table 4.3 Comparison of T_d/O_h ratios in the Al-SBA-15 with various SiO_2/Al_2O_3 ratios

Sample	T_d/O_h ratios
Al-SBA-15(60)	18.96/1
Al-SBA-15(30)	28.72/1
Al-SBA-15(20)	33.34/1

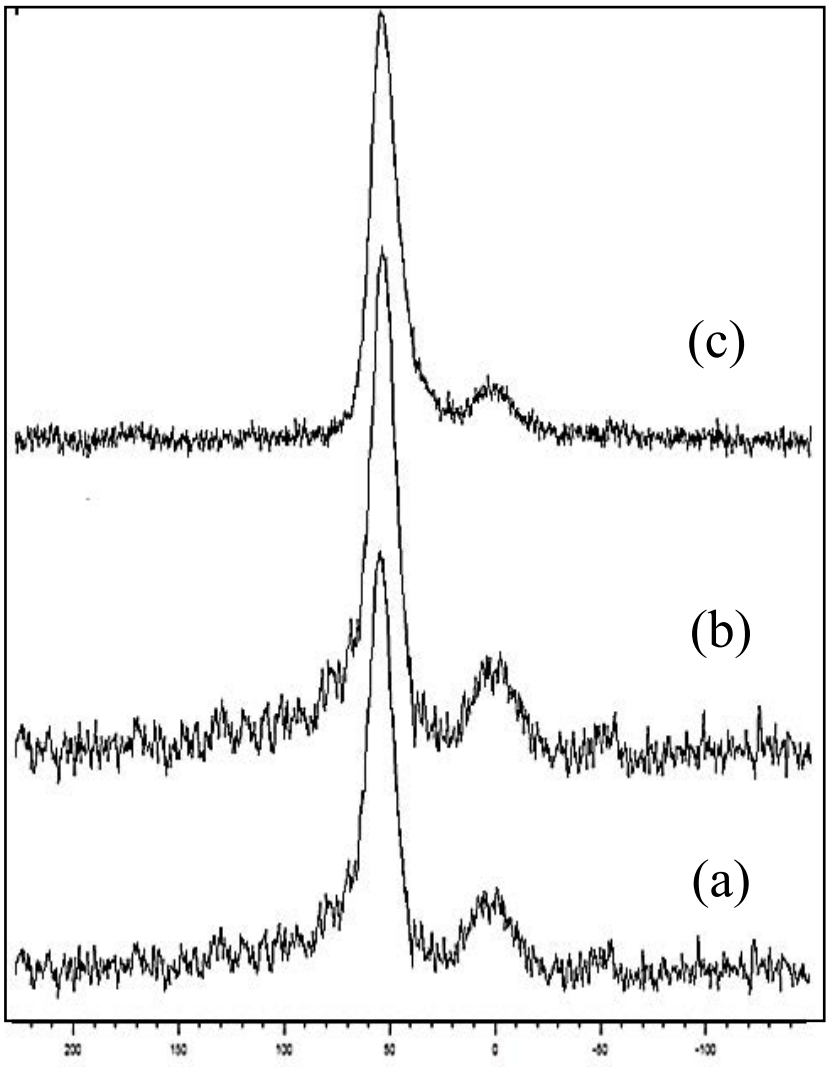

Figure 4.9 ^{27}Al-MAS-NMR spectra of calcined (a) Al-SBA-15(60), (b) Al-SBA-15(30) and (c) Al-SBA-15(20).

4.2.2.4 Scanning electron microscope (SEM)

The morphology of the Al-SBA-15 samples with different SiO_2/Al_2O_3 mole ratios were shown in Figure 4.10. All samples presented rod particles. After aluminum additions, the small rod shape of individual particle remained the same as pure SBA-15. In SEM-EDX method measured the amount of Al metal loading in Al-SBA-15 with various SiO_2/Al_2O_3 mole ratios describing as 20.2%, 28.9% and 60.7% respectively.

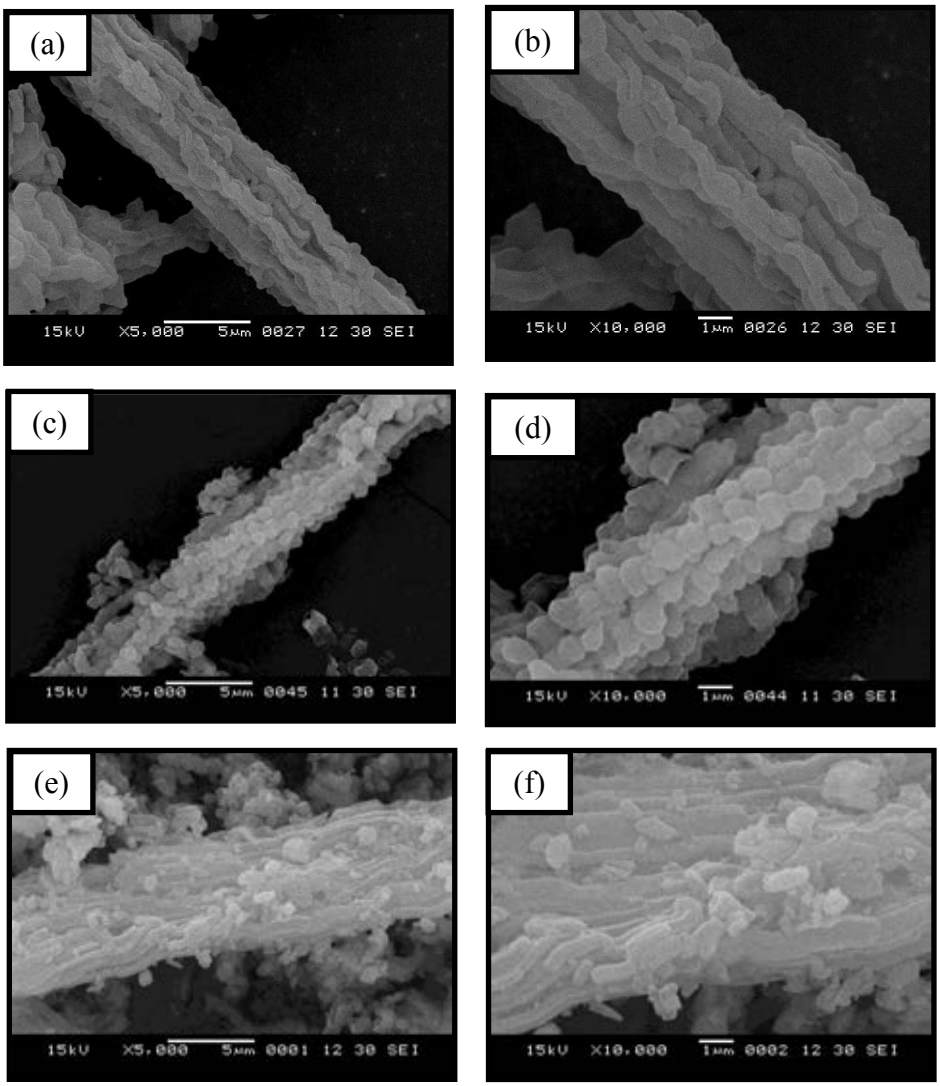

Figure 4.10 SEM images of (a), (b) Al-SBA-15(60), (c), (d) Al-SBA-15(30) and (e), (f) Al-SBA-15(20) at 5,000 and 10,000 magnifications.

4.2.2.5 Transmission electron microscope (TEM)

The TEM images of Al-SBA-15 samples were illustrated in Figure 4.11. All Al-SBA-15 samples showed the well-ordered hexagonal array of mesoporestructure channels similar to the SBA-15 parent. Incorporated Al in the SBA-15 framework leaded to the formation of Al in tetrahedral site which expressed the acidity of Al-SBA-15 structure. Hence, TEM image was confirmed no presented metallic Al particles on SBA-15 surface.

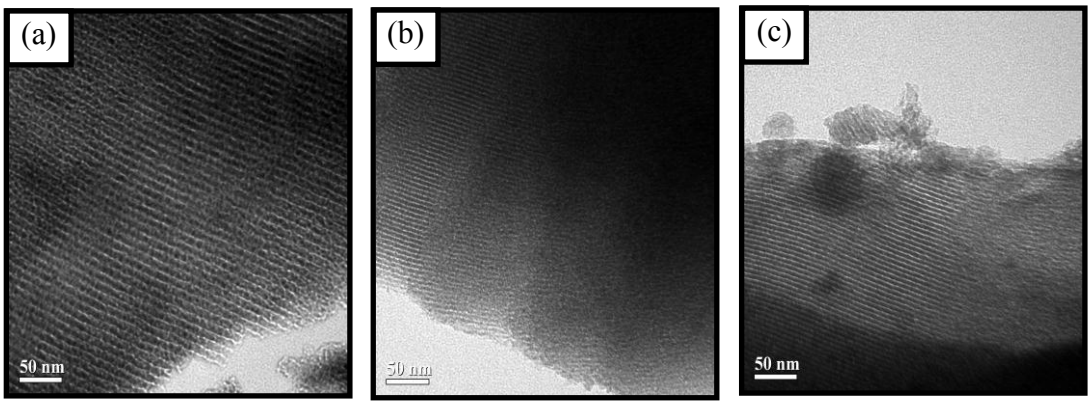

Figure 4.11 TEM images of (a) Al-SBA-15(60), (b) Al-SBA-15(30) and (c) Al-SBA-15 (20).

4.2.3 Impregnation of metal on supported SBA-15 (Ni-SBA-15, Pd-SBA-15)

4.2.3.1 Powder x-ray diffraction (XRD)

The XRD patterns of the Ni-SBA-15 and the Pd-SBA-15 which prepared by impregnation method, displayed in Figure 4.12 and 4.13. Low angle XRD patterns of all samples showed peaks indexed to (100), (110) and (200) plane reflections. All of samples were the characteristic pattern of hexagonal mesoporous. Moreover, the structure of the mesoporous material was intact after impregnation. The peak intensity of the Ni-SBA-15 and Pd-SBA-15 were decreased significantly due to incorporation and blocking of the channels with metal particles. The XRD reflection (100) plane of the Ni-SBA-15 and the Pd-SBA-15 were slightly shifted to higher 2-theta degree because of the constriction of the framework during the recalcination process.

In the wide angle range, pure SBA-15 only showed a broad diffuse peak of amorphous SiO_2. The XRD patterns of Ni-SBA-15 showed diffraction peak at 2-theta = 36.8°, 43.2° and 62.9° were indicated nickel oxide phase (NiO) (JCPDS card, File No. 44-1159) [75]. For the Pd-SBA-15, all diffraction peaks were assigned at 2-theta = 33.72°, 42.60°, 54.70°, 68.8° and 72.2°, which indicated palladium oxide phase (JCPDS card, File No.41-1107) [76, 77].

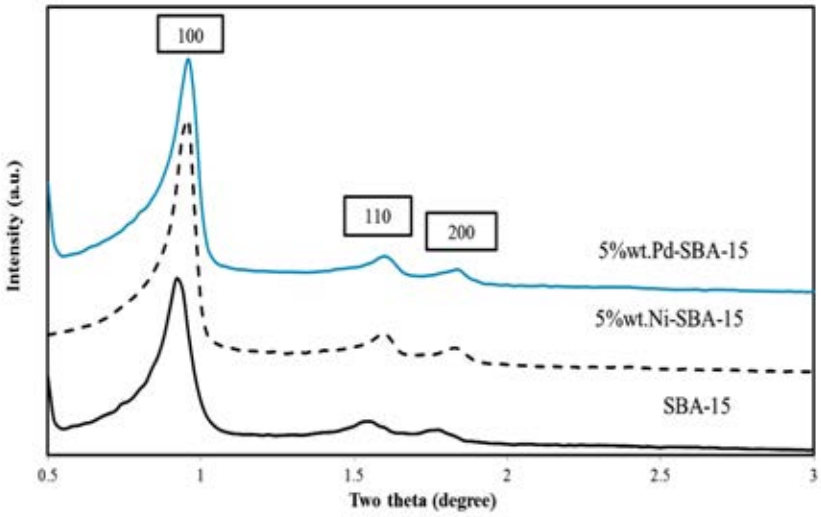

Figure 4.12 XRD patterns of pure SBA-15, Ni-SBA-15 and Pd-SBA-15 at low angle range 0.5-3°.

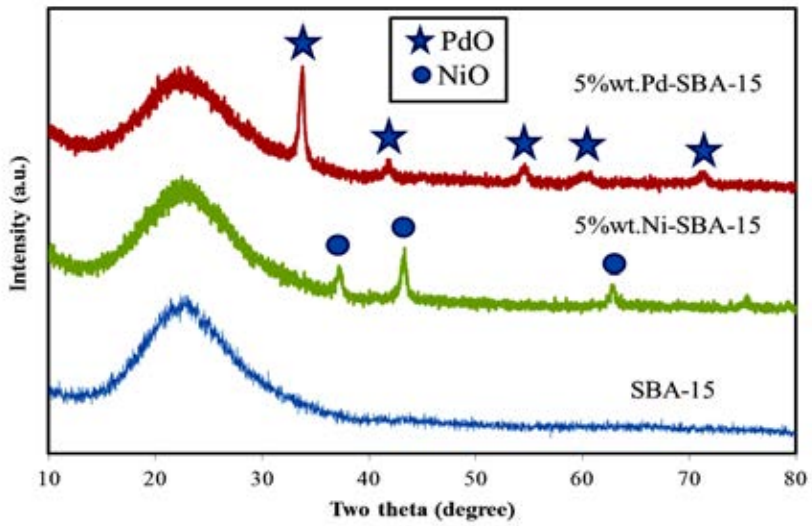

Figure 4.13 XRD patterns of pure SBA-15, Ni-SBA-15 and Pd-SBA-15 at wide angle range 10-80°.

4.2.3.2 Nitrogen adsorption-desorption

The N_2 adsorption-desorption isotherms of the Ni-SBA-15 and the Pd-SBA-15 were shown in Figure 4.14. Both samples exhibited N_2 sorption isotherms of type IV which were the characteristic of mesoporous material. After impregnation, the adsorption-desorption isotherms of the Ni-SBA-15 and the Pd-SBA-15 were similar to the SBA-15 parent. Moreover, the uniform pore structure of the Ni-SBA-15 and the Pd-SBA-15 were maintained.

The specific surface area was calculated using BET method, and the mesopore volume and pore size distribution were calculated using BJH method. The physical properties and pore size distributions were showed in Table 3.4 and in Figure 3.15 respectively. The total specific surface areas and pore volumes of the Ni-SBA-15 and the Pd-SBA-15 were decreased when compared with SBA-15 parent because of metal loading into the surface area and pore channels [76]. However, the narrow pore size distributions of Ni and Pd metals on SBA-15 supported exhibited 8.06 nm similar to SBA-15 parent. In addition, it was observed that the wall thickness was decreased with metal loading into SBA-15 due to the shrinkage during recalcination process.

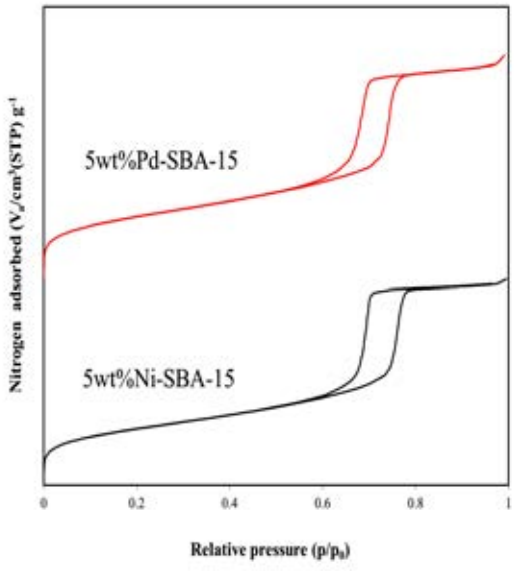

Figure 4.14 Nitrogen adsorption-desorption isotherms of metal on supported SBA-15.

Table 4.4 Physical properties of the Ni-SBA-15 and the Pd-SBA-15

Sample	Total specific Surface Area (m^2/g)[a]	Mesopore volume (cm^3/g)[b]	Pore size distribution (nm)[b]	$d_{(100)}$[c] (nm)	Wall thickness[d] (nm)
SBA-15	847.07	1.0628	8.06	10.26	3.79
Ni-SBA-15	509.67	0.8673	8.06	9.27	2.64
Pd-SBA-15	653.62	0.9499	8.06	9.67	3.11

[a] Determined by BET method,

[b] Determined by BJH-plot method,

[c] Determined by XRD, Jade 5.6,

[d] Determined as: a_0-pore size ($a_0 = 2 \times d_{(100)} / \sqrt{3}$)

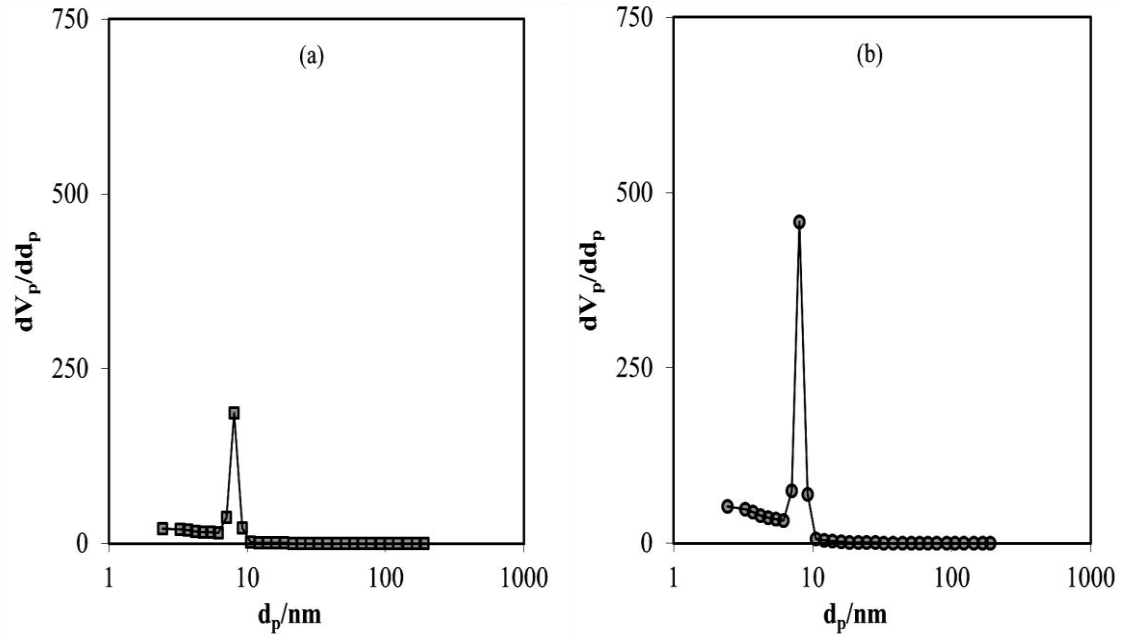

Figure 4.15 Pore size distributions of (a) the Ni-SBA-15 and (b) the Pd-SBA-15.

4.2.3.3 Scanning electron microscope (SEM)

The SEM morphology images of the Ni-SBA-15 and the Pd-SBA-15 samples were showed in Figure 4.16. Both samples performed some small rod particles that were broken from SBA-15. From SEM image of the Ni-SBA-15 was performed fiber-liked bundled. The SEM image, the Pd-SBA-15 was revealed small rod aggregated particles in size about 1.2 × 1.5 μm, and was observed that the Pd metals were deposited on the surface of SBA-15.

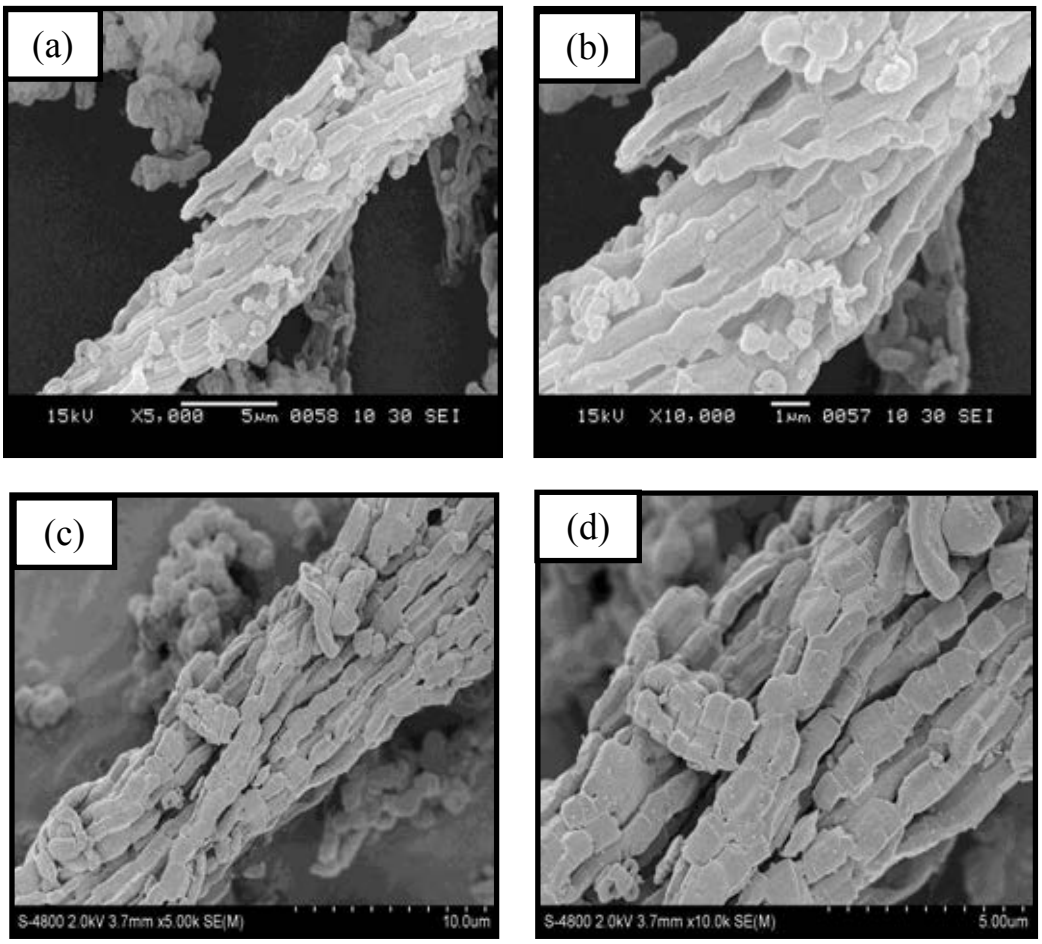

Figure 4.16 SEM images of (a), (b) the Ni-SBA-15 and (c), (d) the Pd-SBA-15 at 5,000 and 10,000 magnifications.

4.2.3.4 Transmission electron microscope (TEM)

The TEM images of the Ni-SBA-15 and the Pd-SBA-15 were showed in Figure 4.17. For both samples clearly observed hexagonal array of uniform mesopore channels. The TEM images presented the agglomeration of Ni and Pd metallic particles in size about 55 and 30 nm, respectively on the structure of SBA-15. The TEM images indicated that the metallic particles where placing outside the channels of the SBA-15, as their metallic particle size larger than the pore size of SBA-15 (estimated by the BJH method to be 8.06 nm.) [77].

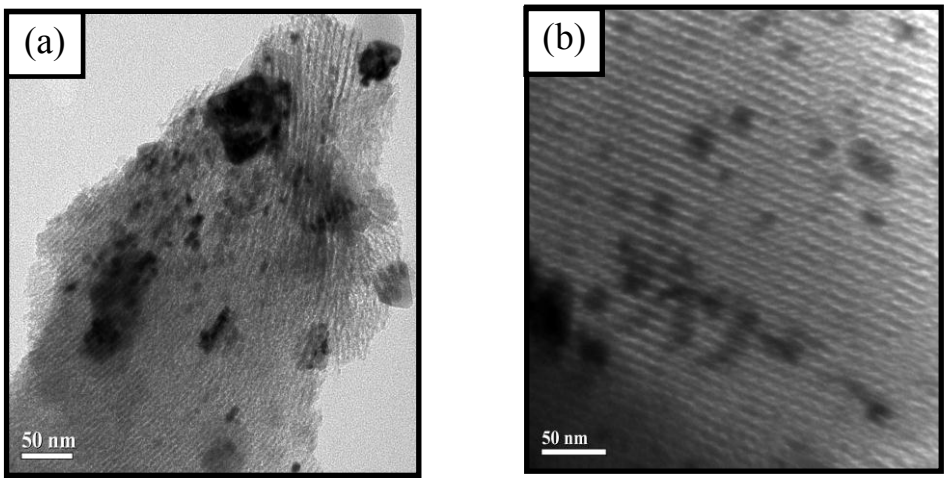

Figure 4.17 TEM images of (a) Ni-SBA-15 and (b) Pd-SBA-15.

4.2.4 Impregnation of metal on supported beta zeolite (Ni-BEA and Pd-BEA)

4.2.4.1 Powder x-ray diffraction (XRD)

The metal supported on commercial beta zeolite, which SiO_2/Al_2O_3 ratios of 30, was prepared by impregnation method following Tunyatorn [62] The commercial beta zeolite and metal supported on commercial beta zeolite were denoted as HBEA and M-BEA (M = Ni, Pd), respectively. The XRD patterns of Ni-BEA and Pd-BEA were exhibited main intensity peak maintained similar to starting HBEA. From Figure 4.18 showed the XRD patterns of HBEA, the Ni-BEA and the Pd-BEA. The diffraction peak at 7.5° and 22.4° were indicated to the characteristic diffraction peak of (101) and (302), respectively, suggesting the high crystallinity of the beta zeolite still remained in both metal BEA samples [78].

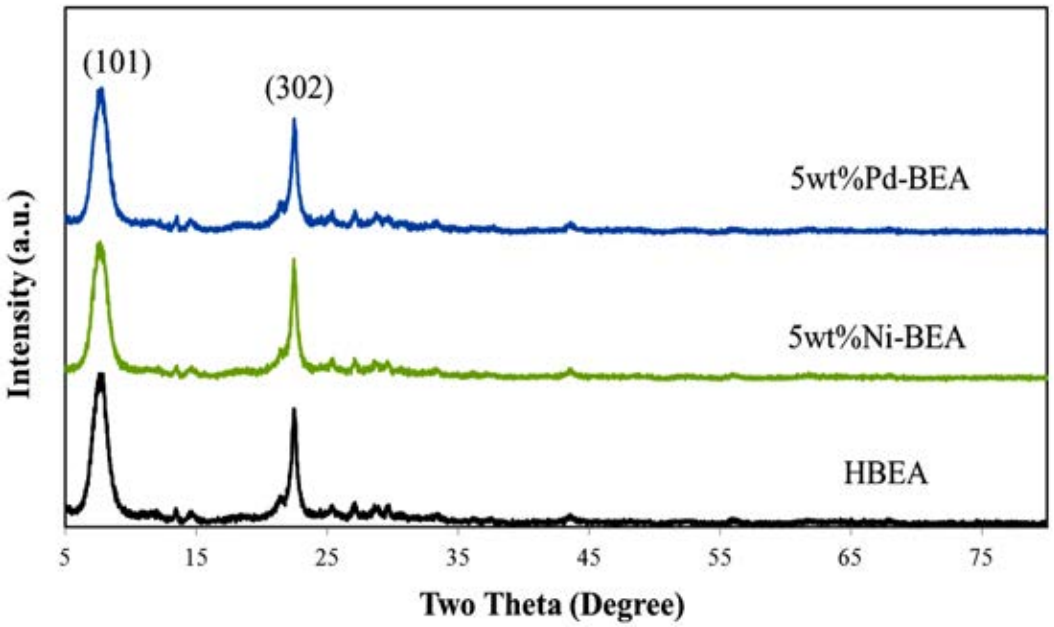

Figure 4.18 XRD patterns of calcined (a) HBEA, Ni-BEA and Pd-BEA.

4.2.4.2 Nitrogen adsorption-desorption

Figure 4.19 and Figure 4.20 showed the N_2 adsorption-desorption isotherm and pore size distribution of HBEA, the Ni-BEA and the Pd-BEA. The adsorption-desorption isotherms presented a type I isotherm which were characteristic pattern of microporous material with the hysteresis loop between relative intensity 0.4 to 0.9. The physical properties of all samples were showed in Table 4.5

The specific surface area, external surface area and micropore volume of Ni-BEA and Pd-BEA were reduced. The blockage and narrowing of some pores due to the metal loading [79, 80].

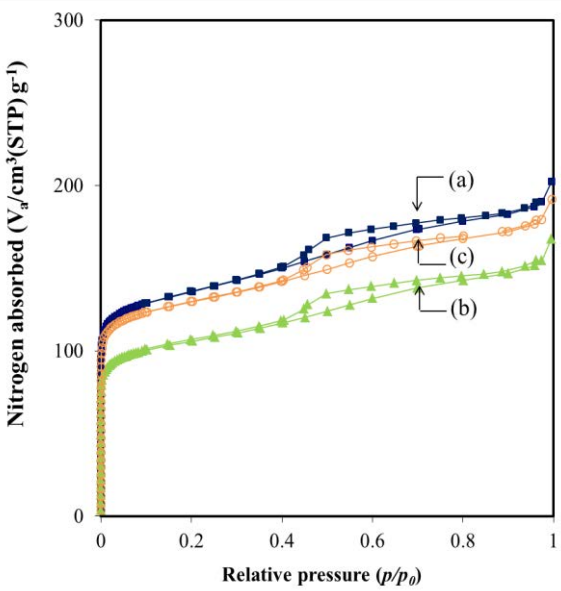

Figure 4.19 Nitrogen adsorption-desorption isotherms of (a) HBEA, (b) Ni-BEA and (c) Pd-BEA.

Table 4.5 Physical properties of the calcined HBEA, the Ni-BEA and the Pd-BEA

Sample	Specific Surface Area (m^2/g)[a]	External Surface Area (m^2/g)[b]	Micropore volume (cm^3/g)[c]	Pore size Distribution (nm)[c]
HBEA	498.42	188.89	0.267	0.6
Ni-BEA	394.23	136.03	0.208	0.6
Pd-BEA	475.34	160.20	0.249	0.6

[a] Determined by BET method

[b] Determined by *t*-method

[c] Determined by MP method

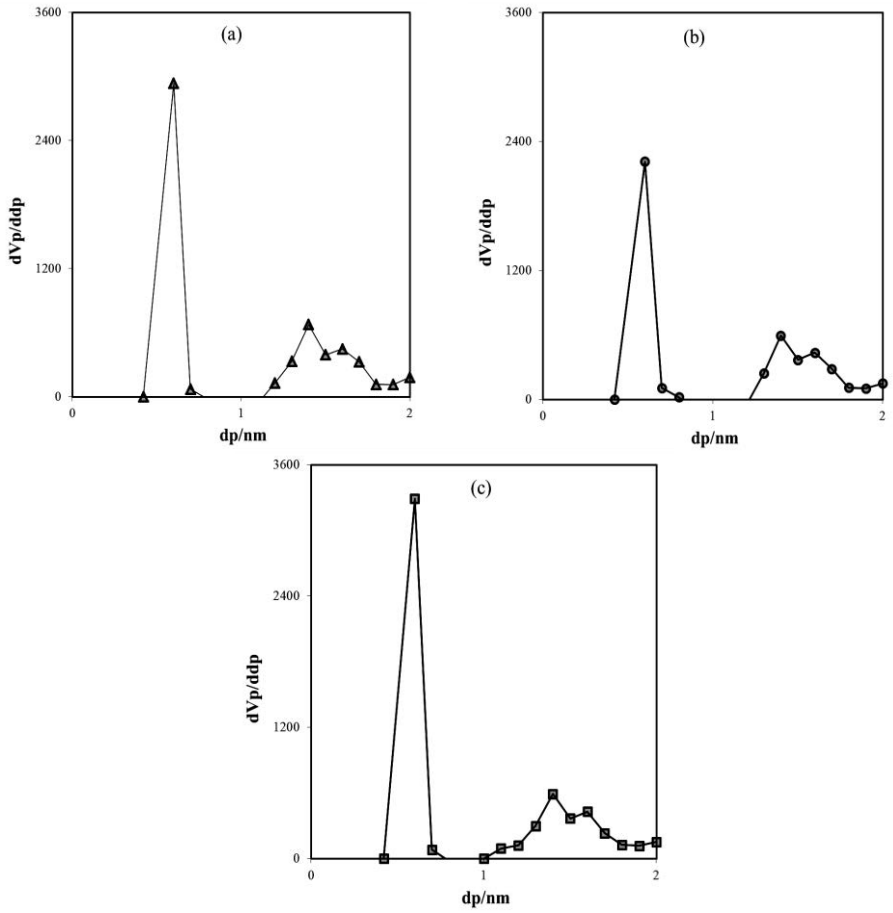

Figure 4.20 Pore size distributions of (a) HBEA, (b) Ni-BEA and (c) Pd-BEA from MP-plot

4.2.4.3 Scanning electron microscope (SEM)

The morphology of HBEA, Ni-BEA and Pd-BEA were showed in Figure 4.21. All samples presented a round granular to form cauliflower agglomeration and the surface was very rouge. In SEM-EDX method measured the amount of the Ni and the Pd metal loading in HBEA describing as only 0.32 and 0.35%, respectively. The results from SEM-EDX showed metal amount much lower than the amount of metal in solution loading (5 wt%) because some parts of metal still remained in solution.

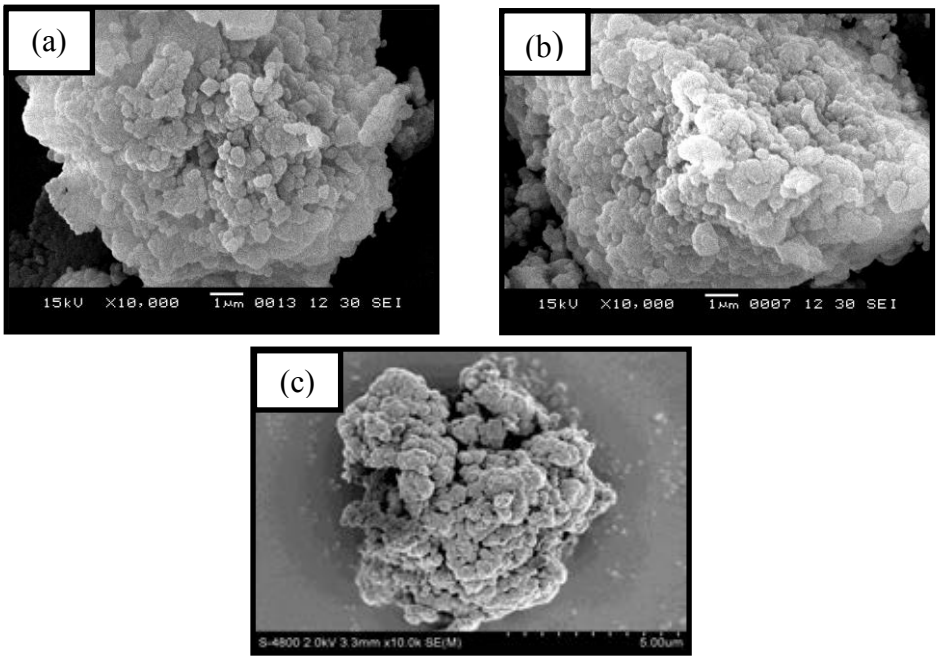

Figure 4.21 SEM images of (a) HBEA, (b) Ni-BEA and (c) Pd-BEA.

4.2.4.4 Transmission electron microscope (TEM)

All TEM images of HBEA, the Ni-BEA and the Pd-BEA were showed in Figure 4.22. The TEM image of the Ni-BEA presented unclear metallic particles on HBEA surface. On the other hand, the TEM image of the Pd-BEA were showed the small metallic particles in sizes about 8-20 nm and the Pd metal particles presented pleasing dispersion over the HBEA surface.

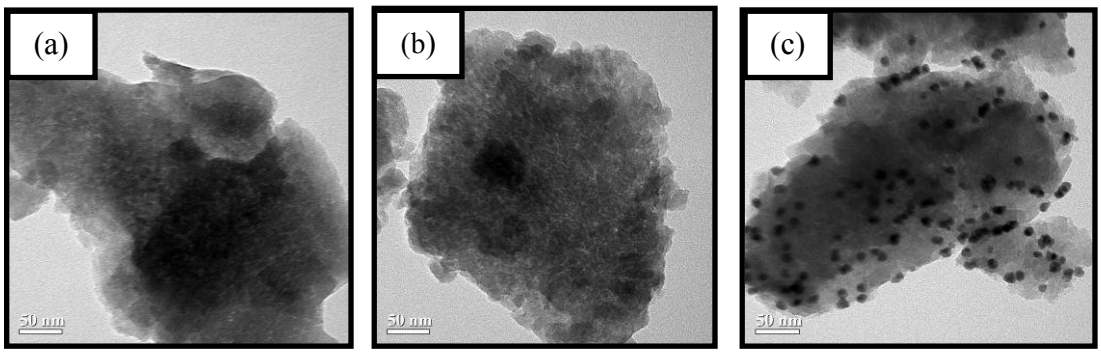

F**igure 4.22** TEM images of (a) HBEA, (b) Ni-BEA and (c) Pd-BEA.

4.3 Catalytic pyrolysis of corncob

In aim of the research was studied the thermal and catalytic pyrolysis of agricultural waste as corncob. The operation worked in the presence of pure SBA-15, Al-SBA-15 with different SiO_2/Al_2O_3 mole ratios and impregnated of metal on supported catalyst. The pyrolysis of corncob was determined the effect of temperature, catalyst type, corncob to catalyst mole ratio.

4.3.1 Effect of reaction temperature

The pyrolysis temperature was a significant parameter that affected the composition of gases and volatile compounds. This research was investigated influence of pyrolysis temperature on product yield which obtained from thermal pyrolysis at 250, 300, 400, 500 and 600°C. The results of thermal corncob pyrolysis at various reaction temperatures were shown in Table 4.6 and Figure 4.23. The value of %conversion was continually increased from 33.20% to 65.40% when reaction temperature was raised from 250 to 600°C. Furthermore, the liquid fraction obtained from pyrolysis of corncob was dark brown liquid with smoky odor. The liquid fraction was separated into two fractions; distillated liquid and heavy liquid (non distillated product). The distillated liquid and the heavy liquid were increased with the increasing of temperature from 11.25% - 26.35% and 7.04% - 12.87%, respectively. In addition, at low temperature 250°C, the volatile composition decomposed to gases and liquid products whereas the residue yield was found high as 66.8% due to incomplete combustion of corncob. At higher temperature 300-600°C, the long-chained compounds were cracked into smaller compounds and converted into the light gases and liquid compounds from 21.60%- 26.60% and 29.07%–38.80%, respectively while the residue yield was decreased as 34.6%.

Table 4.6 Thermal pyrolysis of corncob at various reaction temperatures

	Reaction temperature (°C)				
	250	**300**	**400**	**500**	**600**
%conversion*	33.20	50.13	57.80	61.80	65.40
%yield of product*					
1. Gas	14.87	21.07	24.70	25.00	26.60
2. Liquid	18.33	29.07	33.10	36.80	38.80
Distillated liquid	11.29	20.58	22.69	26.35	25.93
Heavy liquid	7.04	8.49	10.41	10.46	12.87
3. Residue	66.80	49.87	42.20	38.20	34.60
Liquid fraction density (g/cm^3)	0.916	0.973	0.983	0.927	0.944

Condition: reaction time for 40 min, 5 g corncob and N_2 flow 20 cm^3/min.

*Deviation within ±0.50 for conversion, ±0.70 for yield of gas fraction, ±0.90 for yield of liquid fraction, and ±0.50 for yield of residue.

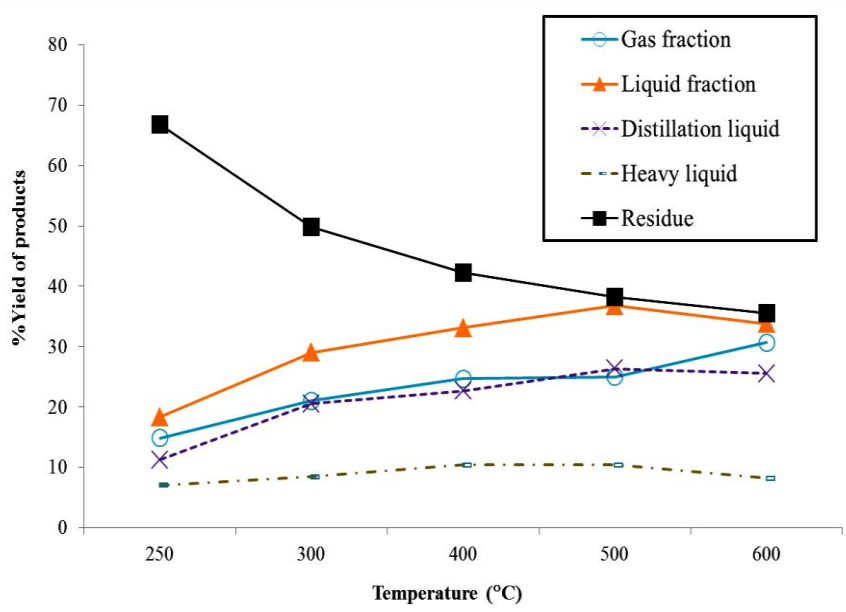

Figure 4.23 %Yield of products from thermal pyrolysis of corncob at different reaction temperatures.

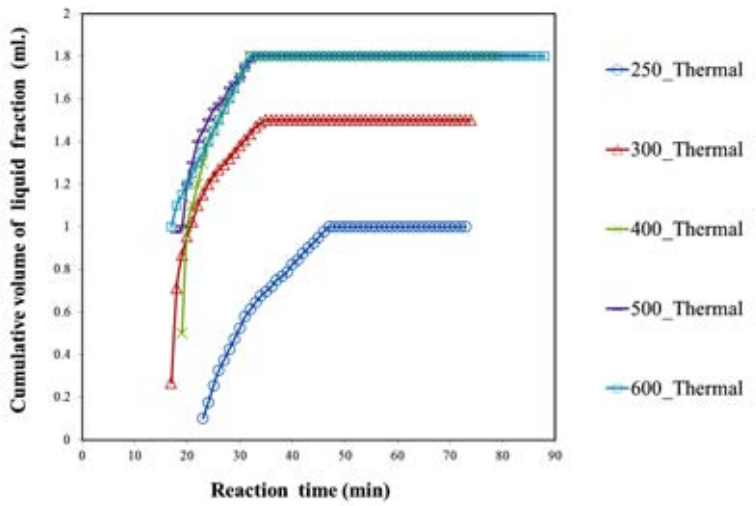

Figure 4.24 Cumulative volume of liquid fraction obtained by thermal pyrolysis of corncob at different reaction temperatures.

Figure 4.24 showed the relationship between the cumulative volume of liquid fractions with time obtained by thermal pyrolysis of corncob at temperature of 250 - 600°C. When the temperature was increased, the total volume of liquid fractions was in order: 250°C < 300°C < 400°C < 500°C < 600°C.

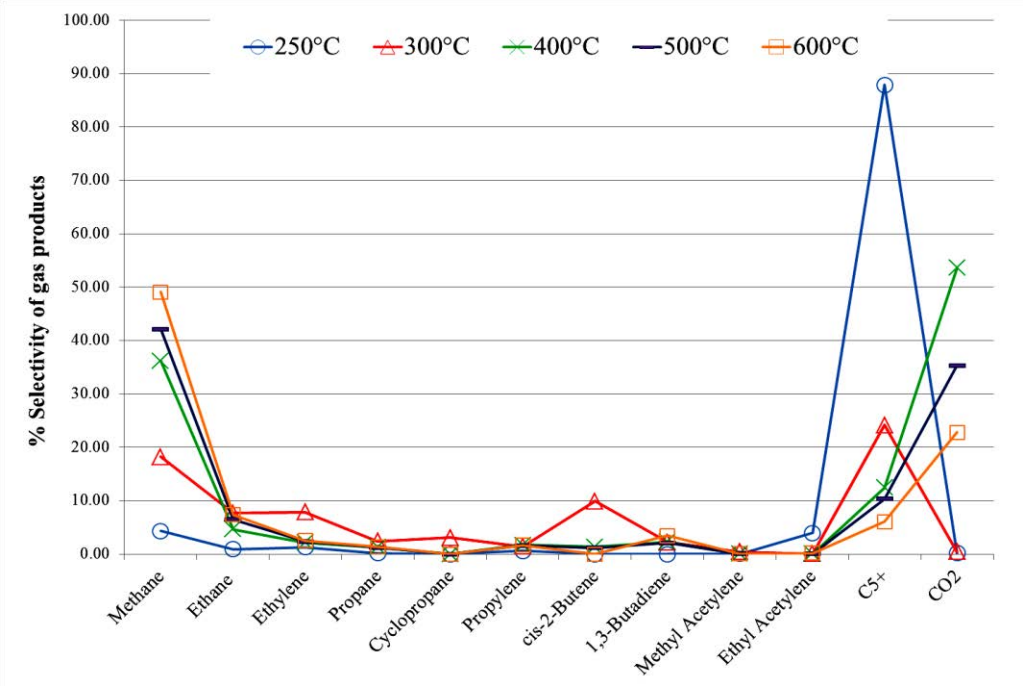

Figure 4.25 Distribution of gas fraction obtained by thermal pyrolysis of corncob at different temperature.

Figure 4.25 showed the gas distributions obtained by thermal pyrolysis of corncob at 250, 300, 400, 500 and 600°C. The major components for thermal pyrolysis of corncob were included methane, C_5^+ and CO_2 whereas C_2-C_4 gases were minor components. When the reaction temperature increased, the gas fraction of lighter hydrocarbon (especially methane) increased, while that of C_5^+ (higher boiling point than that of *n*-pentane) decreased. In addition, it was observed that high temperature (400-600°C) lead to a high percentage of carbon oxides about 22.81-53.59% in the pyrolysis gas products. Hydrogen could not be detected due to the strong dilution with nitrogen flow gas.

The GC/MS analysis was used to determine the distillated liquid product in pyrolysis of corncob which composed of volatile compounds and nonvolatile oligomers. The identification of the product peaks was based on computer matching of the mass spectra with the National Institute of Standards and Technology (NIST) library and the literature research of previous studies [81]. More than 30 product peaks were displayed on the ion chromatograms which the ion chromatograms of the distillated liquid from pyrolysis of corncob were exhibited in Appendices. Some important pyrolysis products of the corncob were listed in Table 4.7. The result of composition in distillated liquid was presented in the mean values of percentage area of the chromatographic peaks. For this experiment was repeated at least three times to confirm the data of the procedure. The GC-MS technique could not give the direct quantitative analysis of the compounds due to the very complex of products and the lack of the commercially available chemical standards. The chromatographic peak area of products was depended on quantity of each chemical. Thus, the corresponding peak areas of products in different chromatograms were compared to reveal the changing yield and selectivity to show the difference of relative content among the detected products [82].

Table 4.7 Compounds identified by GC/MS in the thermal pyrolysis of corncob.

	Retention Time	**Compound Name**	**Formula**	**Molecular Weight**
1	2.27	2-Methyl-butyl propanoic acid ester	$C_8H_{16}O_2$	144
2	2.47	4-Ethyl-phenol	$C_8H_{10}O$	122
3	2.64	4-Ethyl-2-methoxy-phenol	$C_9H_{12}O_2$	152
4	2.96	1-(2-Ethoxyphenyl) acetone	$C_{11}H_{14}O_2$	178
5	3.04	2-Methoxy-4-propyl-phenol	$C_{10}H_{14}O_2$	166
6	4.57	1,2-di-2-Furanyl-2-hydroxy-ethanone	$C_{10}H_8O_4$	192
7	4.93	3-Hydroperoxy-3-hydroxybutan-2-one	$C_4H_8O_4$	120
8	5.35	2-Acetyl-5-methylfuran	$C_7H_8O_2$	124
9	6.98	1-Methoxy-2-propanol	$C_4H_{10}O_2$	90
10	9.65	2-Methoxy phenyl acetate	$C_9H_{10}O_3$	166
11	9.79	2-Methoxy-4-methy phenol	$C_8H_{10}O_2$	138
12	12.56	3-Furaldehyde	$C_5H_4O_2$	96
13	12.85	Hexanoic acid, propyl ester	$C_9H_{18}O_6$	158
14	14.72	3-Hydroxy-2-Butanone	$C_4H_8O_2$	88
15	15.26	3,5-bis-(1,1-Dimethylethyl)-phenol	$C_{14}H_{22}O$	206
16	16.21	3,5-Dimethyl-cyclohexanol	$C_8H_{16}O$	128
17	22.34	Mint furanone	$C_{10}H_{14}O_2$	166
18	23.19	5-Methyl-2-furancarboxaldehyde	C_6H6O_2	110
19	23.56	Furyl hydroxymethyl ketone	$C_6H_6O_3$	126
20	25.86	2,2,4,4-Tetramethyl-3-pentanone	$C_9H_{18}O$	142
21	26.36	Phenol	C_6H_6O	94
22	27.31	3-Ethyl-2-hydroxy-2-cyclopentene-1-one	$C_7H_{10}O_2$	126

23	28.62	2-Furanmethanol, acetate	$C_7H_8O_3$	140
24	28.90	2,5-Dihydroxypropiophenone	$C_9H_{10}O_3$	166
25	29.02	Diethoxymethyl acetate	$C_7H_{14}O_4$	162
26	31.06	1-(3-Methoxyphenyl)-ethanone	$C_9H_{10}O_2$	150
27	31.30	4-Hydroxy-2-butanone	$C_4H_8O_2$	88
28	31.58	Formic acid	CH_2O_2	46
29	32.74	3-Furanmetanol	$C_5H_6O_2$	98
30	36.13	1-Hydroxy-2-propanone	$C_3H_6O_2$	74

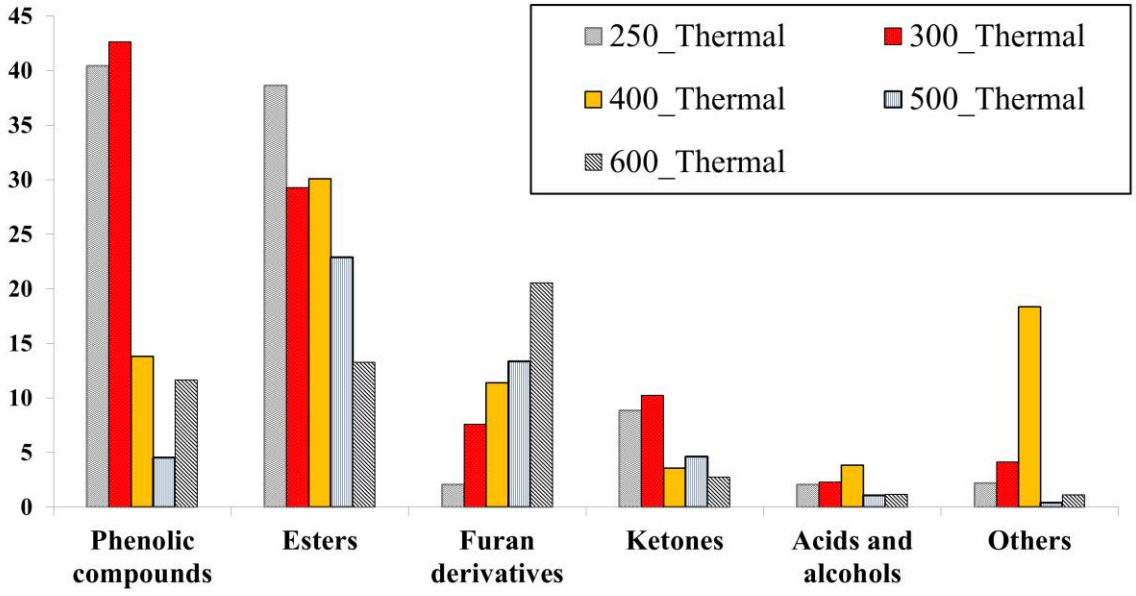

Figure 4.26 Total %selectivity based on peak area of the distillate liquid products obtained by thermal pyrolysis of corncob at different reaction temperature.

The total %selectivity based on peak area of different functional groups in the distillated oil products obtained by thermal pyrolysis of corncob at temperature 250 - 600°C was showed in Figure 4.26. All the compounds were classified into six functional groups including acids and alcohols, furan derivatives, phenolic compounds, light ketones, light esters and others. The increasing of temperature, the furan derivatives groups were increased in about 2.10-20.57% whereas the phenolic

compounds, light esters and light ketones were decreased in about 4.55-42.60%, 13.26-38.61% and 2.76-10.27%, respectively.

The composition of corncob consists of cellulose and hemicellulose (53.40%), and lignin (18.20%). These components were decomposed to volatile compounds and converted to the distillated liquid products at different temperature with corresponding to the thermal stability of corncob in TGA result. The thermal stability of corncob divided into two steps. The first step hemicelluloses and cellulose decomposed at reaction temperature 300-450°C and the second step, heavy volatile and lignin decomposed at higher reaction temperature around 500-900°C. On the other hand, when temperature was increased, the phenolic compounds and the ester compounds were decreased while the furan derivatives were increased. It indicated that product in phenolic and ester group might be converted to high yield of furan derivatives group.

4.3.2 Effect of catalytic type

The corncob biomass was degraded over various catalysts which divided into three groups consist of microporous materials (HBEA with SiO_2/Al_2O_3 was 30), mesoporous materials (SBA-15 and Al-SBA-15 with SiO_2/Al_2O_3 mole ratios were 20, 30 and 60) and metal (Ni and Pd) loading on supported SBA-15 and HBEA. The catalytic pyrolysis was compared with thermal pyrolysis at reaction temperature 300°C for 40 min, heating rate 20°C/min, 10wt% of catalyst to corncob. Table 4.8 showed the values of %conversion and product yield for thermal and catalytic pyrolysis of corncob over the various catalysts.

The values of %conversion in the catalytic pyrolysis of corncob over microporous materials i.e. HBEA, the Ni-BEA and the Pd-BEA catalyst was about 50.93%, 50.70% and 49.90%, respectively. The %conversion values were no significant difference when compared with thermal pyrolysis (50.13%). After metal loading on HBEA supported, the gas yield of the Pd-BEA and the Ni-BEA were decreased to 19.20% and 21.30%, respectively with corresponded to the decreasing of external surface of catalysts. When compared with HBEA catalyst, the external surface of the HBEA was higher than the Ni-BEA and the Pd-BEA related to the primary cracking of the large molecules can be occurred on the external surface of

the HBEA and diffused into the pores. The pyrolysis vapors could be secondary cracking in the catalytic pores which the obtained gas yield was increased [83]. In addition, the %yield of liquid was increased when using metal supported HBEA. Pd-BEA provided the specific surface area and micropore volume were higher than the Ni-BEA and the HBEA. Thus, the Pd-BEA produced the highest liquid yield was about 30.70%, especially, the yield of distillated liquid fraction was high as 24.12%.

Considering the mesoporous material SBA-15, the %conversion value of the catalytic pyrolysis was increased in the range 44.50%-51.90% depending on the amount of aluminum in SBA-15. The %conversion and liquid fraction yield of the Al-SBA-15(20) were found highest as 51.90% and 31.90%, respectively. However, the Al-SBA-15 with low SiO_2/Al_2O_3 mole ratio (higher acidity) was showed a positive effect on liquid yield whereas high SiO_2/Al_2O_3 mole ratio (lower acidity) led to deactivation of catalyst by coke formation. In addition, after incorporated Al into SBA-15, the residue was decreased because heavy molecules of residue could be cracked to light volatile compounds.

Furthermore, for Ni and Pd loaded into supported SBA-15, the %conversion was around 5% higher than pure SBA-15. The gas yield of the Ni-SBA-15 and the Pd-SBA-15 reactions were comparable whereas the liquid yield was increased, especially, the yield of distillated liquid was high as 25.42% in case of the Pd-SBA15 catalyst because Pd-SBA-15 provided acidity and specific surface area higher than the Ni-SBA-15 and SBA-15.

A possible catalytic process was proposed corresponding with the conversion and the product yields shown in Figure 4.27. The product yield would be influenced by catalyst in the following two steps: the primary pyrolysis process, the catalyst would cause the cracking of biomass to gases, water, primary organic vapors and char via thermal pyrolysis (step1). This process temperature was the most important parameter affected to the distribution of product yields. During the catalytic reactions, some of primary organic vapors polymerized directly to form tar and coke (step 3) and induce to the deactivation of catalyst. On the other hand, the catalyst would promote the cracking of primary organic vapors and cracked on active surface of the catalyst which produced light vapors (step 2). The light vapors were undergo reactions such as deoxygenation, cracking, dehydration, decarboxylation or

decarbonylation to form oxygenated compound with different functional groups which increased the volatile (step 4). The oxygenated compounds might also undergo polymerization to form coke (step 5) [83].

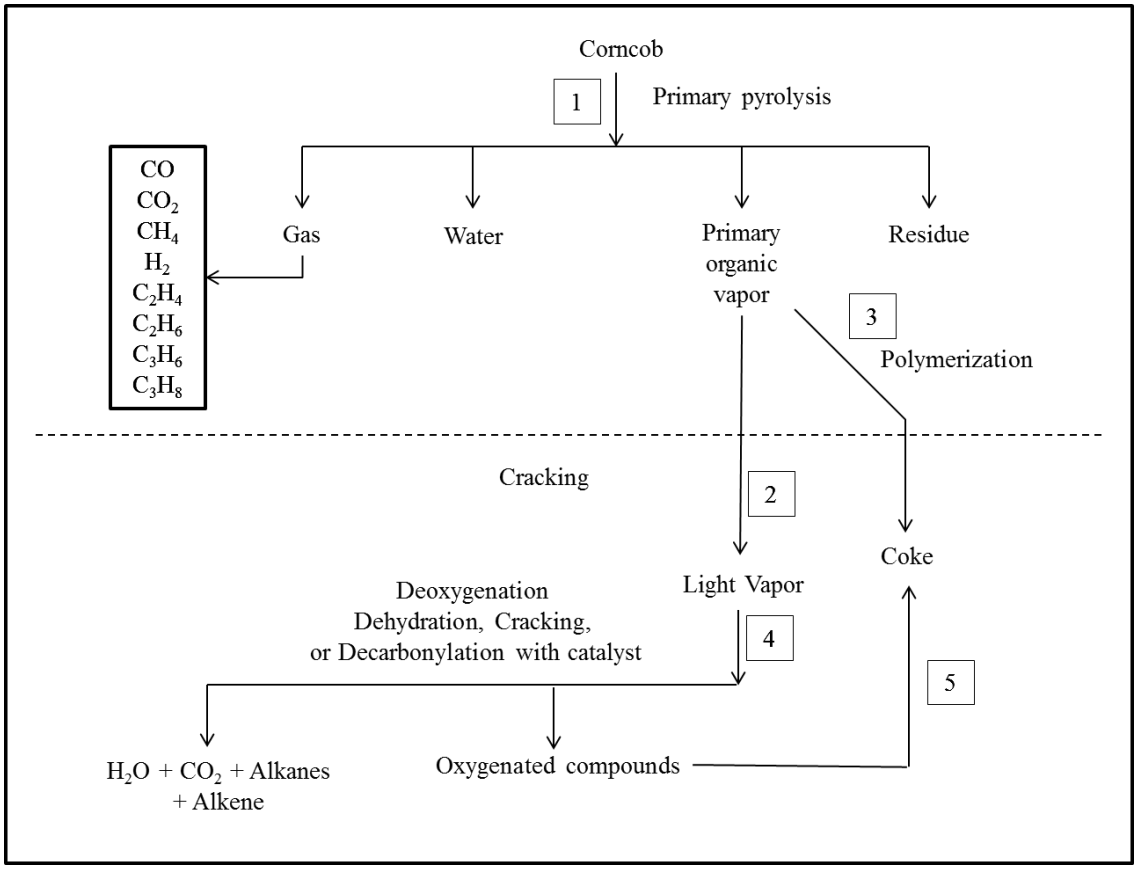

Figure 4.27 Thermal and catalytic process of corncob pyrolysis [18].

Table 4.8 Thermal and catalytic pyrolysis of corncob at 300°C

	Thermal	HBEA	Ni-BEA	Pd-BEA	SBA-15	Al-SBA-15 (60)	Al-SBA-15 (30)	Al-SBA-15 (20)	Ni-SBA-15	Pd-SBA-15
BET surface area (m^2/g)	-	501.60	371.01	538.99	847.07	423.17	408.33	357.60	509.67	653.62
Pore size distribution (nm)	-	0.6	0.6	0.6	8.06	8.06	8.06	8.06	8.06	8.06
External surface area (m^2/g)	-	40.27	14.53	21.55	-	-	-	-	-	-
Pore volume (cm^3/g)	-	0.237	0.209	0.280	1.063	0.865	0.797	0.664	0.867	0.949
%conversion*	50.13	50.93	50.70	49.90	44.50	47.00	50.30	51.90	50.90	50.10
1. % Yields of gas product	21.07	22.67	21.30	19.20	20.00	18.90	19.00	20.00	20.60	18.10
2. %Yield of liquid product	29.07	28.27	29.40	30.70	24.50	28.10	31.30	31.90	30.30	32.00
- %Yield of distillated liquid	20.58	22.43	20.38	24.12	19.04	22.73	24.26	25.15	18.69	25.42
- %Yield of Heavy liquid	8.49	5.84	9.02	6.58	5.46	5.37	7.04	6.75	11.61	6.58
3. %Yield of residue	49.87	49.07	49.30	50.10	55.50	53.00	49.70	48.10	49.10	49.90

Condition: reaction temperature of 300°C, reaction time for 40 min, 5 g corncob, 10wt% of catalyst to corncob and N_2 flow 20 cm^3/min.

*Deviation within ±0.50 for conversion, ±0.70 for yield of gas fraction, ±0.90 for yield of liquid fraction, and ±0.50 for yield of residue.

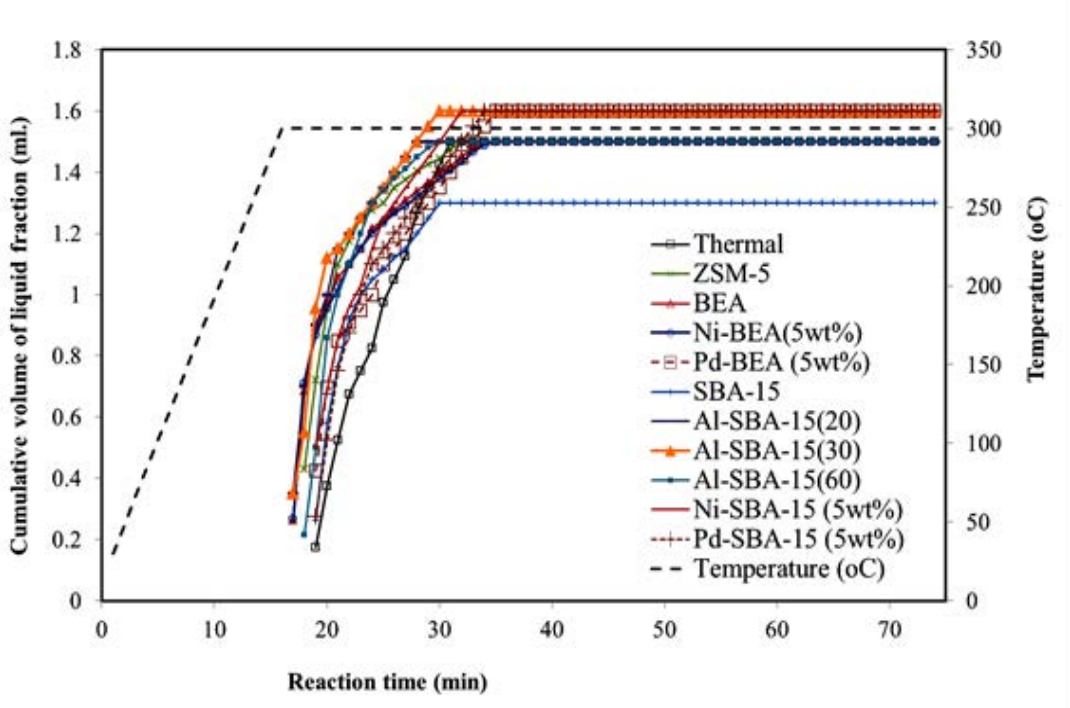

Figure 4.28 Cumulative volume of liquid fraction obtained by thermal and catalytic pyrolysis of corncob over various catalysts.

Figure 4.28 showed the relationship between the cumulative volume of liquid fractions with time obtained by thermal and catalytic pyrolysis of corncob at temperature 300°C. This plot accounts for the kinetic rate of the liquid formation. The amounts of liquid in the cylinder from catalytic pyrolysis were nearly equal to thermal pyrolysis. The initial rates of all catalytic processes were higher than thermal pyrolysis except for SBA-15 catalyst showed lower amount of liquid product than other reactions.

4.3.2.1 Catalytic effect on the distribution of gas products

Figure 4.29 showed the gas distributions obtained by thermal and catalytic pyrolysis of corncob over HBEA, the Ni-BEA and the Pd-BEA at 300°C. The mainly gas components of catalytic pyrolysis of corncob over HBEA similarly thermal pyrolysis were included methane, C_5^+ and CO_2 whereas C_2-C_4 gases were minor components. In three HBEA catalysts, the amounts of light hydrocarbon gas product were decreased whereas that of C_5^+ was increased when compared with thermal pyrolysis. In addition, it was observed that the Ni-BEA catalyst lead to a highest percentage of C_5^+ and CO_2 about 67.67% and 31.60%, respectively.

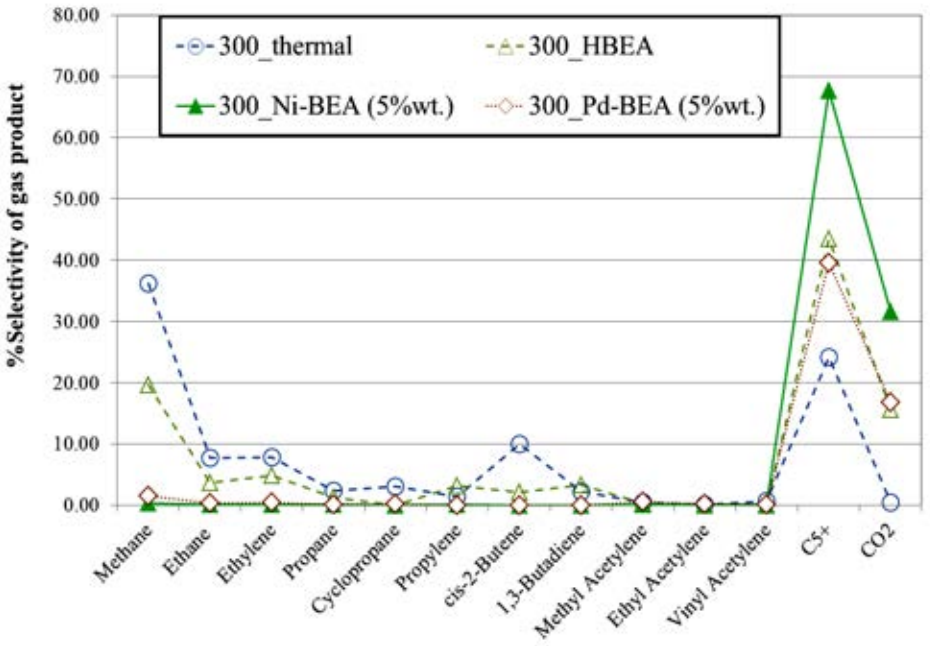

Figure 4.29 Distribution of gas product obtained by thermal and catalytic pyrolysis of corncob over HBEA, Ni-BEA and Pd-BEA at 300°C.

Distribution of gas products in catalytic pyrolysis over SBA-15, Al-SBA-15 and metal-SBA-15 were shown in Figure 4.30. All catalysts gave low amount of light hydrocarbon gases such as methane and C_2-C_4 whereas the C_5^+ was highest gas yield as 77.73% in case of the Al-SBA-15(20). Moreover, the high %yield of CO_2 gas was obtained from catalytic pyrolysis over the Ni-SBA-15 about 56.07%.

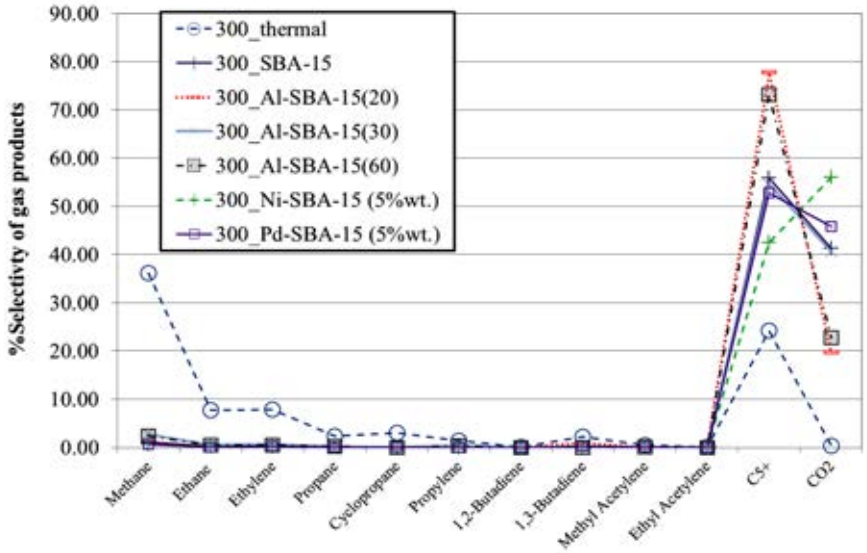

Figure 4.30 Distribution of gas fraction obtained by thermal and catalytic pyrolysis of corncob over SBA-15, Al-SBA-15 with SiO_2/Al_2O_3 mole ratios were 20, 30 and 60) and Ni-SBA-15, Pd-SBA-15 at 300°C.

4.3.2.2 Catalytic effect on the distribution of the distillated liquid products

Figure 4.31 showed summary of total %selectivity based on peak area of different functional groups of the distillated liquid oil obtained by thermal and catalytic corncob pyrolysis over catalysts at 300°C. After catalytic pyrolysis, mainly functional group of liquid product consisted of the light ester group and the phenolic compounds in range 11.93-60.31% and 4.46-19.52%, respectively. In all catalytic pyrolysis products, the phenolic compounds were mainly derived from decomposition of lignin whereas the furan derivatives and other products were mainly derived from hemicellulose and cellulose [84]. However, the phenolic compounds and furan derivatives were decreased whereas the light ester compounds were increased when compared with thermal pyrolysis. This result might be caused by the phenolic compounds and furan derivatives group were converted to light ester compounds.

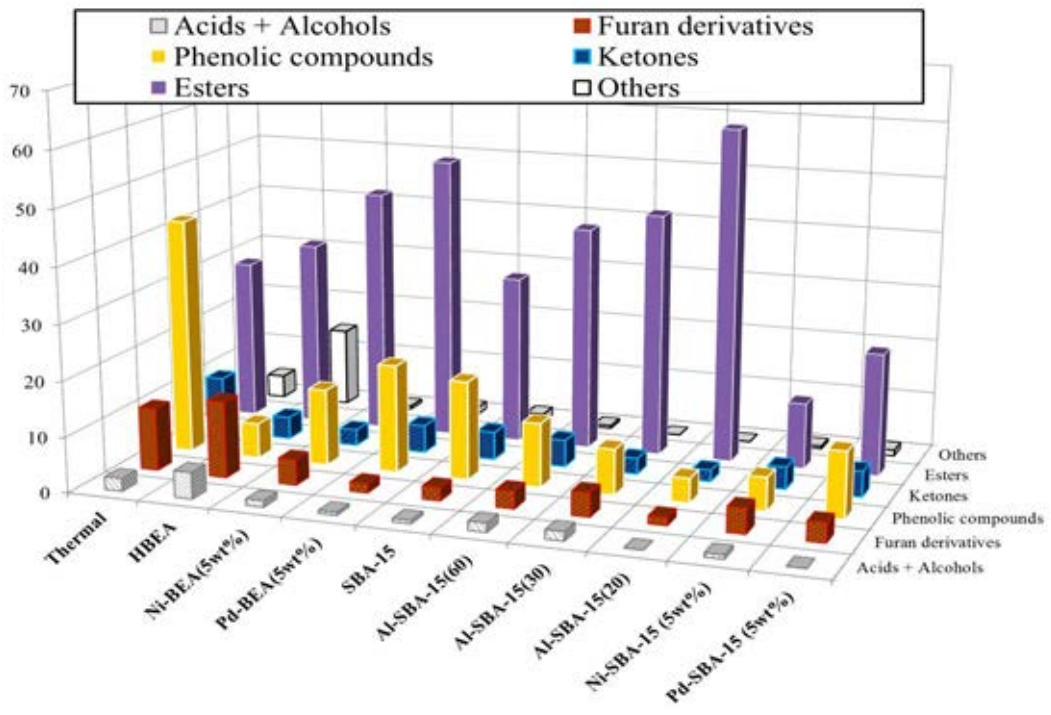

Figure 4.31 The summary of total %selectivity based on peak area of different functional groups in the distillated liquid oil obtained by thermal and catalytic pyrolysis of corncob over various catalysts at 300°C.

4.3.2.3 Catalytic effect on the ester group in the distillated liquid

During pyrolysis, the mainly composition of biomass including cellulose, hemicellulose and lignin were decomposed and formed to light ester group. The major products in light ester group such as 2-methyl-butyl propanoic acid ester (no.1) and 2-methoxy phenyl acetate (no.10) were given in Figure 4.32. After catalytic reaction, 1-methyl-butyl propanoic acid ester (no.1) was degraded from xylose (C5-sugar) which derived the decomposition of hemicellulose and cellulose whereas 2-methoxy phenyl acetate (no.10) was degraded from phenolic compounds which derived the decomposition from lignin [85]. The Al-SBA-15(60) and the Pd-BEA gave high amount of 2-methyl-butyl propanoic acid ester (no.1). While Al-SBA-15(20) were exhibited given highest amount of 2-methoxy-phenyl acetate (no.10) compared with other reactions. The 2-methoxy-phenyl acetate (no.10) was important most important intermediate chemical for sweet odor in food and beverage industry.

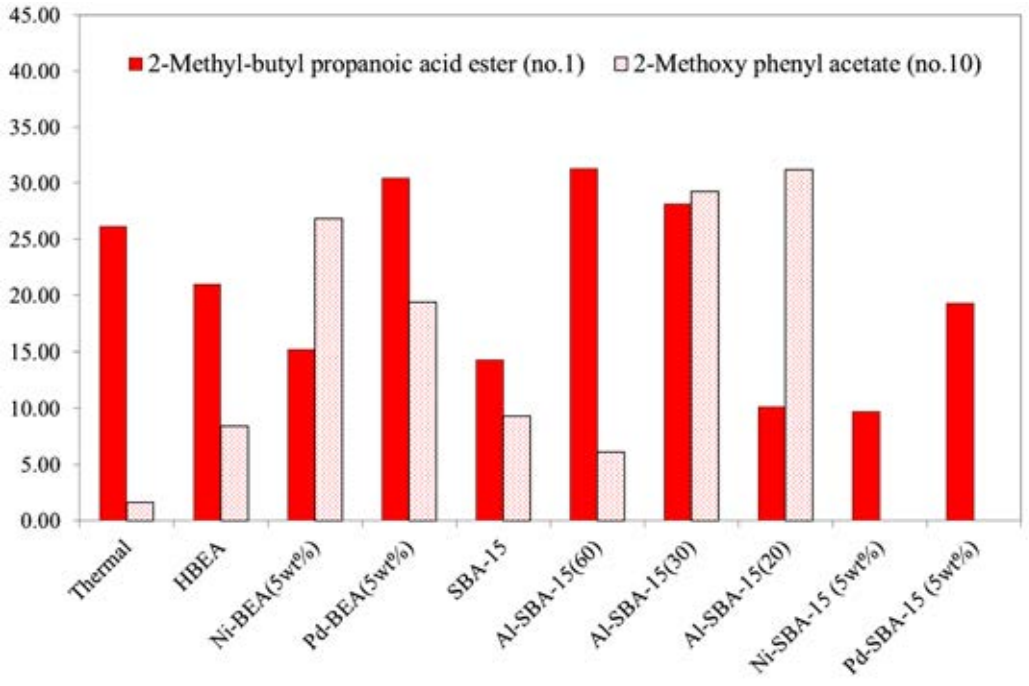

Figure 4.32 %Selectivity based on peak area of 2-methyl-butyl propanoic acid ester (no.1) and 2-methoxy phenyl acetate (no.10) in the distillated liquid products obtained by thermal and catalytic pyrolysis of corncob.

4.3.2.4 Catalytic effect on the phenolic group in the distillated liquid

The thermal and catalytic pyrolysis effect on major phenolic group was shown in Figure 4.33. The methoxy-containing compounds and mono-functional phenol were included in the phenolic compound groups such as 4-ethylphenol (no.2), 4-ethyl-2-methoxyphenol (no.3), 2-methoxy-4-propyl phenol (no.5) and 2-methoxy-4-methylphenol (no.11) which the phenolic compounds were mainly produced from lignin at low reaction temperature 250-300°C. The 4-ethylphenol (no.2) and 4-ethyl-2-methoxyphenol (no.3) were formed in high percentage which related to the degradation of *p*-coumaryl alcohol from the decomposition of lignin. The 4-ethylphenol (no.2) and 4-ethyl-2-methoxyphenol (no.3) were most important in wine smoky aroma in food industry [15]. After catalytic pyrolysis, some of the phenolic compounds were reduced or eliminated. The phenolic compounds were cracked to gases or deoxygenated to form aromatic hydrocarbons [83].

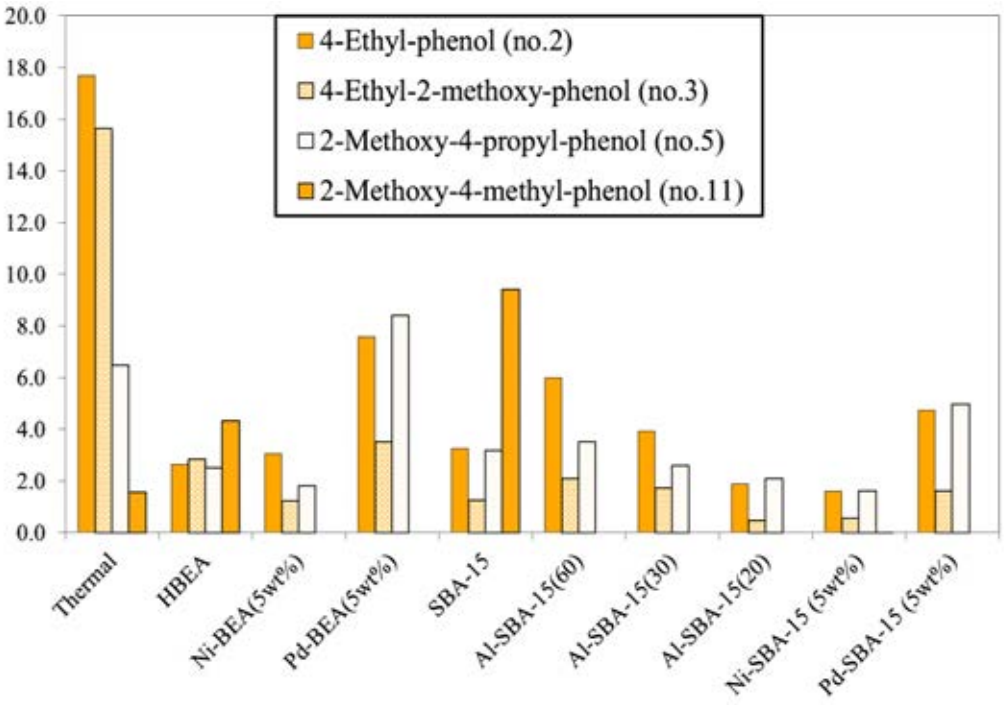

Figure 4.33 %Selectivity based on peak area of the phenolic compounds in the distillated liquid products obtained by thermal and catalytic pyrolysis of corncob.

4.3.2.5 Catalytic effect on the furan group in the distillated liquid

The thermal and catalytic pyrolysis effect on the furan derivatives group was shown in Figure 4.34. In furan derivative groups were high percentage of contained 1,2-di-2-furanyl-2-hydroxy-ethanone (no.6) and 2-acetyl-5-methylfuran (no.8) which the furan derivatives were mainly decomposed from cellulose and hemicellulose in pyrolysis at high temperature 500-600°C because hemicellulose and cellulose were involved depolymerization, ring scission reaction and formation of furan derivatives, light aldehydes, light ketones, alcohols and esters [85, 86]. Hemicellulose and cellulose were found abundant xylose (C5-sugar) which degradation during pyrolysis and produced to furan and related derivatives [15]. After catalytic pyrolysis, the selectivity of furan derivatives was decreased to lower than 4% expect for 1,2-di-2-furanyl-2-hydroxy-ethanone (no.6) was increased about 10% when catalyzed by HBEA catalyst. The 1,2-di-2-furanyl-2-hydroxy-ethanone (no.6) or furoin is organic compound which synthesized from furfural was used as a plasticizer in food industry, photosensitive agents and intermediate chemical for pharmaceutical industry.

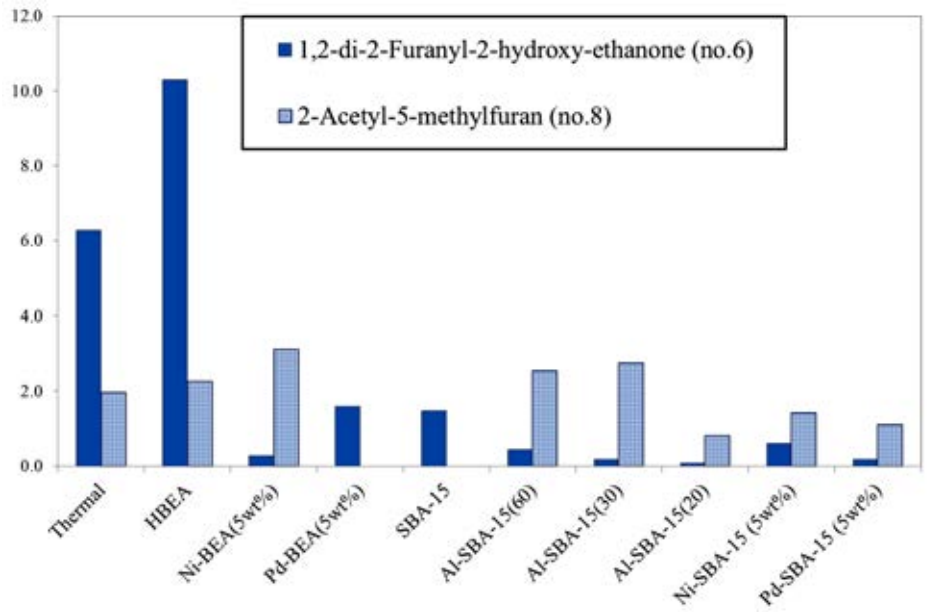

Figure 4.34 %Selectivity based on peak area of the furan derivative compounds in the distillated liquid products obtained by thermal and catalytic pyrolysis of corncob.

4.3.2.6 Catalytic effect on the acid and alcohol groups in the distillated liquid

The thermal and catalytic effects on the acid and alcohol groups were shown in Figure 4.35. 1-methoxy-2-propanol (no.9), 3,5-dimethyl-cyclohexanol (no.16) and formic acid (no.28) were main products which these were undesirable compounds due to corrosion problems. All catalysts could reduce or nearly eliminated these acids and alcohols which the catalytic provided the improvement of the liquid oil quality [22].

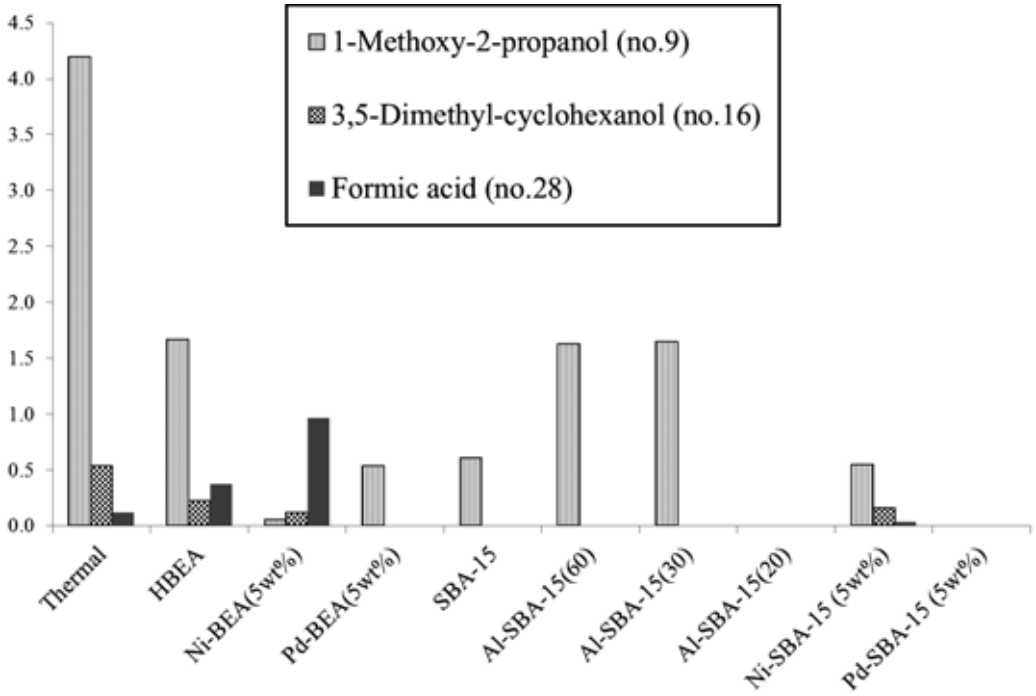

Figure 4.35 %Selectivity based on peak area of acids and alcohols in the distillated liquid products obtained by thermal and catalytic pyrolysis of corncob.

4.3.3 Effect of corncob to catalyst ratio

The %conversion and product yield obtained by catalytic pyrolysis of corncob over the Al-SBA-15(20) with different amounts of catalyst weight ratio were shown in Table 4.9 and Figure 4.36. The %conversion obtained from 5wt% catalytic amount was rose from 45.50% to 62.50% when catalytic amount was increased to 15wt%. It was indicated that the conversion depended on the catalytic content. Moreover, yield of gas and liquid fractions were increased with the increasing of amount of catalyst. The distillated liquid yield and heavy liquid were also affected by catalytic amount and was ordered by amount of catalyst as 15wt% > 10wt% > 5wt%. Generally, the increasing of catalytic amount lead to the rising of acidity and product yields. On the other hand, the amount of residue was decreased because solid residue was converted to gas and liquid yield when the catalytic amount was increased.

Table 4.9 Catalytic pyrolysis of corncob over the Al-SBA-15(20) at 300°C various amounts of catalyst

	Catalyst amount to corncob		
	5wt%	**10wt%**	**15wt%**
%conversion*	45.50	48.20	62.50
%yield of product*			
1. Gas	16.00	18.90	28.90
2. Liquid	29.50	29.30	33.60
Distillated liquid	20.55	23.79	28.09
Heavy liquid	8.90	5.51	5.51
3. Residue	54.50	51.80	37.50
Liquid fraction density (g/cm^3)	0.988	0.975	0.976

Condition: reaction time for 40 min, 5 g corncob and N_2 flow 20 cm^3/min.

*Deviation within ±0.50 for conversion, ±0.70 for yield of gas fraction, ±0.90 for yield of liquid fraction, and ±0.50 for yield of residue.

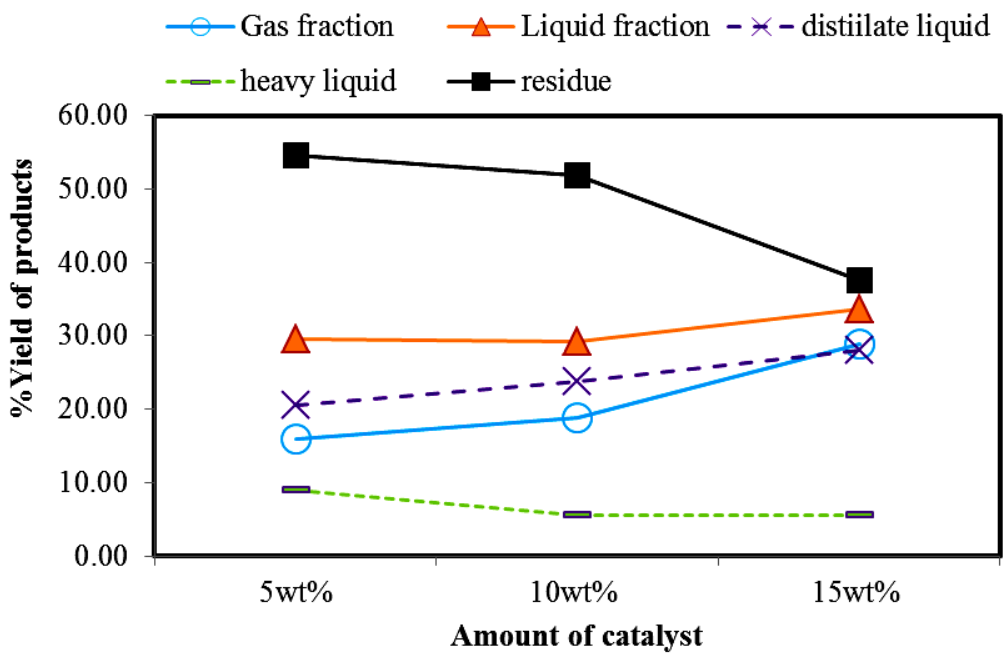

Figure 4.36 %Yield of products from catalytic pyrolysis of corncob over the Al-SBA-15(20) various catalytic amount at 300°C.

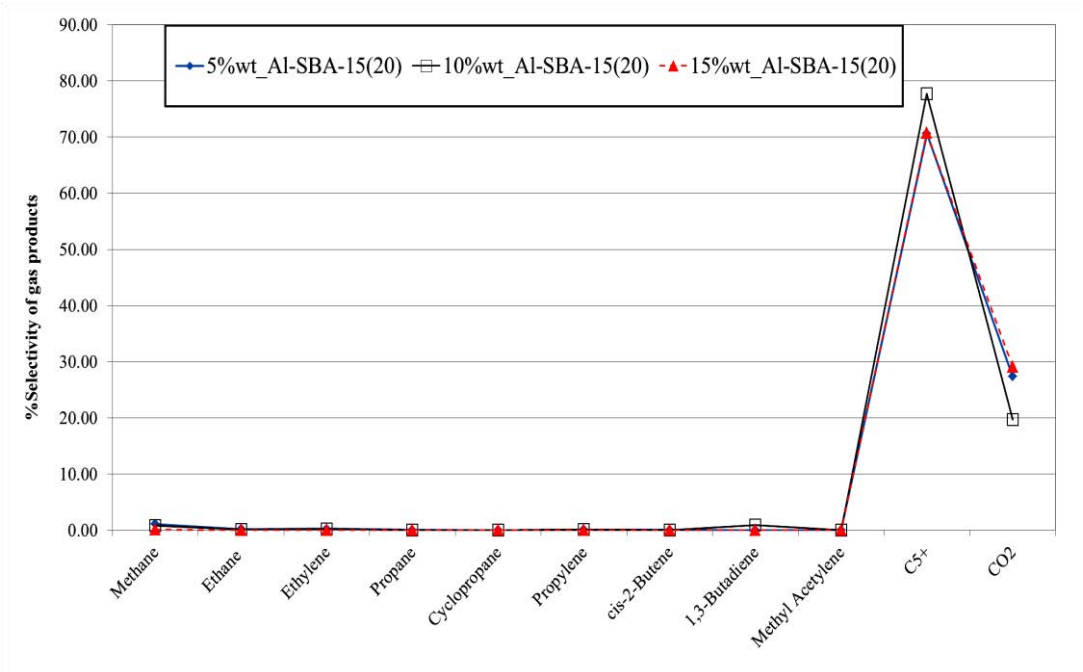

Figure 4.37 Distribution of gas fraction obtained by catalytic pyrolysis of corncob over the Al-SBA-15(20) at 300°C various catalytic amounts.

The catalytic amount affect on gas and distillated liquid product distribution was studied using different amount of the Al-SBA-15(20) were presented in Figure 4.37 and Figure 4.38. The major gas products included only C_5^+ and CO_2 when amount of catalyst was increased from 5wt% to 15wt% did not affect to these gas products. However, the highest yield ester group in distillated liquid (60.31%) was obtained at the catalytic amount of 10wt%Al-SBA-15(20). Main chemical product in ester group was 2-methoxy phenyl acetate (no.10) or guaiacyl acetate which this product smells sweet and used for aroma and flavor in food industry [87].

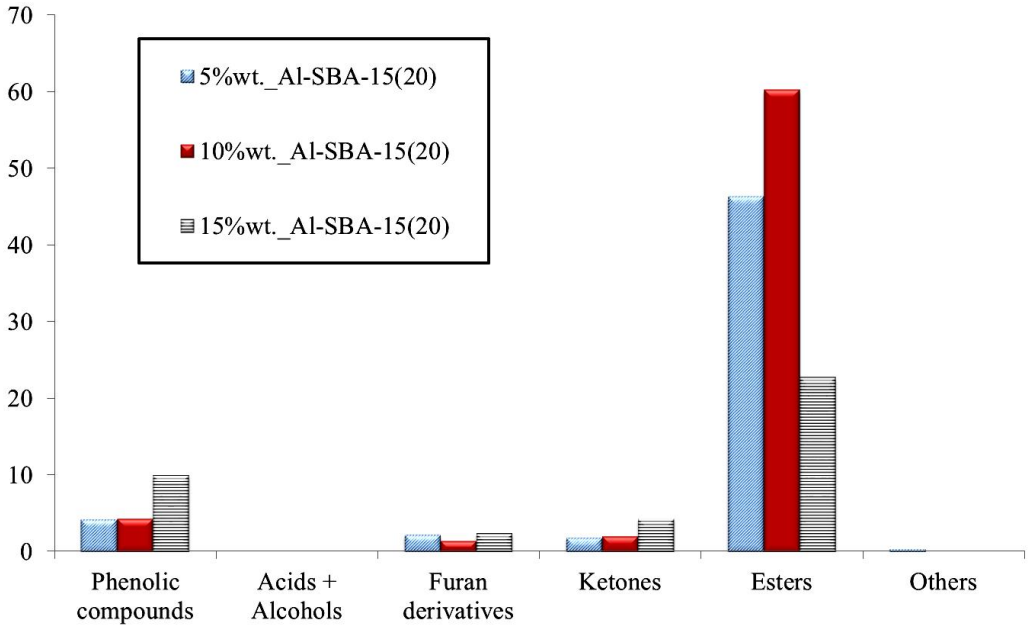

Figure 4.38 Total %selectivity based on peak area of the distillated liquid products obtained by corncob pyrolysis over various amount of Al-SBA-15(20).

4.3.4 Reused catalyst

The spent Al-SBA-15(20) catalyst from catalytic pyrolysis of corncob was reused by washed with acetone and dried in oven and then calcined in air at 550°C for 4 h. The reused catalyst was characterized by XRD, N_2 adsorption-desorption, SEM and tested for catalytic activity of corncob pyrolysis at 300°C for 40 min.

4.3.4.1 Powder x-ray diffraction (XRD)

The reused Al-SBA-15(20) was a mixture of white and black powder after calcination. The XRD pattern of the reused catalyst was presented in Figure 4.39 compared with the fresh catalyst which still remained characteristic peaks of hexagonal phase like the fresh catalyst. Additionally, the one very intense peak (100) and the two weak peaks indexed to (110) and (200) diffractions of reused catalyst exhibited lower intensity due to formation of coke.

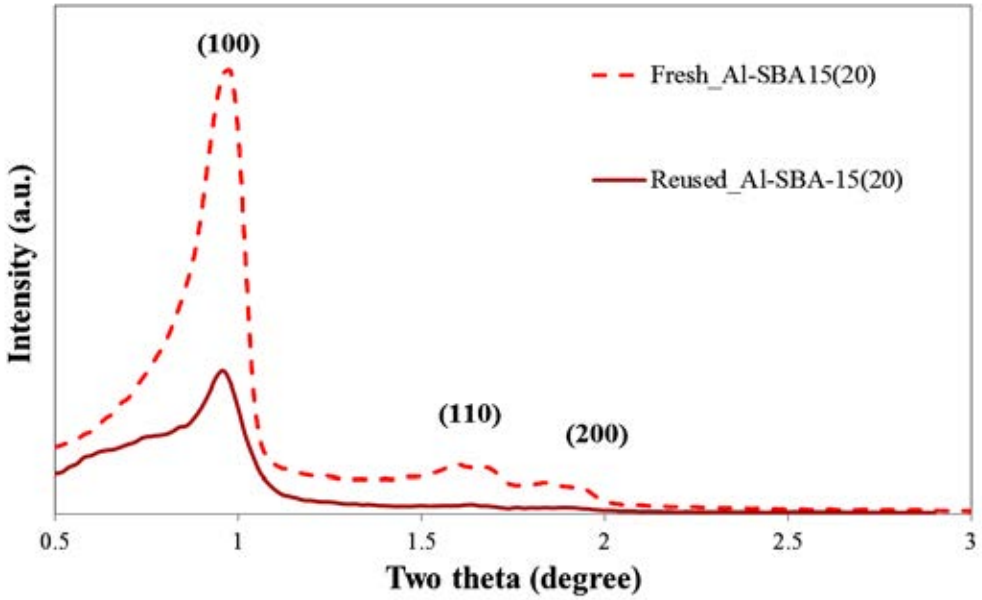

Figure 4.39 XRD patterns of calcined the fresh Al-SBA-15 (20) and the reused Al-SBA-15 (20).

4.3.4.2 Nitrogen adsorption-desorption

The N_2 adsorption-desorption isotherms of the reused Al-SBA-15(20) catalyst was shown in Figure 4.40. The reused catalyst exhibited the characteristic type I isotherm of microporous material. Table 3.7 showed the physical properties of reused Al-SBA-15(20) compared with fresh Al-SBA-15. The reused Al-SBA-15(20) gave total specific surface area only 295.61 m^2g^{-1} and pore size distribution of 2.43 nm which lower than fresh catalyst due to coke formation in mesoporous pore.

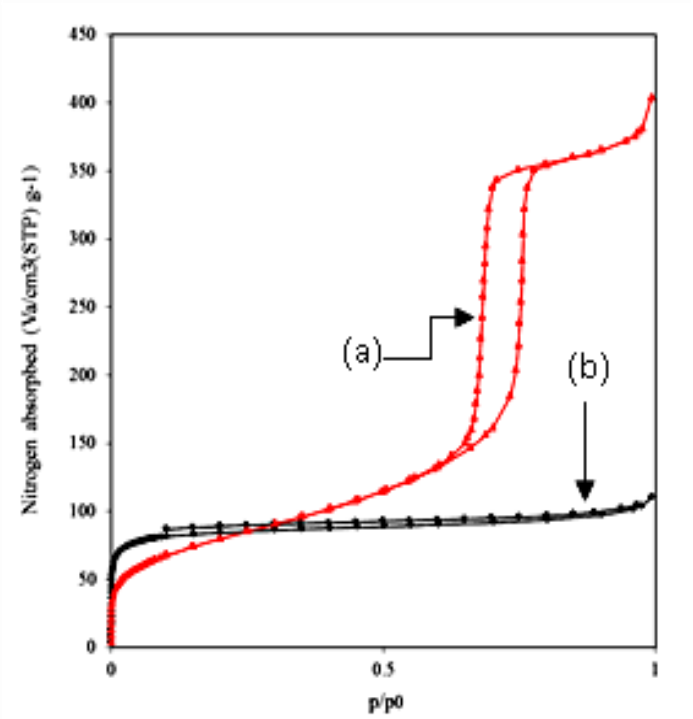

Figure 4.40 Nitrogen adsorption-desorption isotherms (a) the fresh Al-SBA-15(20) and (b) the reused Al-SBA-15(20).

Table 4.10 Physical properties of the fresh Al-SBA-15(20) and the reused Al-SBA-15(20)

Sample	Total specific Surface Area (m^2/g)[a]	Mesopore volume (cm^3/g)[b]	Pore size distribution (nm)[b]	$d_{(100)}$[c] (nm)	Wall thickness[d] (nm)
Fresh Al-SBA-15(20)	357.60	0.6636	8.06	9.18	2.54
Reused Al-SBA-15(20)	295.61	0.1687	2.43	9.21	8.20

[a] Determined by BET method,

[b] Determined by BJH-plot method,

[c] Determined by XRD, Jade 5.6,

[d] Determined as: a_0-pore size ($a_0 = 2 \times d_{(100)} / \sqrt{3}$)

4.3.4.3 Scanning electron microscope (SEM)

The SEM images of the fresh and the reused Al-SBA-15(20) catalysts were shown in Figure 4.41. After the catalytic pyrolysis of corncob, the reused Al-SBA-15(20) catalyst showed agglomerated of particles.

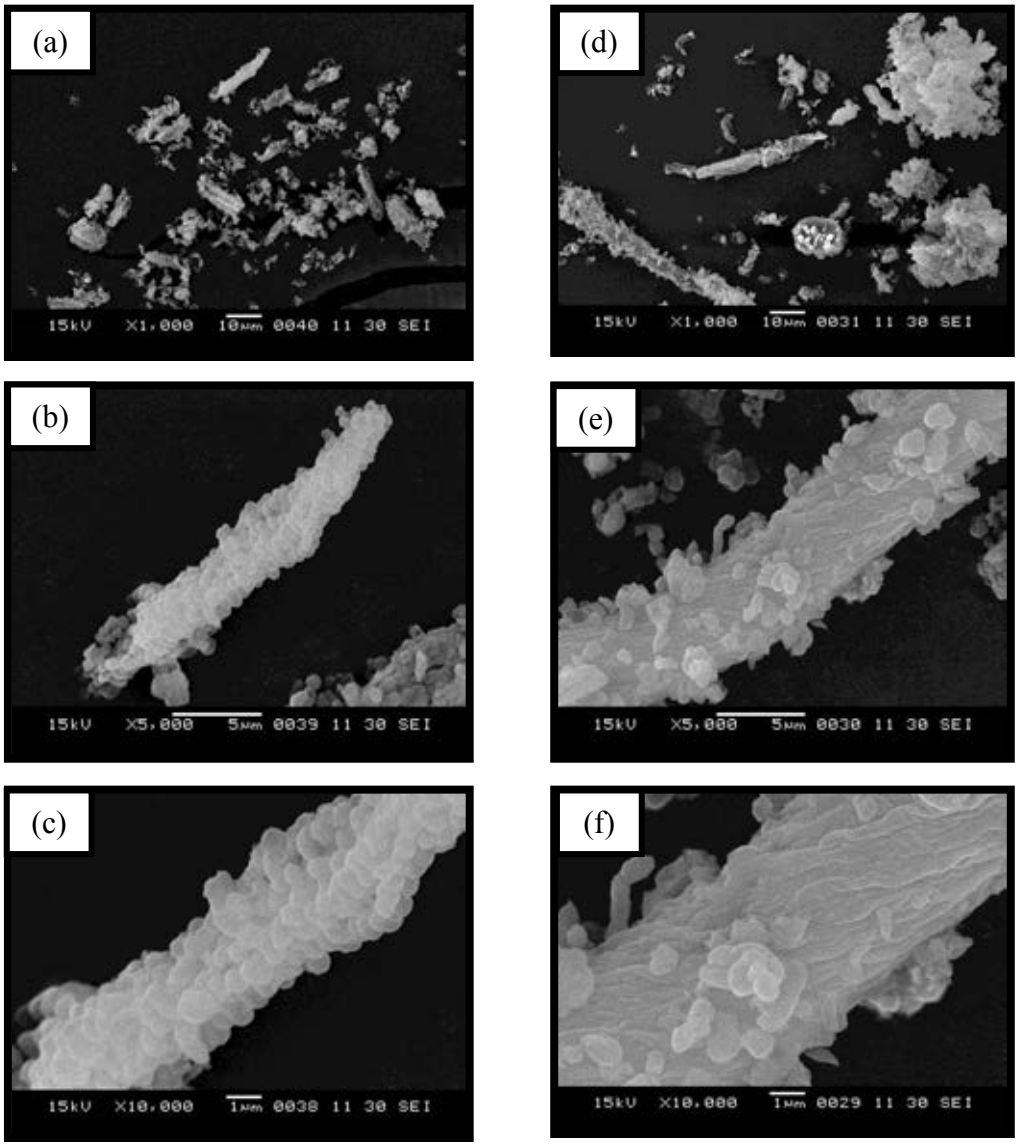

Figure 4.41 SEM images (a), (b), (c) of the fresh Al-SBA-15(20) and (d), (e), (f) of the reused Al-SBA-15(20) with different magnification.

4.3.4.4 Activity of reused Al-SBA-15(20) catalyst in corncob pyrolysis

Table 4.11 summarized the %conversion and products yield obtained in catalytic pyrolysis of corncob over reused Al-SBA-15(20) at 300°C for 40 min. The %conversion value of the reused catalyst was accounted 49.90% which higher than fresh catalyst as 2.9%. The gas yield and liquid yield were no significant difference between the fresh catalyst and reused catalyst. The reused Al-SBA-15(20) increased gas and distillated liquid yield because biomass residue still remained in the reused catalyst which was decomposed to volatile compound.

Table 4.11 Catalytic pyrolysis of corncob over the fresh and the reused Al-SBA-15(20) catalyst

	Thermal	**Fresh Al-SBA-15(20)**	**Reused Al-SBA-15(20)**
%conversion*	50.13	47.00	49.90
%yield of product*			
1. Gas	21.07	18.90	20.60
2. Liquid	29.07	28.10	29.30
Distillated liquid	20.58	22.73	24.41
Heavy liquid	8.49	5.37	4.89
3. Residue	49.87	53.00	50.10
Liquid fraction density (g/cm^3)	0.973	0.990	0.980

Condition: reaction time for 40 min, 5 g corncob and N_2 flow 20 cm^3/min.

*Deviation within ±0.50 for conversion, ±0.70 for yield of gas fraction, ±0.90 for yield of liquid fraction, and ±0.50 for yield of residue.

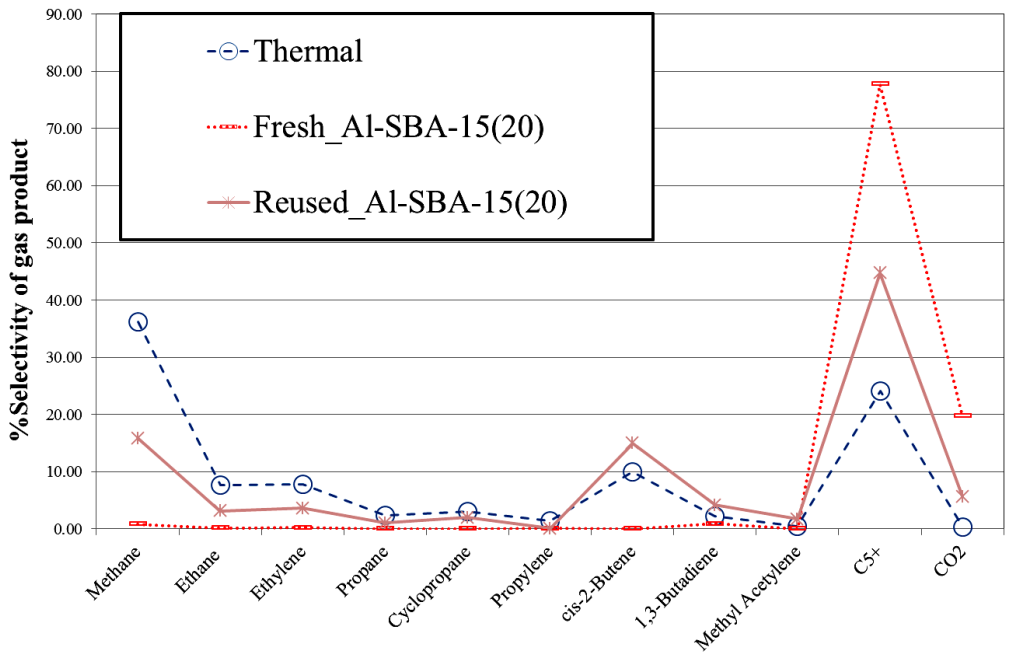

Figure 4.42 Distribution of gas fraction obtained by catalytic pyrolysis of corncob over the fresh Al-SBA-15(20) and the reused Al-SBA-15(20) catalyst.

Distribution of gas fraction by catalytic pyrolysis over the fresh Al-SBA-15(20) and the reused Al-SBA-15(20) catalysts were shown in Figure 4.42. The main components for catalytic pyrolysis over the reused Al-SBA-15(20) contained methane and C_1-C_4 gases reduced by half of thermal reaction while gas component of the fresh Al-SBA-15(20) gave C_5^+ and CO_2 as main gas product. The reducing of the reused Al-SBA-15(20) pore diameter resulted to the selectivity of smaller gas products.

Figure 4.43 showed product distribution of distillated liquid obtained by catalytic pyrolysis over the fresh Al-SBA-15(20) and the reused Al-SBA-15(20) catalyst. The fresh Al-SBA-15(20) was selective to 2-methoxy phenyl acetate (no.10) while reused Al-SBA-15(20) showed high amount of 2-methyl-butyl propanoic acid ester (no.1) same as non-catalytic reaction.

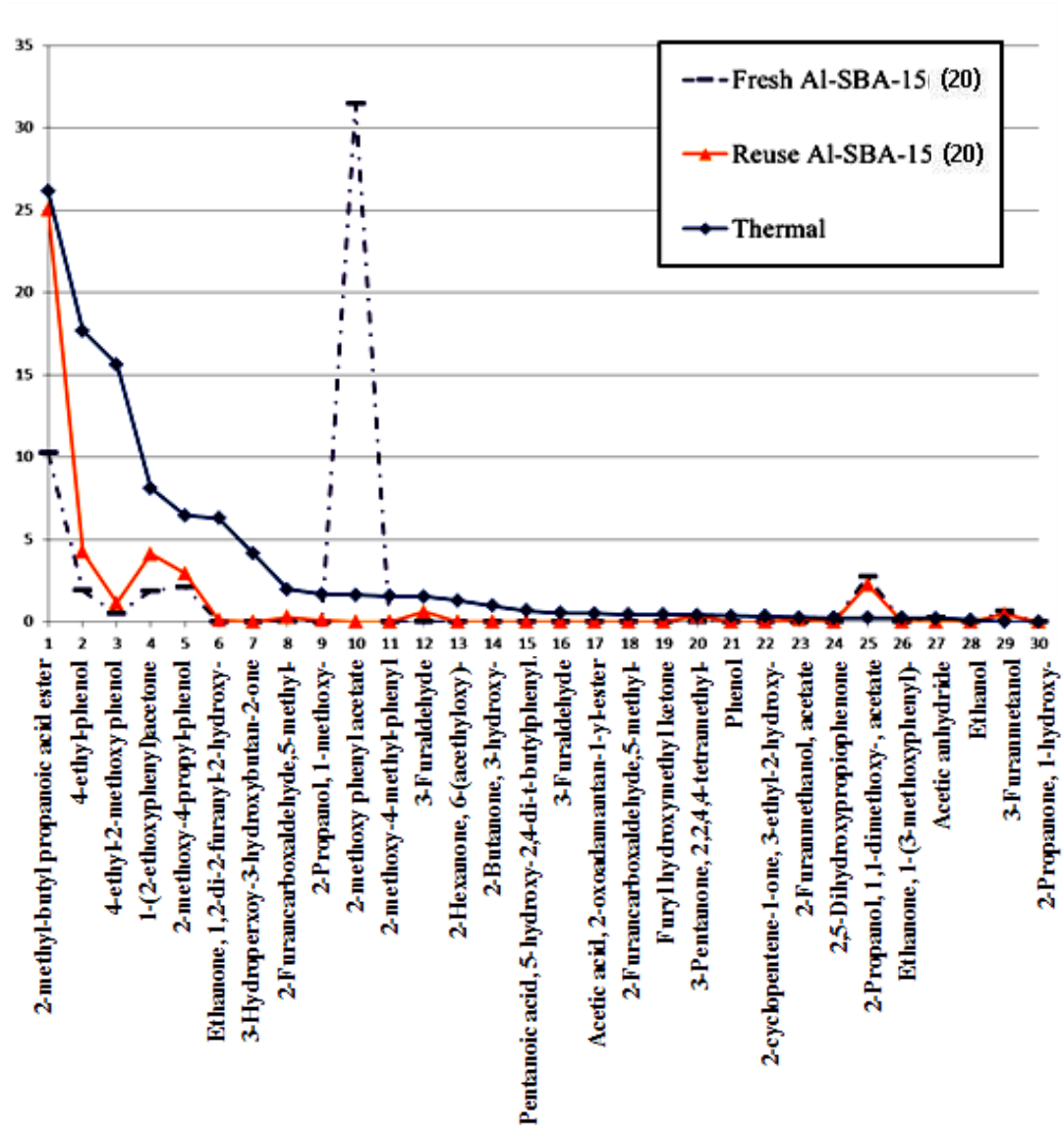

Figure 4.43 Distribution of the distillated liquid fraction obtained by catalytic pyrolysis of corncob over the fresh and reused Al-SBA-15(20) catalysts.

CHAPTER V

CONCLUSION

The SBA-15 was synthesized under hydrothermal condition. The Al-SBA-15 was prepared by post-synthesis method and the Ni, Pd metal supported SBA-15 materials were prepared by impregnation. The XRD patterns of all samples indicated the hexagonal structure same as the SBA-15 parent. N_2 adsorption-desorption isotherms exhibited a type IV pattern which showed typical shape of mesoporous materials. All samples presented aggregated particles with fiber-linked bundled from SEM-images. The TEM images of the Al-SBA-15 showed the well-ordered hexagonal array of one-dimensional channels same as the SBA-15 parent which Al atoms were into porous material framework corresponded to NMR technique. In case of the Ni and Pd metal supported SBA-15 presented the dispersion of metallic particle about 55 and 30 nm, respectively

The Ni and Pd metal supported commercial HBEA were prepared by impregnation method. The XRD patterns of the Ni-BEA and the Pd-BEA exhibited high crystallinity of the beta zeolite similar to starting HBEA. N_2 adsorption-desorption isotherms presented a type I pattern which showed characteristic pattern of microporous material. All samples presented a round granular to form cauliflower agglomeration from SEM images. The TEM image of the Ni-BEA no clearly showed metallic particles on HBEA surface whereas the TEM image of the Pd-BEA showed small metallic particles in sizes about 8-20 nm.

The pyrolysis temperature was an important parameter affected to decomposition of biomass. From TGA results, cellulose and hemicellulose decomposed about 53.4wt% at temperature 300-450°C and lignin and other heavy volatile were decomposed about 18.1wt% at temperature 500-900°C. The %conversion, gas yield and liquid yield were increased to 33.20-65.40%, 14.87-26.60% and 18.33-38.80%, respectively whereas residue was decreased from 66.80-34.60% with the increasing of temperature. The main gas products were methane, C_5^+ and CO_2 whereas C_2-C_4 gases were minor components. The distillated liquid products were divided into six

functional groups including acid and alcohol groups, furan derivatives, phenolic compounds, light ketones, light esters and others.

The catalysts were applied for catalytic pyrolysis process of corncob at low temperature 300°C. All catalyst could promote the light ester group whereas the phenolic and furan groups were decreased and especially showed significant difference in distillated liquid of the Al-SBA-15(20) and the Pd-BEA as catalysts. These catalysts gave the highest light ester group such as 2-methyl-butyl propanoic acid ester (no.1) and 2-methoxy phenyl acetate (no.10) which the most important in intermediate chemical for sweet odor and apple, banana aroma in food industry.

The suggestions for future work

1. Study the optimum condition of the vapor-phase catalytic pyrolysis of corncob using Al-SBA-15 for avoidance of the mixture of catalyst and starting materials.
2. Study the catalytic pyrolysis of other biomass such as sugarcane and cassava for upgrading agricultural waste in Thailand.
3. Study the quantitative main composition of corncob (cellulose, hemicellulose and lignin) by solvent extraction.

REFERENCES

[1] Bosetti, A. and Perego, C. Biomass to fuels: The role of zeolite and mesoporous materials. Microporous and Mesoporous Materials. 144(2011): 28-39.

[2] Renewable energy consumption [online]. Available from: http://www.eia.doe.gov/emeu/mer/contents.html [2012, May 29].

[3] Balat, M., Balat, M., Kirtay, E. and Balat, H. Main routes for the thermo-convertion of biomass into fuels and chemicals Part 1: Pyrolysis systems. Energy Conversion and Management. 50(2009): 3147-3157.

[4] Nattaporn Suwannakhanthi, N. Overview for Thailand‟s renewable energy focusing on biomass energy. Department of alternative energy development and efficiency. Thainland: Burean of Energy Research, pp.1-14, 23 August 2004.

[5] Rydholm, SA., Pulping processes, New York: Jonh Wiley and Sons. (1965).

[6] Shinya, Y. and Yakihiko, M. The Asian biomass handbook. Japne: The Japan Institute of Energy. (2008).

[7] Aho, A., Kumar, N., Eranen, K., Salmi, T., Hupa, M. and Murzin, D.Y. Catalytic pyrolysis of biomass in a fluidized bed reactor: influence of the acidity of H-beta zeolite. Process Safety and Environmental Protection. 85(2007): 473-480.

[8] Judit, A., *et al*. In situ catalytic upgrading of biomass derived fast pyrolysis vapours in a fixed bed reactor using mesoporous materials, Microporous and Mesoporous Materials. 96(2006): 93-101.

[9] Xi-feng, Z., Qiang, L., Wen-zhi, L. and Dong, Z. Analytical pyrolysis-gas chromatography/mass spectrometry (Py-GC/MS) of sawdust with Al/SBA-15 catalysts. Journal of Analytical and Applied Pyrolysis. 84(2009), 131-138.

[10] Stucky, D.G., et al. Triblock copolymer syntheses of mesoporous silica with periodic 50 to 300 angstrom pores. Science. 297(1998): 548-552.

[11] Ooi, Y.S. and Bhatia, S. Aluminum-containing SBA-15 as cracking catalyst for the production of biofuel from waste used palm oil. Microporous and Mesoporous Materials. 102(2007): 310–317.

[12] Paul, T.W. and Serpil, B. The influence of temperature and heating rate on the slow pyrolysis of biomass. Renewable Energy. 7(1996): 233-250.

[13] Ke-Chang, X., Qing, C., Wei-Ren, B. and Shu-Guang, S. Pyrolytic behavior of waste corn cob. Bioresource Technology. 94(2004): 83-89.

[14] Suneerat Pipatmanomai, Janewit Wannapeera and Nakorn Worasuwannarak. Product yields and characteristics of rice husk, rice straw and corncob during fast pyrolysis in a drop-tube/fixed-bed reactor, Songklanakarin Journal of Science Technology. 30(3) (2008): 393-404.

[15] Azeez, A.M., Meier, D., Jurgen, O., and Willner, T. Fast pyrolysis of African and European lignocellulosic biomasses using Py-GC/MS and fluidized bed reactor. Energy and Fuel. 24(2010): 2078-2085.

[16] Murzin, D.Y., Aho, A., Kumar, N., Eranem, K. Salmi, T. and Hupa, M. Catalyst pyrolysis of woody biomass in a fluidized bed reactor: influence of the zeolite structure. Fuels. 87(2008): 2493-2501.

[17] Murzin, D.Y., Aho, A., Kumar, N., Eranem, K. Salmi, T. and Hupa, M. Catalytic pyrolysis of biomass in a fluidized bed reactor: influence of the acidity of H-beta zeolite. Trans IChemE. 85 (B5) (2008): 473-480.

[18] Xiao, R., Zhang, H., Huang, H. and Xiao, G. Comparison of non-catalytic and catalytic fast pyrolysis of corncob in a fluidized bed reactor. Bioresource Technology. 100(2009): 1428-1434.

[19] Akwasi, B.A., David, M.J. and Charles, M.A. Screening acidic zeolites for catalytic fast pyrolysis of biomass and its components, Analytical and Applied Pyrolysis. 92(2011): 224-232.

[20] Samolada, M.C., Papafotica, A. and Vasalos, I.A. Catalyst evaluation for catalytic biomass pyrolysis, Energy and Fuels. 14(2000): 1161-1167.

[21] Funda, A. and Asli, I.M. Influence of temperature and alumina catalyst on pyrolysis of corncob, Fuel. 88(2009): 1991-1997.

[22] Xiangling, J., Lianxun, G., Peng, H., Xiaomei, W. and Xuepeng, Q. One-step synthesis of palladium/SBA-15 nanocomposites and its catalytic application, Molecular Catalysis A: Chemical. 272(2007): 136-141.

[23] Calles, J.A., Lindo, M., Vizcaino, A.J. and Carrero, A. Ethanol steam reforming on Ni/Al-SBA-15 catalysts: effect of the aluminum content, International, Journal of Hydrogen Energy. 35(2010): 5895-5901.

[24] Sineenat Rodjeen. Catalytic pyrolysis of biomass in a circulating fluidized bed. Master"s Thesis, Program of Chemical Technology, Faculty of Science, Chulalongkorn University, 2004.

[25] Zhu, X., Zhang, Y., Lu, Q. and Tang Z. Catalytic upgrading of biomass fast pyrolysis vapors with Pd/SBA-15 catalysts, Industrial and Engineering Chemistry Research. 49(2010): 2573-2580.

[26] Ralph, P.O. and Lynn L.W. The handbook of mechanical engineering second edition. United States of America: The Japan Institute of Energy, 2008.

[27] Ebeling, J.M. and Jenkins, B.M. Physical and chemical properites of biomass fuels, American society of agricultural engineer winter meeting, Chicago, 13-16 December.

[28] Overend, R. and Wright, Lynn L. Biomass Energy. New York: Taylor and Francis Group, LLC, 2007

[29] Demirbas, A., Biofuels sources, biofuel policy, biofuel economy and global biofuel projections. Energy Conversion and Management. 49 (2008): 2106-2116.

[30] Wild P.J., Relth H. and Heeres, H.J. Biomass pyrolysis for chemicals, biofuels. 2(2), (2011): 185-208.

[31] Asri, G. and Ichiro, N. Effect of cellulose and lignin content on pyrolysis and combustion characteristics for several types of biomass, Renewable Energy. 32, (2007): 649-661.

[32] Dermirbas, A. Effect of temperature and particle size on bio-char yield from pyrolysis of agricultural residues. Journal of Analytical and Applied Pyrolysis. 72(2004): 243-248.

[33] Folch-Mallol, J. and Quiroz-Castaneda, R.E. Plant cell wall degrading and modeling proteins: current perspectives. Biotechnologia Applicada, 28(2011): 205-215.

[34] Pandey, M.P. and Sookim, C. Lignin depolymerization and conversion: A review of thermochemical methods. Chemical Engineering and Technology. 34(1) (2011): 29-41.

[35] Bridgwater, A.V. Review of fast pyrolysis of biomass and product upgrading. Biomass and Bioenergy. 38(2011): 1-27.

[36] Sadaka, S. Pyrolysis, Associate scientist. Department of Agricultural and Biosystems Engineering. Navada: Ivowa State University, 2007.

[37] Serrano, D.P., Aguado, J., Escola, J.M., Roriguez, J.M., Moreslli, L. and Orsi, R. Thermal and catalytic cracking of a LDPE-EVA copolymer mixture, Journal of Analytical Pyrolysis. 68 (2003): 481.

[38] Flanigen, E.M. Zeolite and Molecular Sieve An Historical Perspective in Bekkum, HV., Flanigen, E.M. and Jansen, J.C. Introduction to Zeolite Science and Pracitice, Studies in Surface Science and Catalysis. 58. Amsterdam: Elsevier. 1991.

[39] Barrer, R.M. Hydrothermal Chemistry of Zeolites. London: Acadamic Press. 1982.

[40] Meier, M.W., Olson, D.H., and Boerlocher, C. Atlas of Zeolite structure type. 4th edition Amsterdam: International Zeolite Association.

[41] Juttu, G. Modified Microporous Aluminosilicates As Novel Solid Acid Catalyst. Ph.D.‟s Thesis, University of Delaware, 2001.

[42] Lin, Y.H., Yang, M.H., Yeh, T.F. and Ger, M.D. Catalytic degradation of HDPE over mesoporous and microporous catalytic in a fluidized-bed reactor. Polymer Degradation and Stability. 86(2004): 121.

[43] Garforth, A., Fiddy, S., Lin, Y.H., and Sharratt, P.N. Catalytic degradation of HDPE: An evaluation of mesoporous and microporous catalysts using thermal analysis. Thermochimica Acta. 294(1997): 65.

[44] Aguado, J., Sotelo, J.L., Serrano, D.P., Callers, J.A., and Escola, J.M. Catalytic conversion of polyolefins into liquid fuels over MCM-41: Comparison with ZSM-5 and amorphous SiO_2-Al_2O_3. Energy Fuels. 11(1997): 1225.

[45] Wadlinger, R. L., Kerr, G. T., Rosinski, E. J. A crystalline zeolite with improved adsorption and catalytic properties. *United States Patent* 3308069. (1967)

[46] Baerlocher, C., Meier, W.M., Olson, D.H. Atlas of zeolite framework types 5th Ed. Amsterdam: Elsevier, 2001.

[47] De Vries, A.H., Sherwood, P., Collins, S.J., Rigby, A.M., Rigutto, M., Kramer, G.J. Zeolite structure and reactivity by combined quantum chemical-classical calculations. Journal of Physical Chemistry. *B*103(1999): 6133-6141.

[48] Treacy, M. M.J., Newsam, J.M. Two new three-dimensional twelve-ring zeolite frameworks of which zeolite beta is a disordered intergrowth. Nature. 332(1988): 249-251.

[49] Rungsirisakun, R., Jansang, B., Pantu, P., Limtrakul, J. The adsorption of benzene on industrially important nanostructured catalysts (H-BEA, H-ZSM-5, and H-FAU): confinement effects. Journal of Molecular Structure. 733(2005): 239-246.

[50] Newsam, J.M., Treacy, M. M.J., Koetsier, W.T., de Gruyter, C. B. Structural characterization of zeolite beta. Proceeding of Royal Society A. 420(1988): 375-405.

[51] Guisnet, M., Ayrault, P., Coutanceau, C., Alvarez, M. F., Datka, J. Acid properties of dealuminated beta zeolites studied by IR spectroscopy. Journal of Chemical Society Faraday Transactions. 93(1997): 1661-1665.

[52] Abd El-Wahab, M. M. M. and Said, A. Phosphomolybdic acid supported on silica gel and promoted with alkali metal ions as catalyst for the esterification of acetic acid by ethanol. Journal of Molecular Catalysis. 240(2005): 109.

[53] Weitkamp. Zeolites and catalysis. Solid State Ionics. 131(2000): 175-188.

[54] Ying, J.Y., Mehnert, C.P. and Wong, M.S. Synthesis and application of supramolecular-templated mesoporous materials. Angewandte Chemie International Edit. 38(1999): 56.

[55] Kresge, C.T., Leonowicz, M.E., Roth, W.J., Vartuli, J.C. and Beck, J.S. Ordered mesoporous molecular sieves synthesized by a liquid crystal template mechanism. Nature. 359 (1992): 710.

[56] Soler-Illia, G. J. A. A., Sanchez, C., Lebeau, B. and Patarin, J. Chemical strategies to design textured materials: from microporous and mesoporous oxides to nanonetworks and hierarchical structures. Chemical Reviews. 102(2002): 4093.

[57] Tanev, P.T. and Pinnavavia, T. J. A neutral templating route to mesoporous molecular sieve. Science. 267 (1995): 865.

[58] Melosh, N.A., Lipic, P., Bates, F.A. and Stucky, G.D. Molecular and mesoscopic structure of transparent block copolymer silica monoliths. Macromolecules. 32(1999): 4332.

[59] Soler-Illia, G. J. A. A., Crepaldi, E. L., Grosso, D. and Sanchez, C. Block copolymer-templated mesoporous oxides. Current Opinion in Colloid and Interface Scienc. 8(2003): 109.

[60] Beck, J. S., Leonowicz, M. E., Roth, W. J., Vartuli, J. C. and Kresge, C. T. A new family of mesoporous molecular sieves prepared with liquid crystal templates. Journal of the American Chemical Society. 114(1992): 10834.

[61] Gabriel, B.L. SEM: A User‟s Manual for Material Science, Ohio: American Society for Metal, 1985.

[62] Tunyatorn Tongtooltush. Catalytic cracking of glycerol using metal-supported SBA-15. Master‟s Thesis, Program of Petrochemistry and Polymer Science, Faculty of Science, Chulalongkorn University. 2009.

[63] Moore, D.M. and Reynolds, Jr.R. C. X-ray Diffraction and the Identification and Analysis of Clay of Instrument Analysis. 4th ed. pp.363-364. New York: Harcourt Brace College Publishers, 1997.

[64] Skoog, D.A. Principles of Instrumental Analysis. 4th ed. pp. 363-364. New York: Harcourt Brace College Publishers, 1997.

[65] Basic operating principles of the sorptomatic. [Online]. Available from: http://saf.chem.ox.ac.uk./Instruments/BET/sorpoptprin [2011, September 9].

[66] Analysis software user‟s manual, BELSORP, BEL JAPAN, INC.

[67] Hunger, M., Schenk, U., Breuninger, R., Glaser, R., and Weikamp, J. Characterization of the acid sites in MCM-41 type materials by spectroscopic and catalytic technique. Microporous Mesoporous Materials. 27(1999): 261.

[68] Microscope. [Online]. Available from: http://www1.stkc.go.th/stportal Document/ stportal_1170654028.doc [2010, September 2].

[69] Standard Practice for Proximate analysis of Coal and Coke, ASTM D317-73(84): 1989.

[70] Wannapeera, J. al et. Product yields and characteristics of rice husk, rice straw and corncob during fast pyrolysis in a drop-tube/fixed-bed reactor. *Songklanakarin.* Science and Technology. 30(3)(2008): 309-404.

[71] Zabaniotou, A. *et al.* Investigating the potential for energy, fuel, materials and chemicals production from corn residues (cobs and stalks) by non-catalytic and catalytic pyrolysis in two reactor configurations. Renewable and Sustainable Energy Reviews. 13 (2009): 750-762.

[72] Gomez-Cazalilla, M., Merida-Robles, J.M., Gurbani, A., Rodriguez-Castellon, E. and Jimenez-Lopez, A. Characterization and acidic properties of Al-SBA-15 materials prepared by post-synthesis alumination of a low-cost ordered mesoporous silica. Journal of Solid State Chemistry. 180(2007): 1130-1140.

[73] Rangsan Chakkasemkij. Catalytic cracking of waste from biodiesel production using Al-SBA-15. Master"s Thesis, Program of Petrochemistry and Polymer Science, Faculty of Science, Chulalongkorn University, 2008.

[74] Zeng, S., Blanchard, J., Breysse, M., Shi, Y., Shu, X., Nie, H., and Li, D. Post-synthesis alumination of SBA-15 in aqueous solution: A versatile tool for the preparation of acidic Al-SBA-15 supports. Journal Microporous and Mesoporous Materials. 85(2005): 297-304.

[75] Cao, L., Jia, Z., Ji, S., and Hu, J. Catalytic steam reforming of biomass over Ni-based catalysts: Conversion from poplar leaves to hydrogen-rich syngas. Journal Natural Gas Chemistry. 20(2011): 377-383.

[76] Lu, Q., Tang, Z., Zhang, Y., and Zhu, X. Catalytic upgrading of biomass fast pyrolysis vapors with Pd/SBA-15 catalysts. Journal Industrial Engineering Chemistry. 49(2010): 2573-2580.

[77] Wang, H. and Liu, C. Preparation and characterization of SBA-15 supported Pd catalyst for CO oxidation. Journal Applied Catalysis B: Environmental. 106(2011): 672-680.

[78] Aguado, J., Serrano, D.P., Escola, J.M., Garagorri, E., and Fernandez, J.A.Catalytic conversion of polyolefins into fuels over zeolite beta. Journal Polymer Degradation and Stability. 69(2000): 11-16.

[79] Tidahy, H.L., Siffert, S., Lamonier, J.-F., Cousin, R., Zhilinskaya, E.A., Aboukais, A., Su, B.-L., Canet, X., Weireld, G. De., Frere, M., Giraudon, J.-M., Leclercq, Influence of the exchanged cation in Pd/BEA and Pd/FAU zeolites for catalytic oxidation of VOCs. Journal Applied Catalysis B: Environmental. 70(2007): 377-383.

[80] Tang, T., Yin, C., Wang, L. and Ji, Y. Good sulfur tolerance of a mesoporous Beta zeolite-supported palladium catalyst in the deep hydrogenation of aromatics. Journal of Catalysis. 257(2008): 125-133.

[81] Jale. Y., Christoph. K., Mehmet. S. and Mithat. Y., Fast pyrolysis of agricultural wastes: characterization of pyrolysis products. Journal Fuel Processing Technology. 88(2007): 942-947.

[82] NIST. [online]. Available from: http://webook.nist.gov/chemistry [2012, January 18].

[83] Qiang, L., Zhi-F, Z., Chang-Qing, D. and Xi-Feng, Z. Catalytic upgrading of biomass fast pyrolysis vapors with nano metal oxides: An analytical Py-GC/MS study. Energies. 3(2003): 1805-1820.

[84] Illiopoulou. E.F., Antonako. E.V., Karakoulia. S.A., Vasalos. I.A., Lappas. A.A. and Trantafyllidis. K.S. The influence of temperature on the yields of compounds existing in bio-oils obtained from biomass samples via pyrolysis. Chemical Engineering. 134(2007): 51.

[85] Mustafa. B., Mehmet. B., Elif. K and Havva. B. Main routes for the thermo-conversion of biomass into fuels and chemicals. Part 1: Pyrolysis systems. Energy Conversion and Management. 50(2009): 3147-3157.

[86] Xi-Feng, Z. Qiang, L. Wan-Ming, X., Wen-Zhi, L. and Qing-Xiang, G. Catalytic pyrolysis of cellulose with sulfated metal oxides: A promising method for obtaining high yield of light furan compounds. Bioresource Technology. 100(2009):4871-4876.

[87] 2-methoxy phenyl acetate. [online]. Available from: http://www.perflavory.com/docs/doc1025261.html [2012, February 26].

[88] Yan-fen. L., Shu-rong. W. and Xiao-qian. M. Study of reaction mechanisms in cellulose pyrolysis. Preprint Papers-American Chemical Society, Division of Fuel Chemistry. 49(1) (2004): 407.

[89] Chang-qing. D., Zhi-fei. Z. and Yong-ping. Y. Characteristics and mechanism study of analytical fast pyrolysis of poplar wood. Energy Conversion and Management. 57 (2012): 49-59.

[90] Yusaku. S., Selhan. K., Thallada. B. and Akinori. M.Comparative studied of oil compositions produced from sawdust, rice husk, lignin and cellulose by hydrothermal treatment. Fuel. 84 (2005): 875-884.

[91] Gu. S., Shen. D.K. and Bridgwater. A.V. Study on the pyrolytic of xylan-based hemicelluloses using TG-FTIR and Py-GC-FTIR. Journal of Analytical Applied Pyrolysis. 87 (2010): 199-206.

[92] Grushin. V.V., Kabro. A. and Escudero-Adan. E.C. Biomass conversion to High value chemicals: from furfural to chiral hydrofuroins in two steps. Organic Letters. 4 (2012): 680-684.

APPENDICES

A. Proximate analysis ASTM D3172

1.1 Moisture content: ASTM D3173-73

- Grid and sieve samples to size a 250 μm. (mesh No.60). The samples 1.0 g. loaded to crucible and put into the oven at temperature 105°C for 1 hour and then kept into desiccator for 1 hour. Weigh record before and after drying and calculate moisture content in equation A-1.

$$\text{Moisture content (\%)} = 100(W_1 - W_2)/W \qquad \text{(A-1)}$$

W_1 = Weight of crucible and cap and sample before dry (g.)

W_2 = Weight of crucible and cap and sample after dry (g.)

W = Weight of sample (g.)

1.2 Ash content: ASTM D3174-82

- Using the crucible with cap and place them in the muffle furnace at 575 ± 25°C for four hours until constant weight and then kept into the desiccator for 1 hour. Weighed the crucibles to the nearest 0.1 mg. and recorded this weight.

- Weighed 1.0 g. biomass into the crucible with cap. Record the samples weight. Before samples were analyzed taken into oven at temperature 105°C, the sample should be stored in a desiccator until use.

- Place the crucible in the muffle furnace and begin the ramping program.

Hold at 105°C for 12 minutes

Ramp to 250°C at 10°C/minute

Hold at 250°C for 30 minutes

Ramp to 575°C at 20°C/minute

Hold at 575°C for 180 minutes

Allow temperature to drop to 105°C

Hold at 105°C until samples are removed

- Carefully remove the crucible from the directly furnace into a desiccator and cool. Record sample weigh. Weigh the crucibles and ash to the nearest 0.1 mg.

- Place the samples back into the muffle furnace at 575 ± 25°C and ash to constant weight. Constant weight is defined as less than ±0.3 mg change in the weight upon one hour of re-heating the crucible and Calculate ash content, shown as equation A-2.

$$\text{Ash content (\%)} = 100(W_3 - W_4)/W \quad \text{(A-2)}$$

W_3 = Weight of crucible and cap and ash after dry (g.)
W_2 = Weight of crucible and cap and before dry (g.)
W = Weight of sample (g.)

1.3 Volatile matter: ASTM D3175 -77

- Using the crucible with cap and place them in the muffle furnace at 950 ± 25°C for 30 minutes until constant weight and then kept into the desiccator for 1 hour. Weigh the crucibles to the nearest 0.1 mg. and record this weight.

- Weighed 1.0 g. biomass into the crucible with cap. Record the samples weight. Before samples were analyzed taken into oven at temperature 105°C, the sample should be stored in a desiccator until use.

- Place the samples into the muffle furnace at 950°C for 7 minutes and then remove into the desiccator for 1 hour. Weigh sample record and calculate volatile matter follow as A-3

$$\text{Volatile matter (\%)} = [100(W_5 - W_6)/W] - \text{Moisture content} \quad \text{(A-3)}$$

W_5 = Weight of crucible and cap and sample before dry (g.)
W_6 = Weight of crucible and cap and sample after dry (g.)
W = Weight of sample (g.)

1.4 Fixed carbon: ASTM D3172 -73

$$\text{Fixed carbon (\%)} = 100 - (\%\text{Moisture} + \%\text{Ash} + \%\text{Volatile matter}) \quad \text{(A-4)}$$

B.1 Calculation of %Selectivity of gas fraction

$$\%\text{Yield product of X} = \frac{\text{Concentration of X} \times 100}{\text{Total concentration of products}} \quad \text{(A-5)}$$

$$\text{Concentration of X} = \frac{b \times c}{a} \quad \text{(A-6)}$$

a = Peak area of X in standard gas products

b = %molar of X in standard gas products

a = Peak area of X in sample products

B.2 Calculation of %Product yield of liquid fraction

$$\%\text{Yield product of X} = \frac{b}{a}\ 00 \quad \text{(A-7)}$$

b = Peak area of X in sample liquid products

a = Total peak area of X in sample liquid products

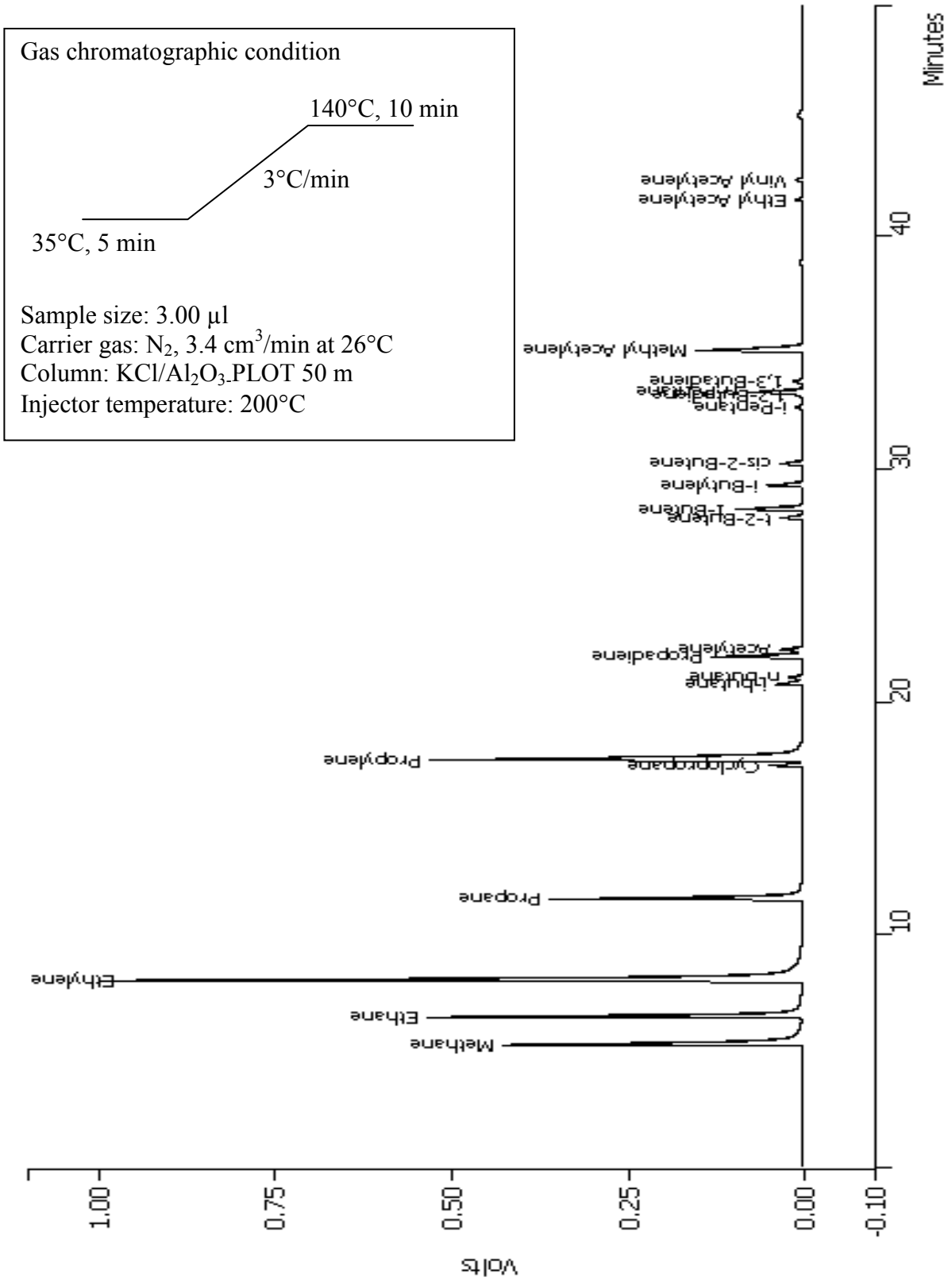

Figure B-1 Gas chromatogram of standard mixture hydrocarbon gas.

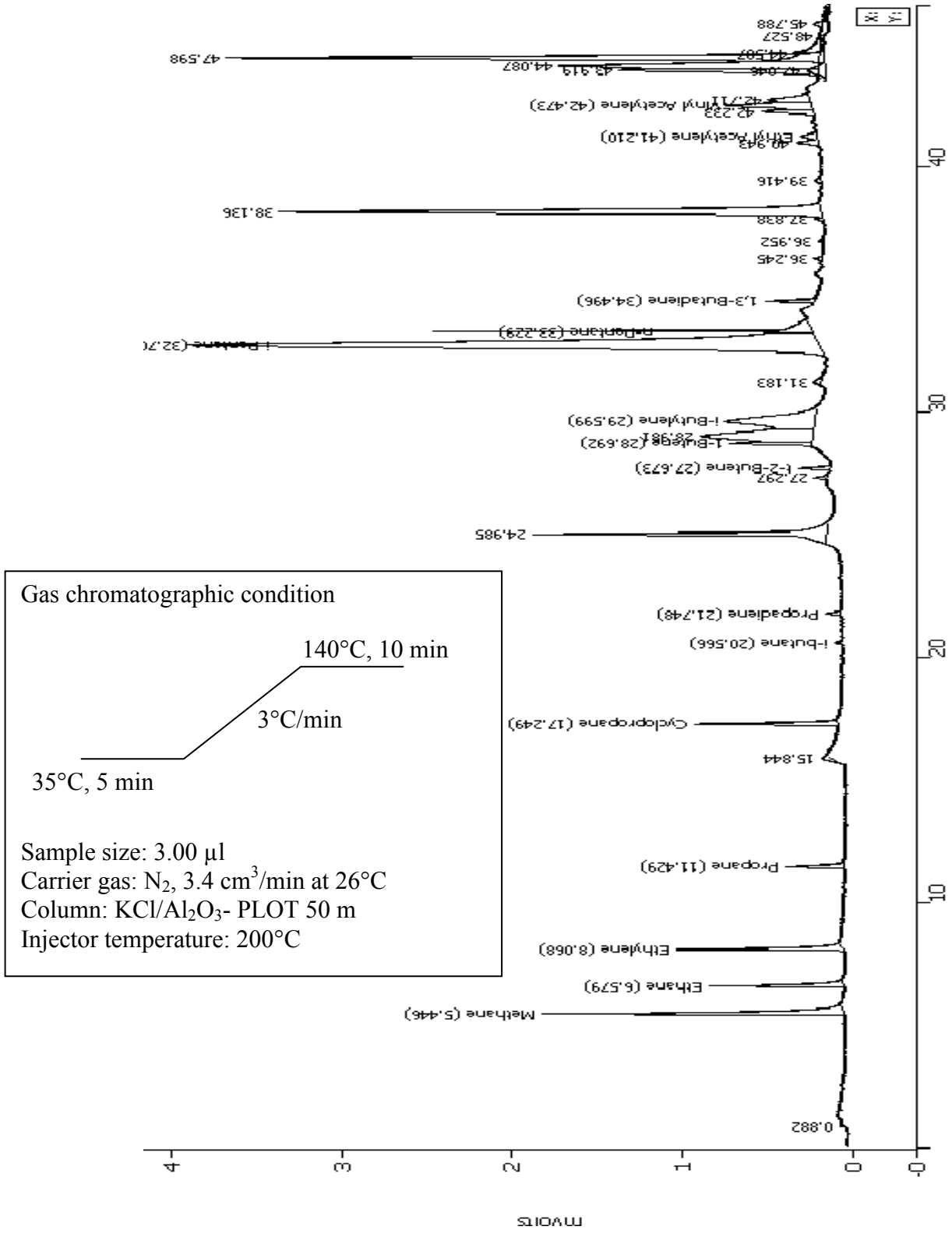

Figure B-2 Gas chromatogram of products from catalytic pyrolysis of corncob over Al-SBA-15 (SiO_2/Al_2O_3=20) at 300°C.

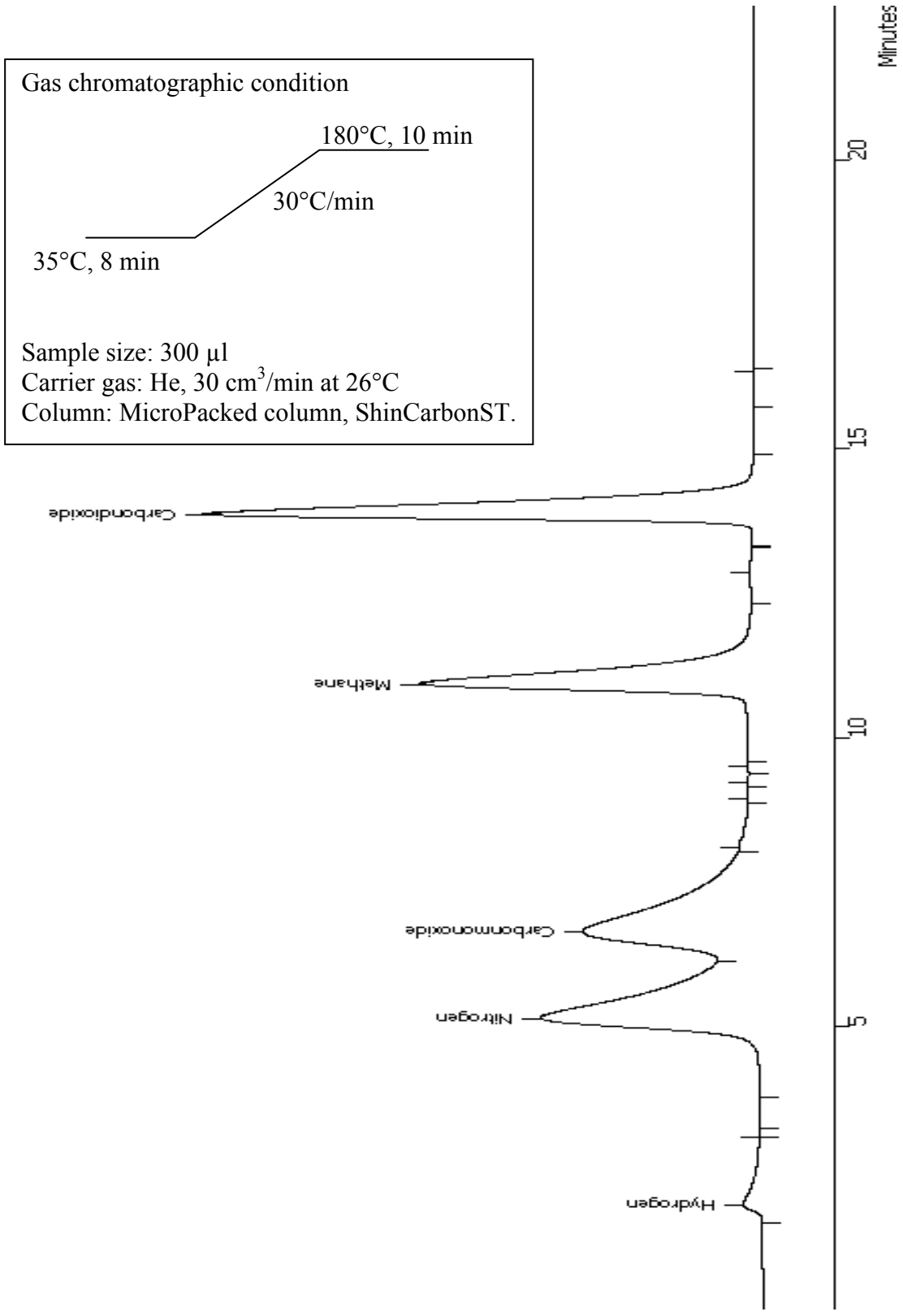

Figure B-3 Gas chromatogram of standard mixture permanent gas.

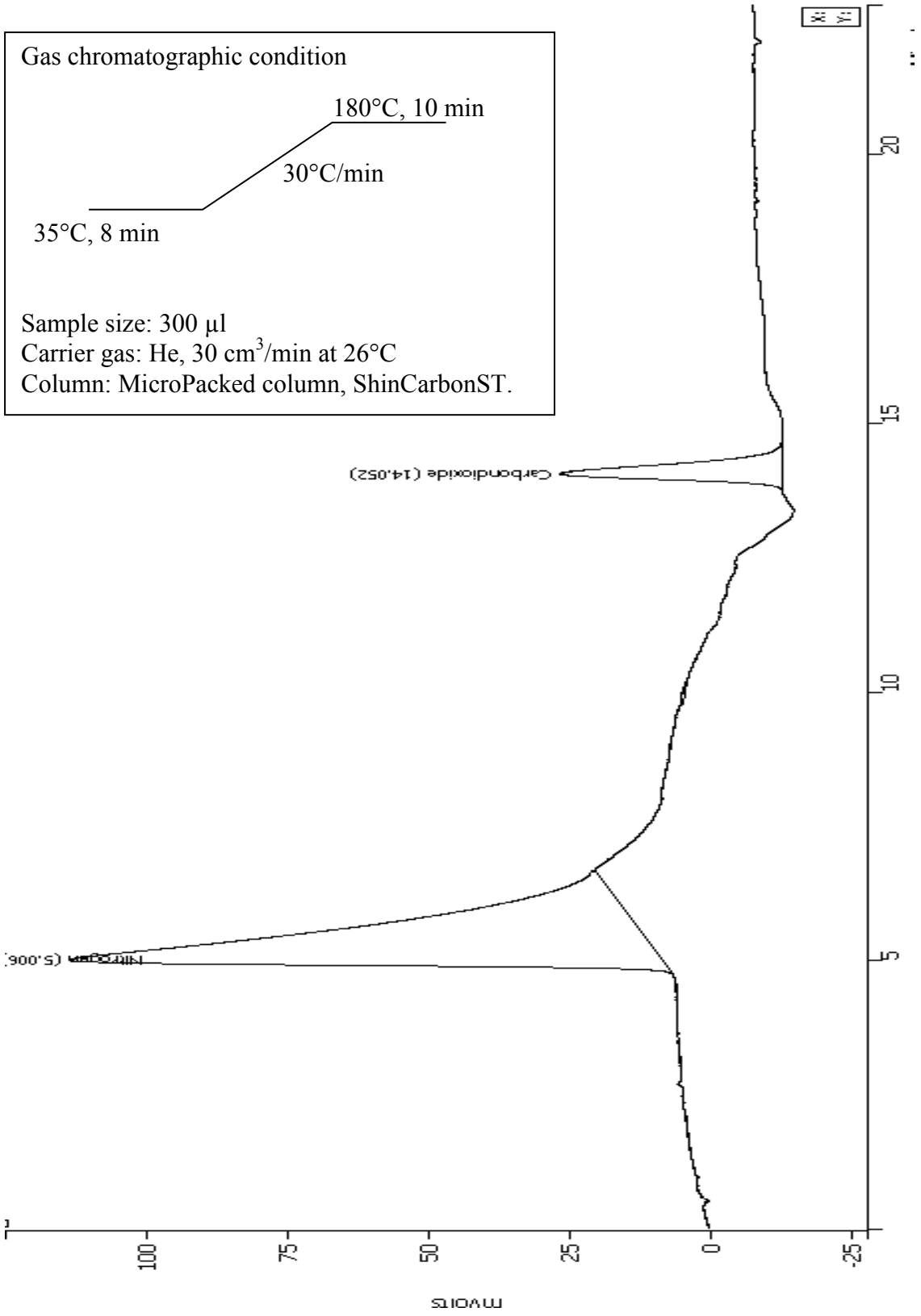

Figure B-4 Gas chromatogram of gas product from catalytic pyrolysis of corncob over Al-SBA-15 (SiO_2/Al_2O_3=20) at 300°C.

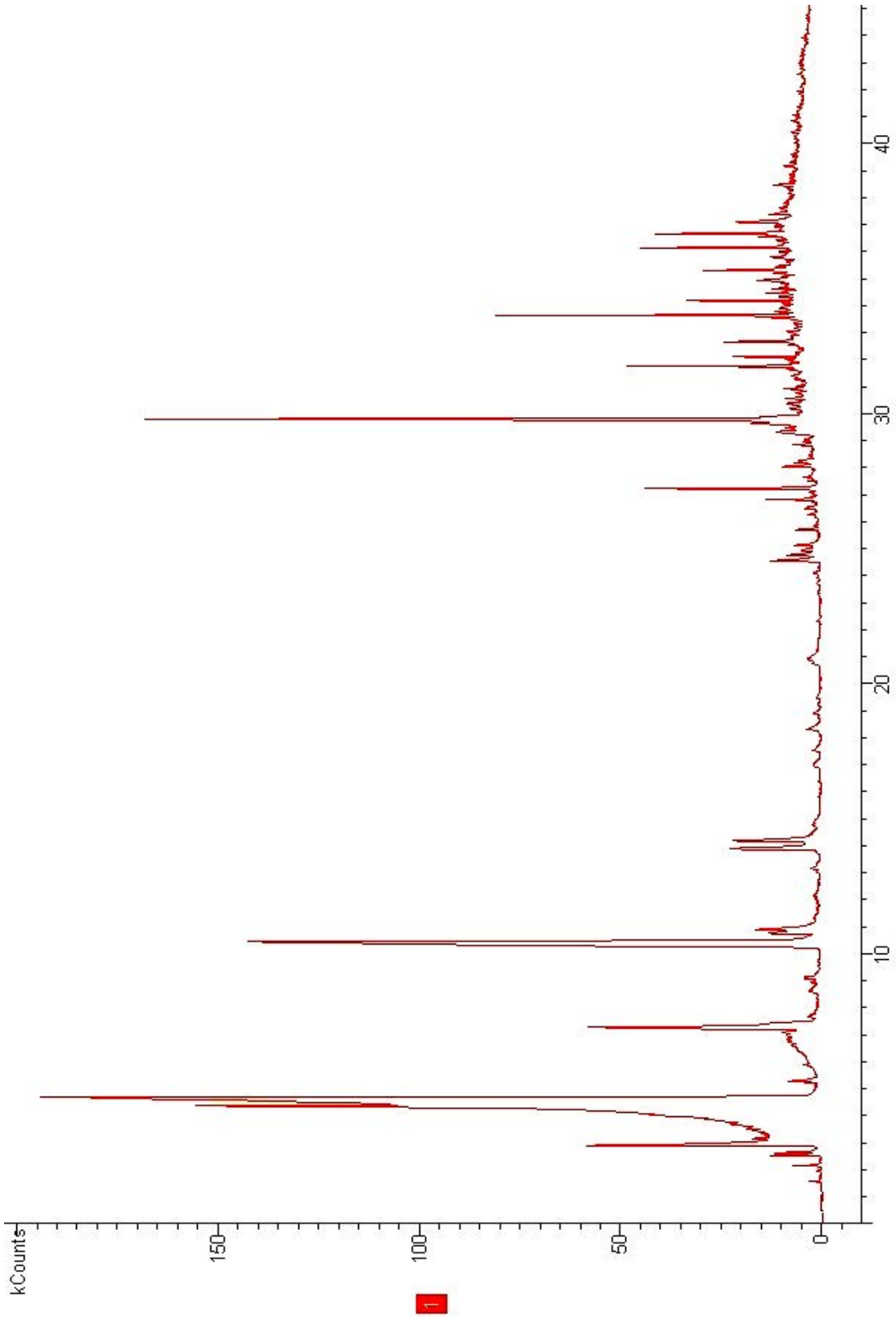

Figure B-5 Liquid chromatogram of product from thermal pyrolysis of corncob at 300°C.

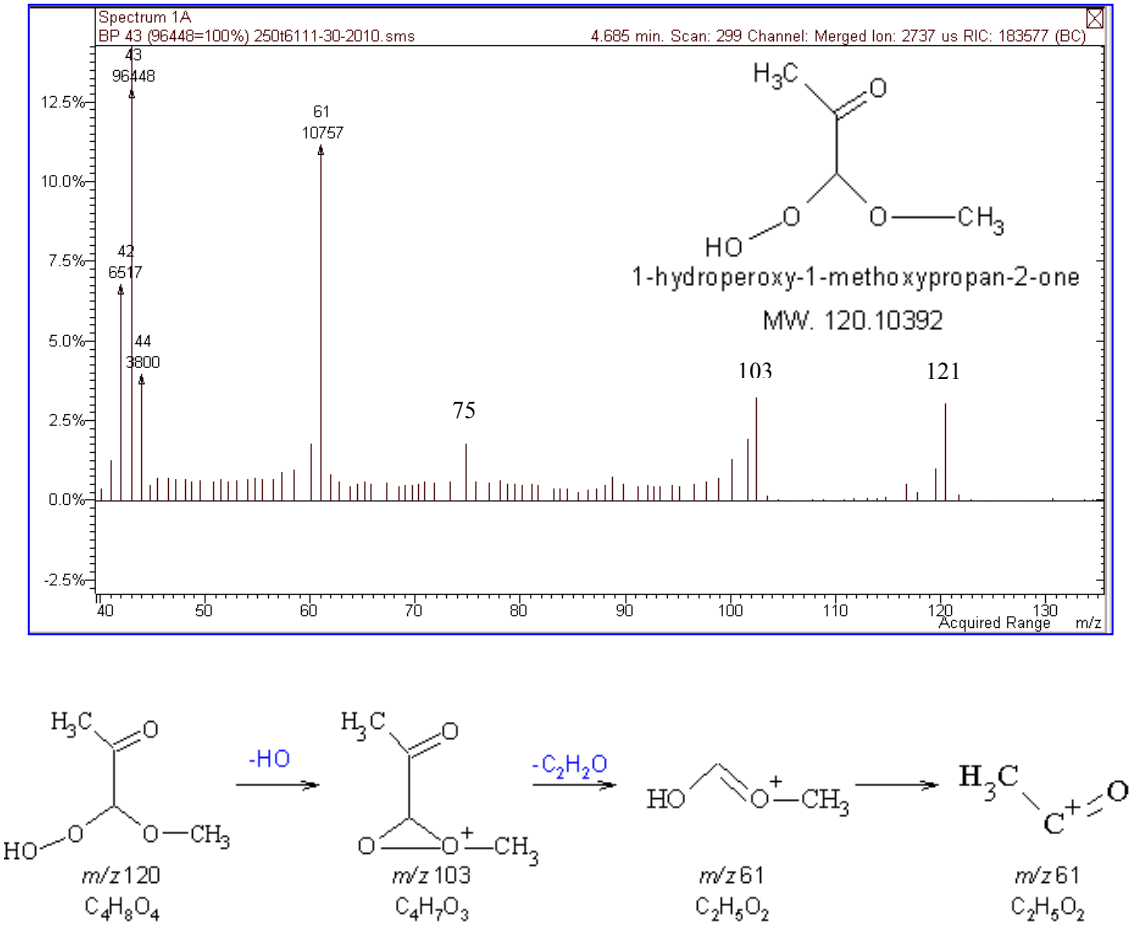

Figure B-6 Mass spectra of 1-hydroperoxy-1-methoxypropan-2-one.

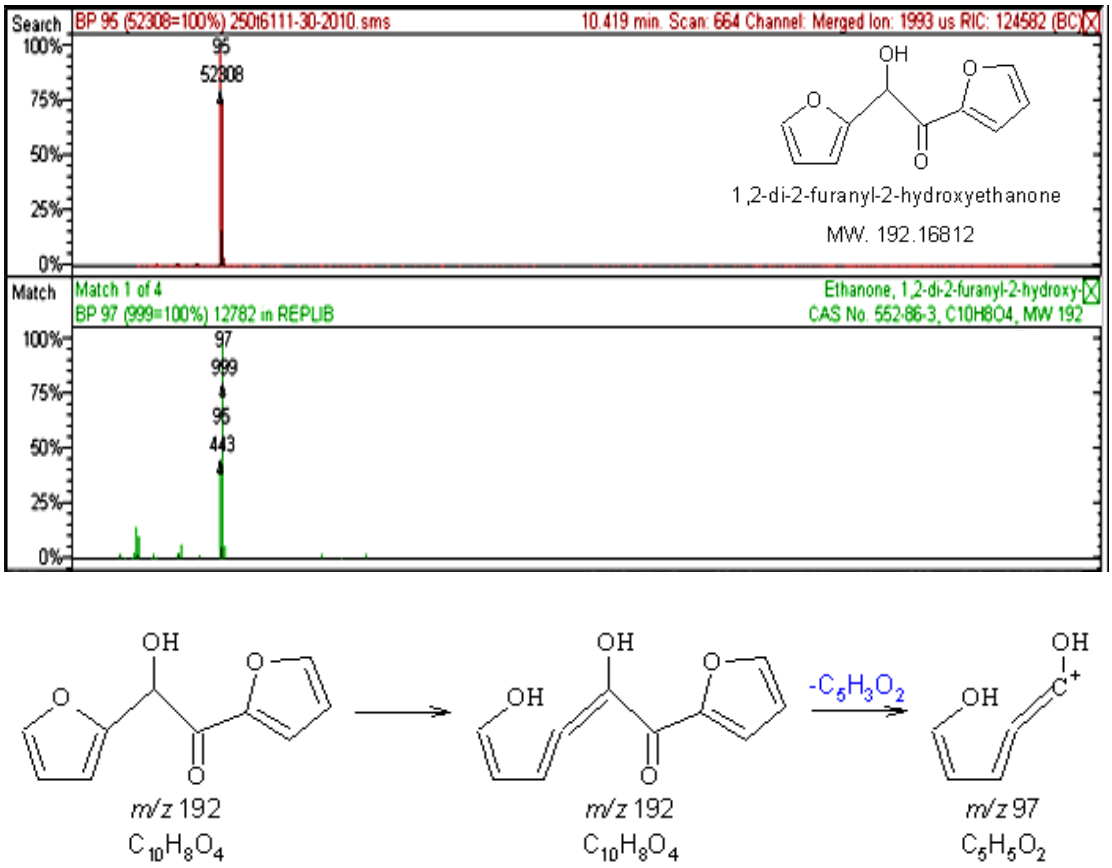

Figure B-7 Mass spectra of 1,2-di-2-furanyl-2-hydroxyethanone.

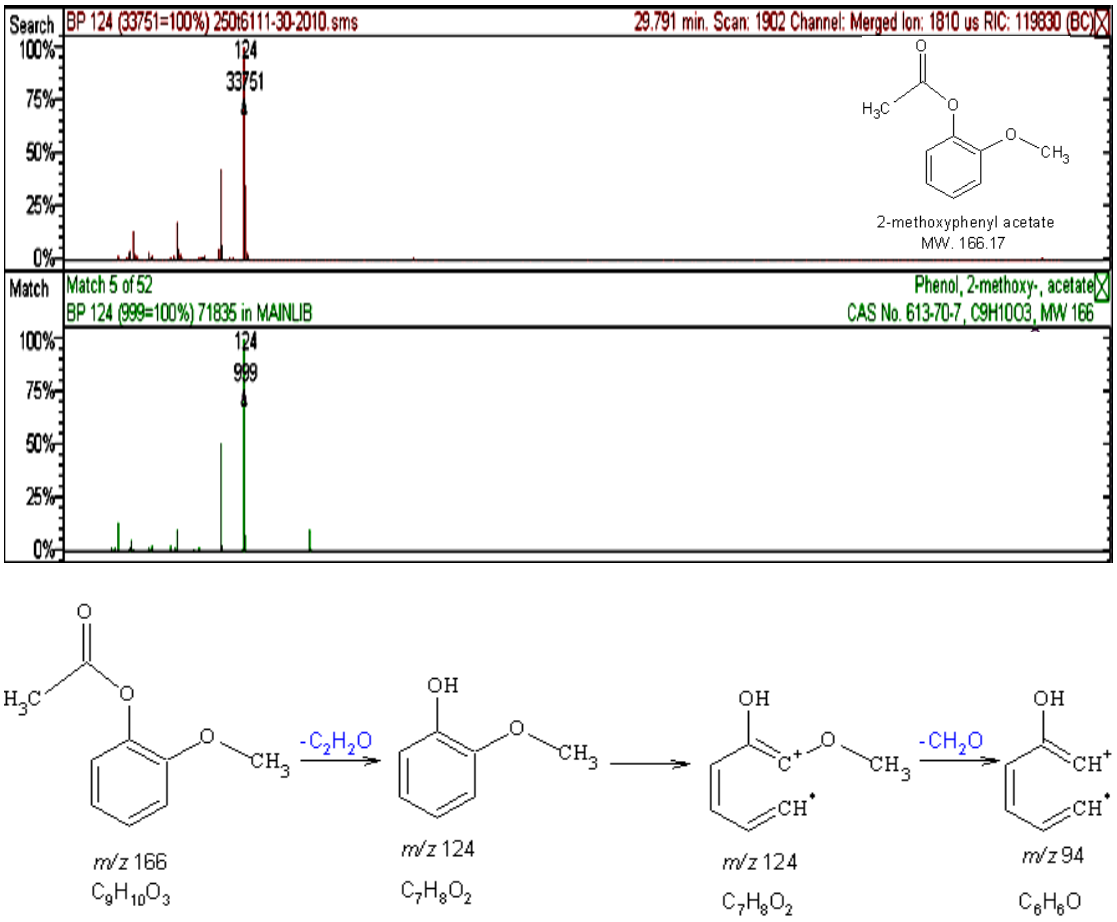

Figure B-8 Mass spectra of 2-Methoxyphenyl acetate.

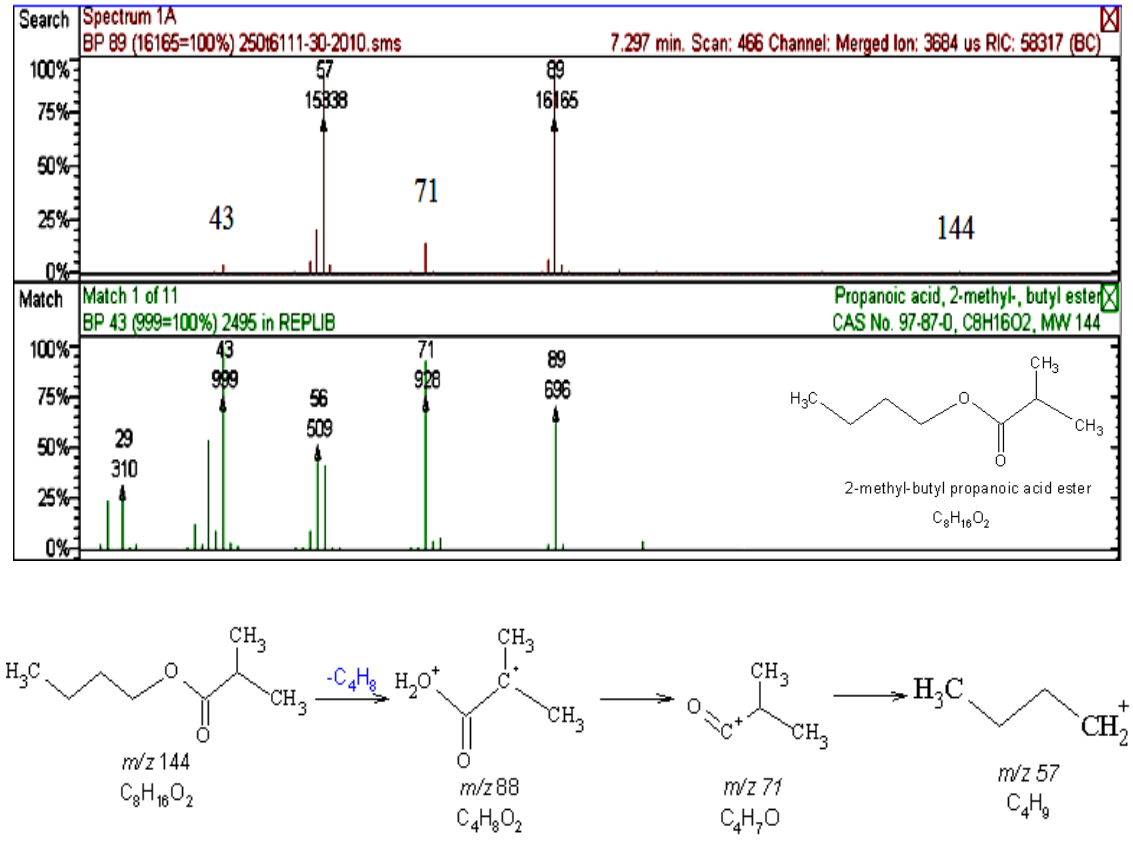

Figure B-9 Mass spectra of 2-Methyl-butyl propanoic acid ester.

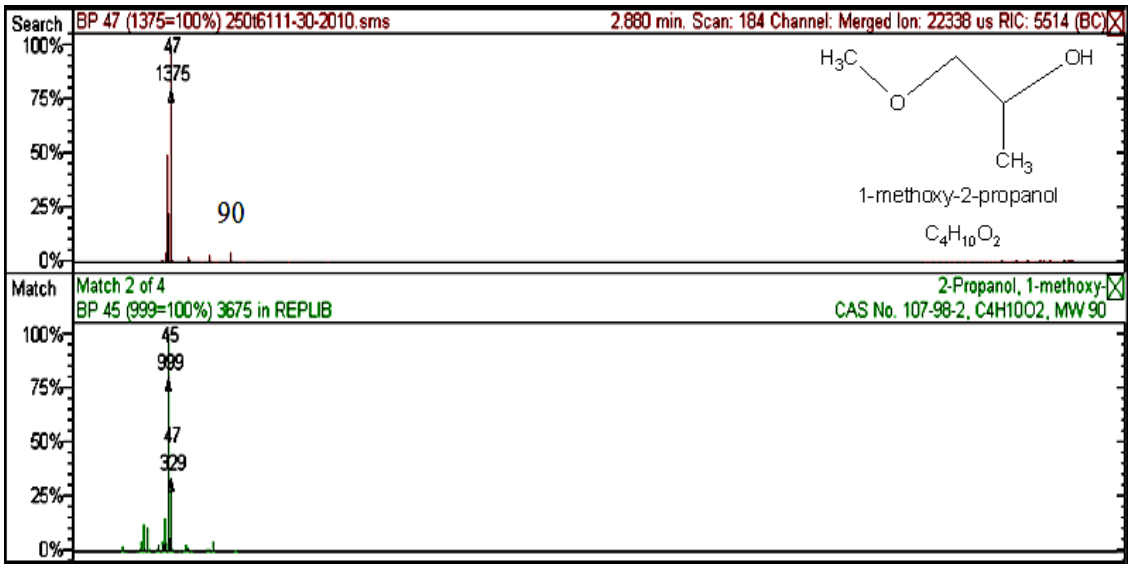

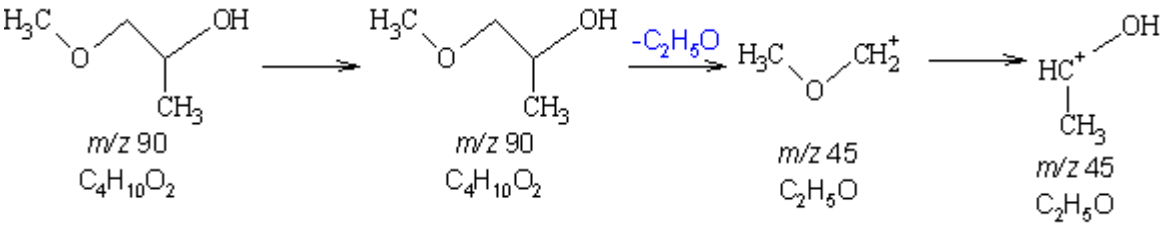

Figure B-10 Mass spectra of 1-Methoxy-2-propanol.

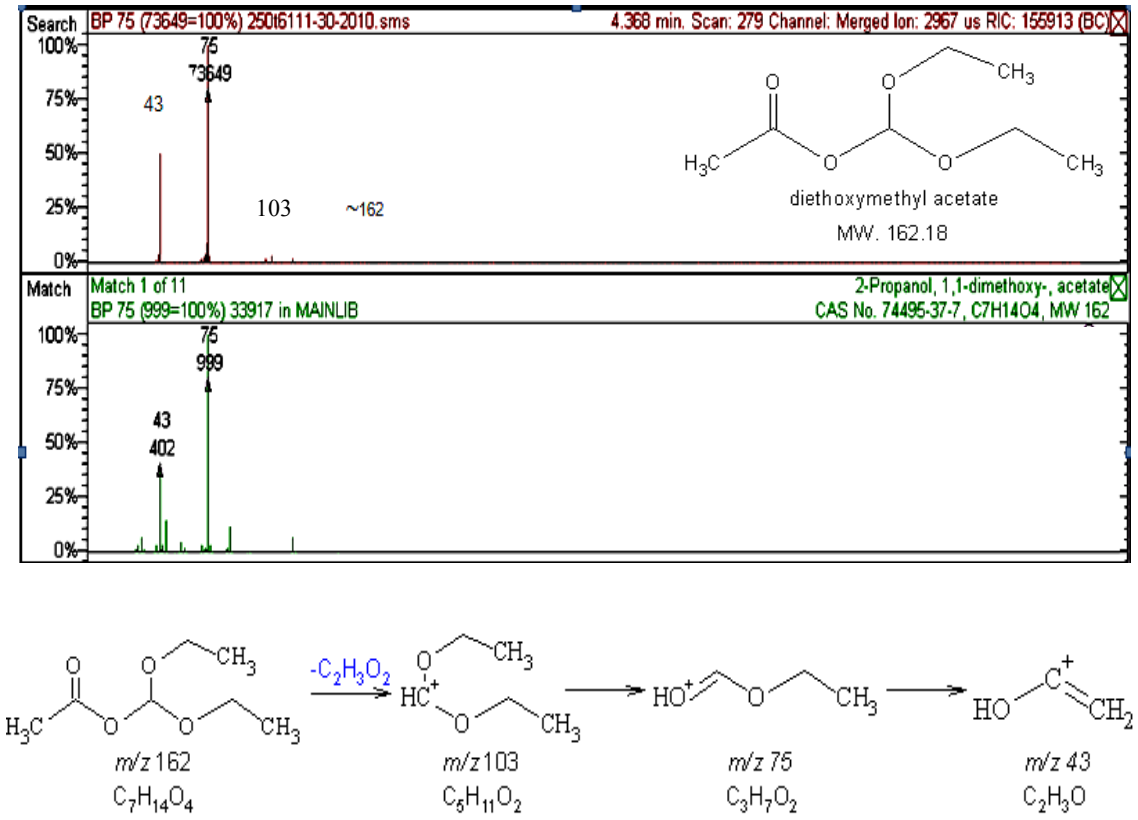

Figure B-11 Mass spectra of Diethoxymethyl acetate.

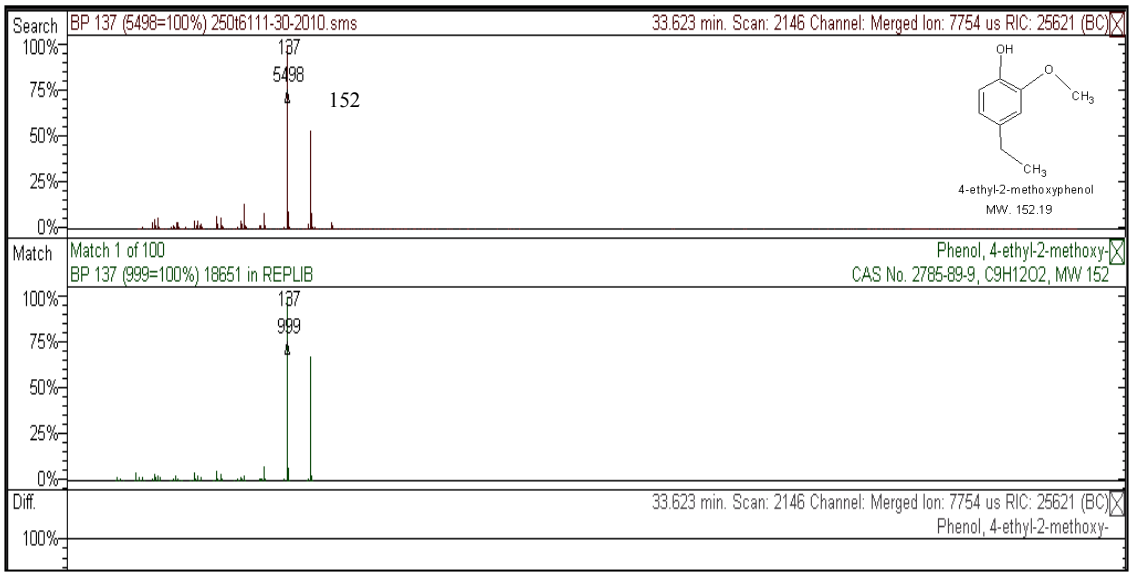

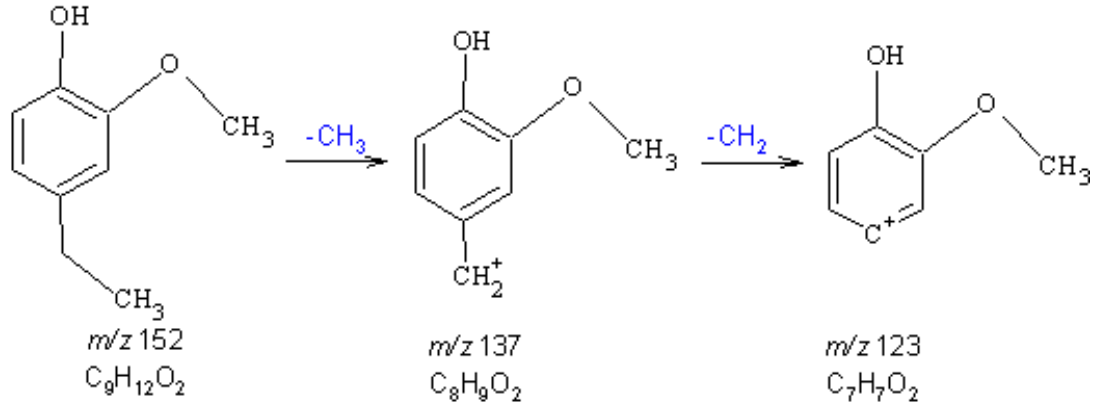

Figure B-12 Mass spectra of 4-Ethyl-2-methoxy phenol.

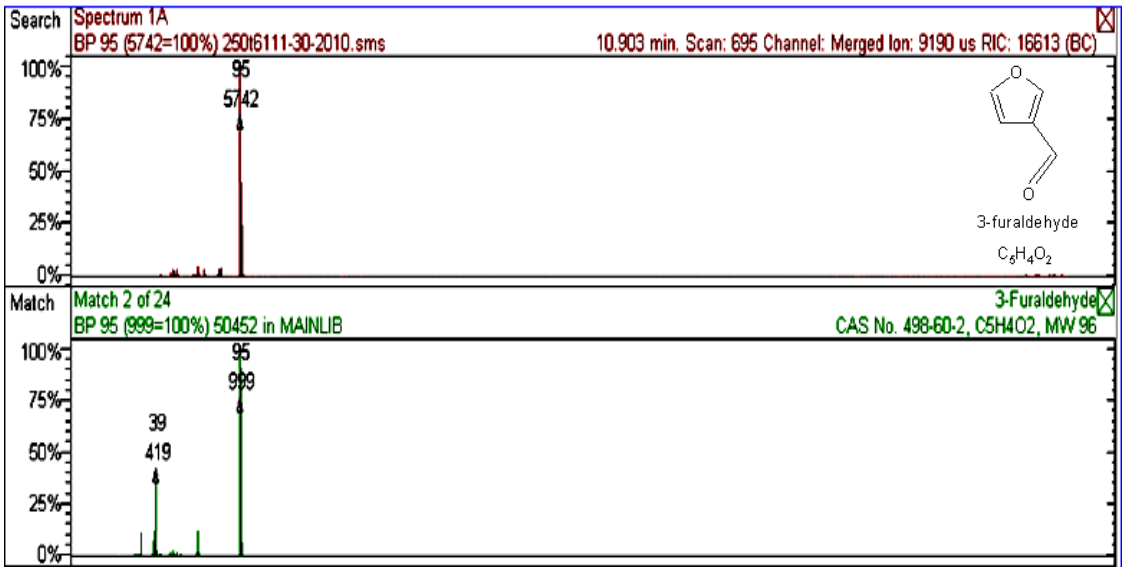

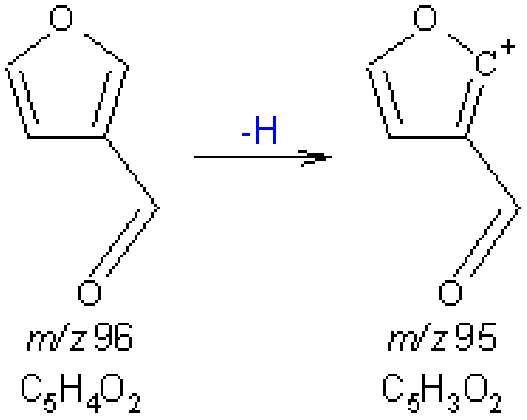

Figure B-13 Mass spectra of 3-Furaldehyde.

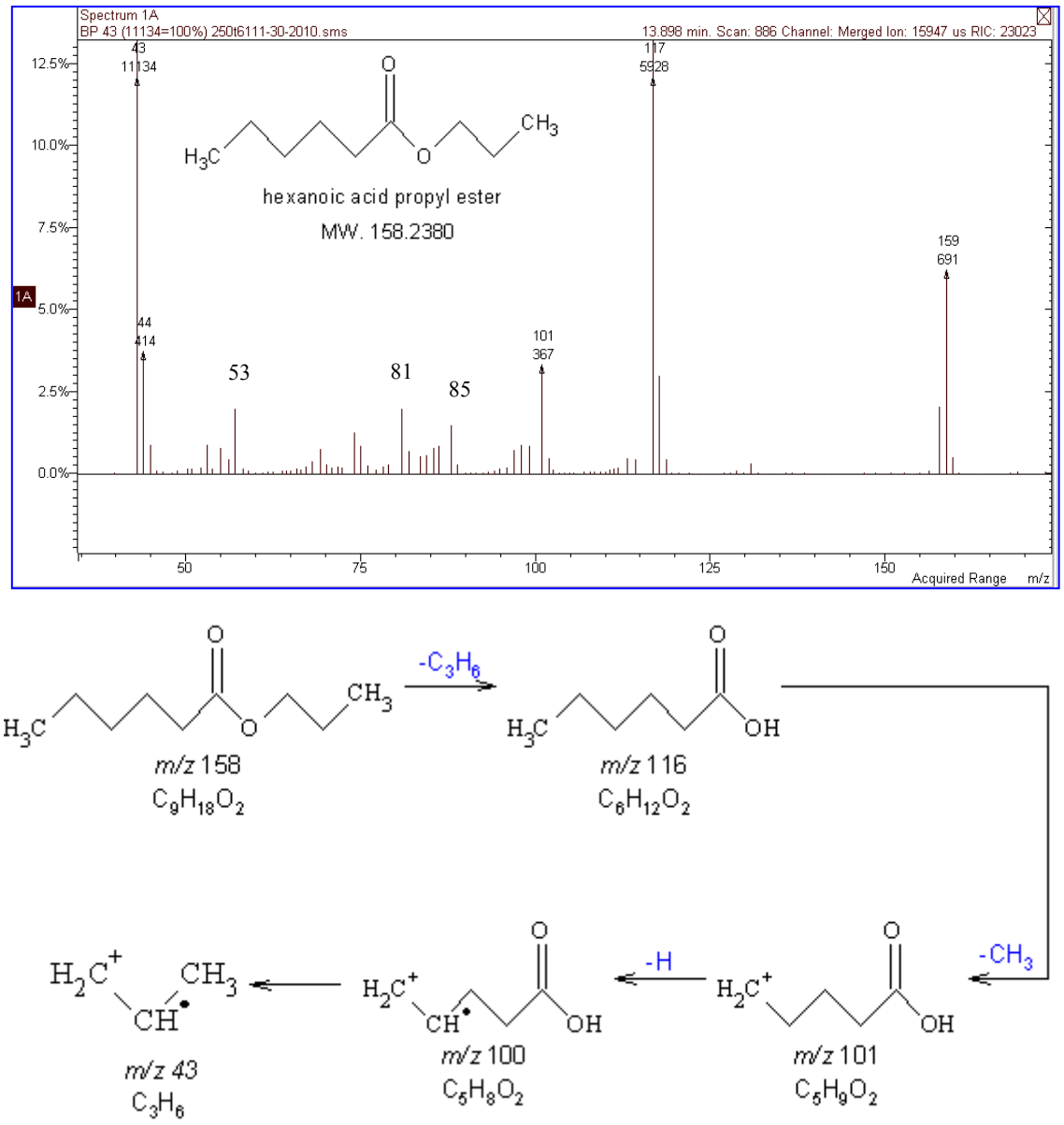

Figure B-14 Mass spectra of Hexanoic acid propyl ester.

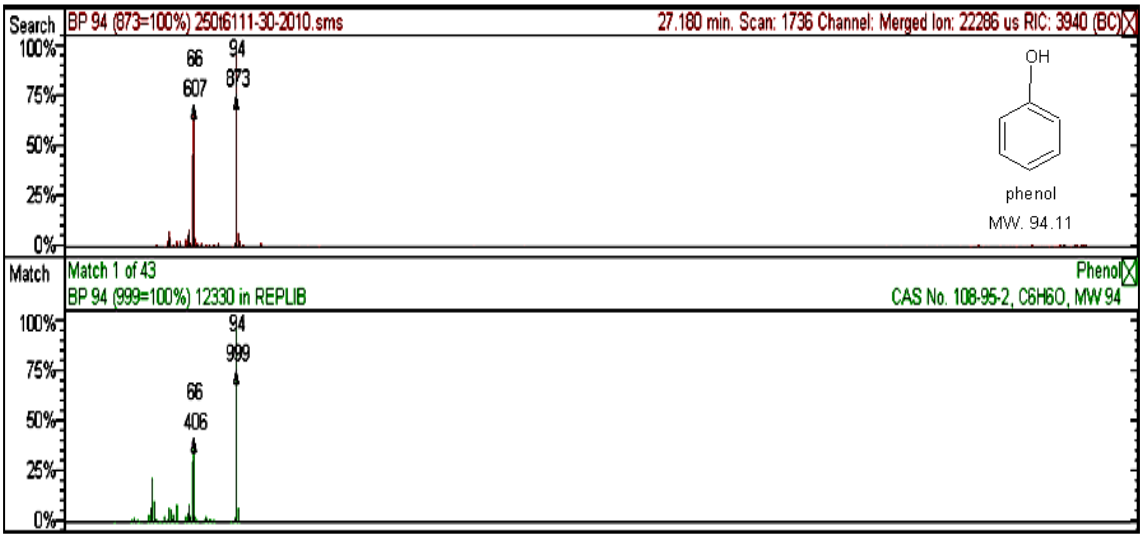

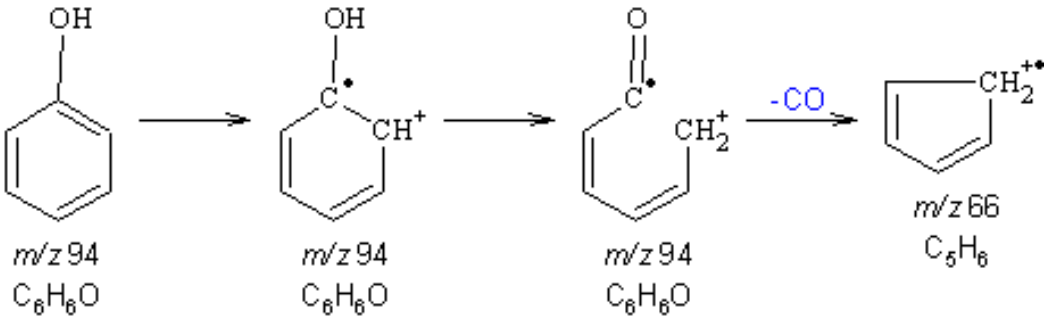

Figure B-15 Mass spectra of phenol.

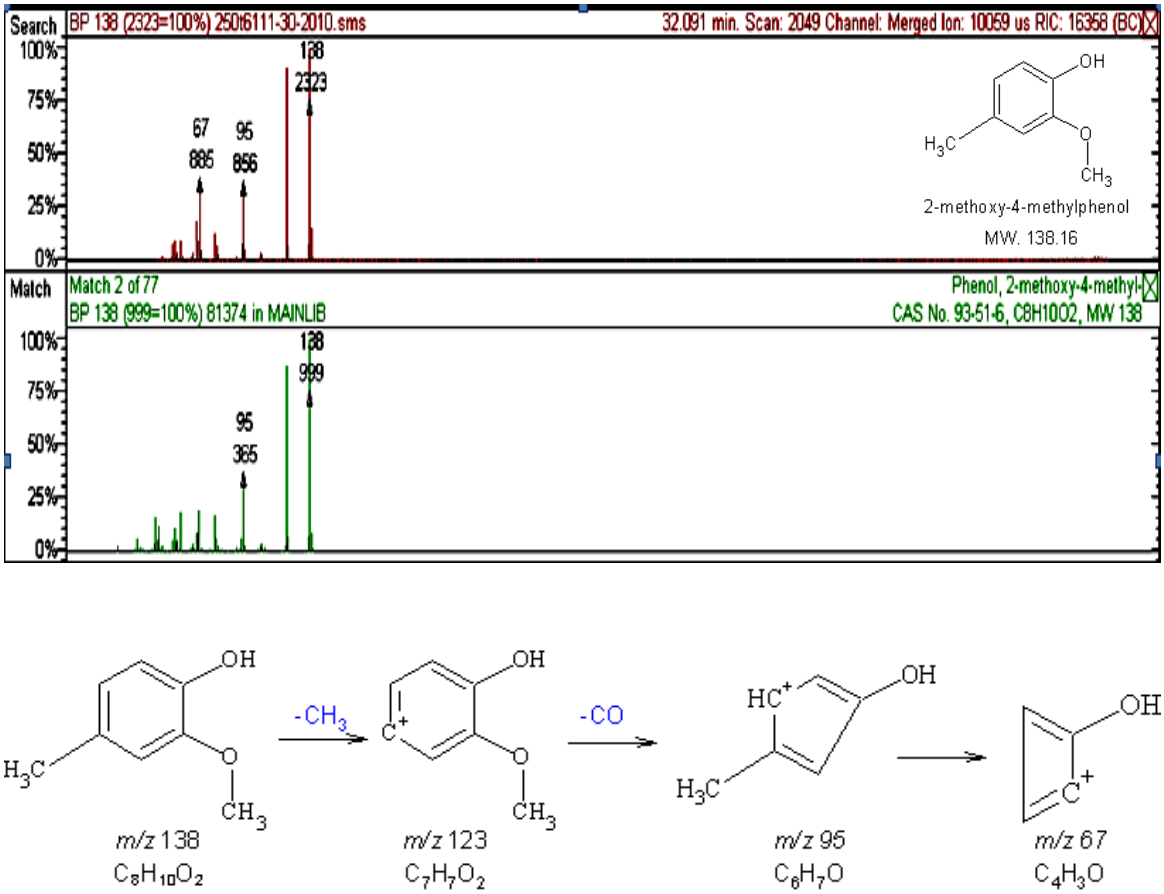

Figure B-16 Mass spectra of 2-Methoxy-4-methylphenol.

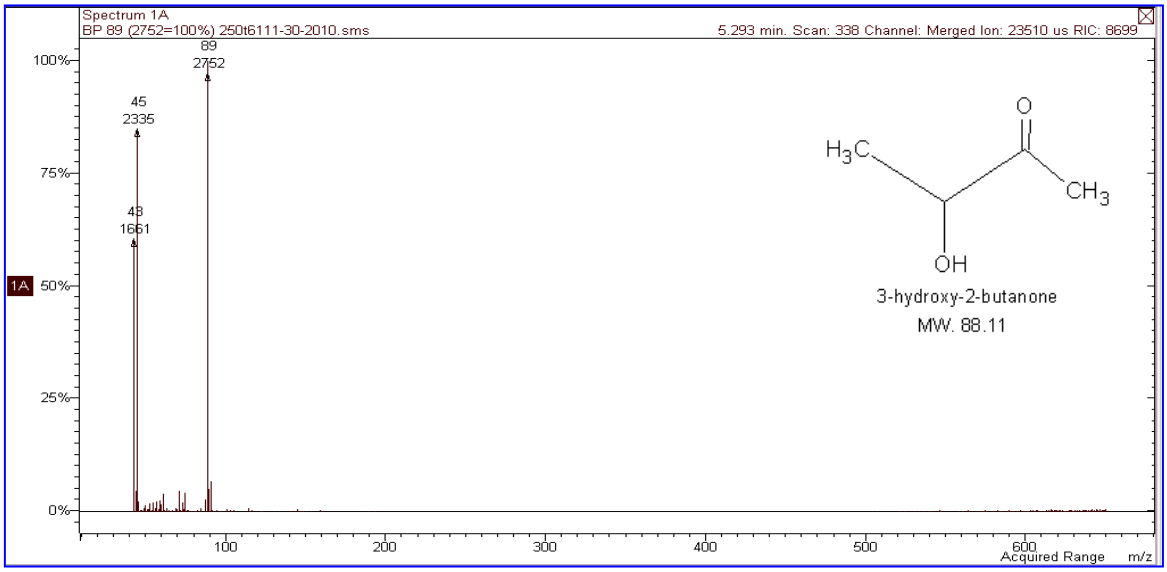

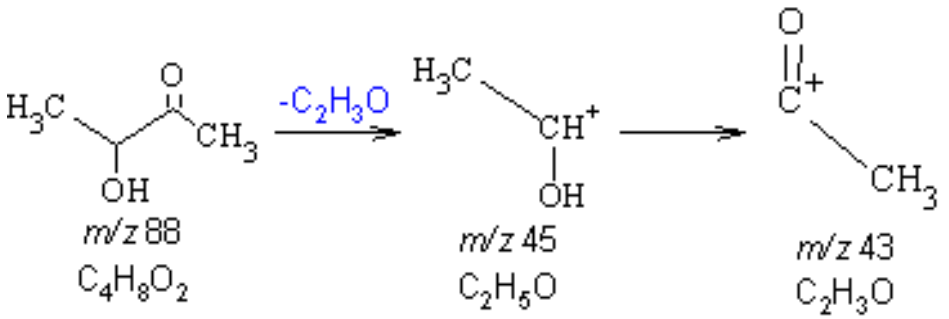

Figure B-17 Mass spectra of 3-hydroxy-2-butanone.

C.1 Proposed mechanism of product in ester group

2-methoxyphenyl acetate (no.10) was derived from the decomposition of monomeric lignin unit and then reacted with acetic acid via nucleophilic aromatic substitution. The proposed pyrolytic pathway of 2-methoxyphenyl acetate (no.10) was shown in Figure C-1. The monomeric lignin unit was deprotonated and then gave benzyne intermediate. In the addition step, acetic acid could be derived from the fragmentation of cellulose (Figure C-2) or the deacetylation of hemicellulose (Figure C-3). Acetic worked as nucleophile attacked to triple bond of benzyne intermediate and then produced the 2-methoxyphenyl acetate product (no.10) [88, 89].

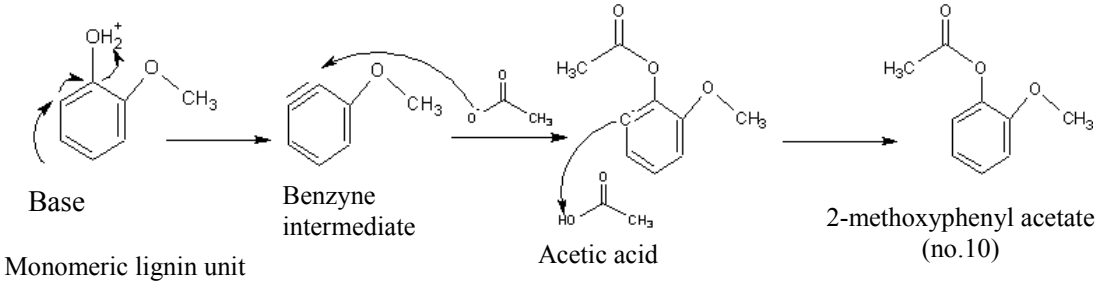

Figure C-1 The proposed pyrolytic pathway of 2-methoxyphenyl acetate (no.10).

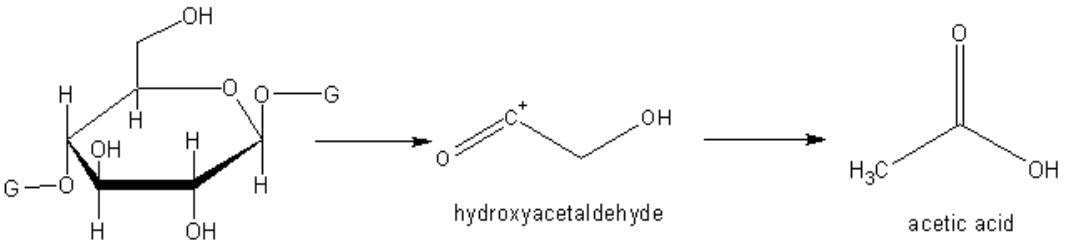

Cellulose unit

Figure C-2 The proposed pyrolytic pathway of pyrolysis cellulose unit.

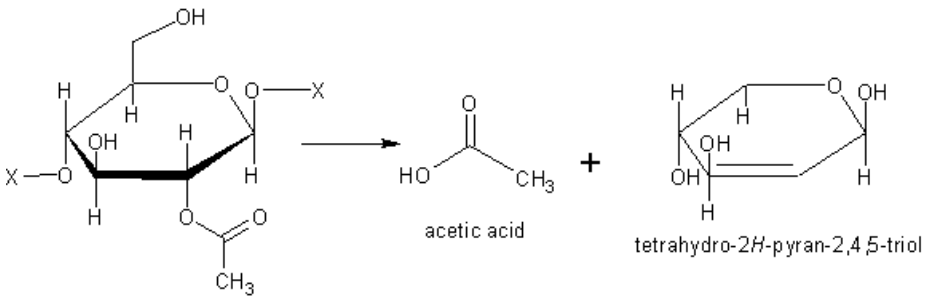

O-acetyl xylan unit

Figure C-3 The proposed pyrolytic pathway of *O*-acetyl xylan unit from hemicellulose.

C.2 Proposed mechanism of product in phenolic compound

The 4-ethylphenol (no.2) and 4-ethyl-2-methoxyphenol (no.3) were related to the degradation of *p*-coumaryl alcohol from the decomposition of monomeric lignin unit. The two pathways of both compounds were proposed in Figure C-4 [90]. The cleavage of α- and β- carbon bond in pathway-I and demethoxylation led to 4-ethyl-2-methoxyphenol (no.3) and 4-ethylphenol (no.2). If the bond between oxygen and β-position carbon of *p*-coumaryl alcohol was cleaved in pathway-II, 4-ethylphenol (no.2) and 4-ethyl-2-methoxyphenol (no.3) were formed via demethylation and dehydroxylation, respectively.

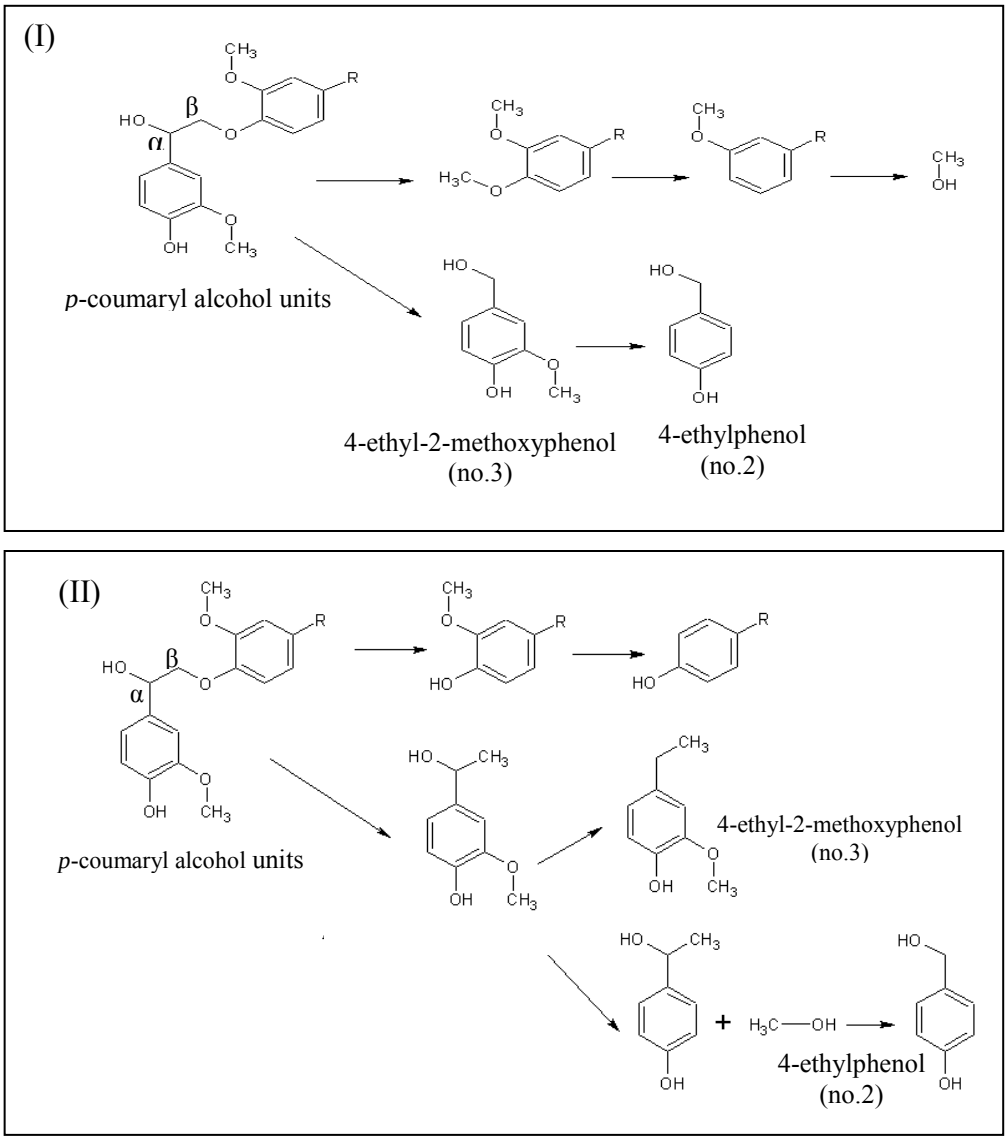

Figure C-4 The proposed pyrolytic pathway of 4-ethylphenol (no.2) and 4-ethyl-2-methoxyphenol (no.3).

C.3 Proposed mechanism of product in furan derivatives

The furan derivatives might be decomposed from cellulose. The proposed reaction pathway of 1,2-di-2-furanyl-2-hydroxy-rthanone or furoin (no.6) was shown in Figure C-5. The cleavage of the bond between oxygen and C-1 or C-6 position and dehydration led to furfural formation. After that furoin was produced via dimerization of furfural [91, 92].

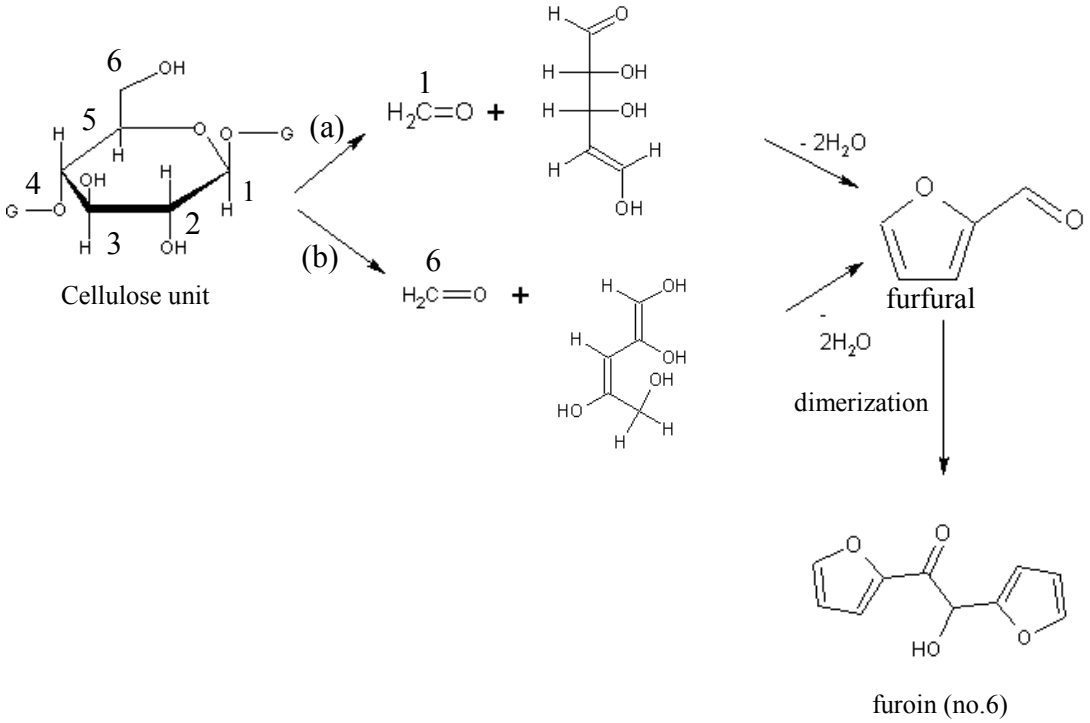

Figure C-5 The proposed pyrolytic pathway of 1,2-di-2-furanyl-2-hydroxy-ethanone (no.6).

C.4 Proposed mechanism of product in acid group

The acid products, i.e. formic acid and acetic acid were commonly detected in distillated liquid fraction from the pyrolysis of hemicelluloses. The formation mechanism for formic acid (no.29) and acetic acid were proposed in Figure C-6. The 4-*O*-methylglucurono-xylan unit was eliminated to hydroxy-aldehydes, furfural and small carboxylic molecules [91].

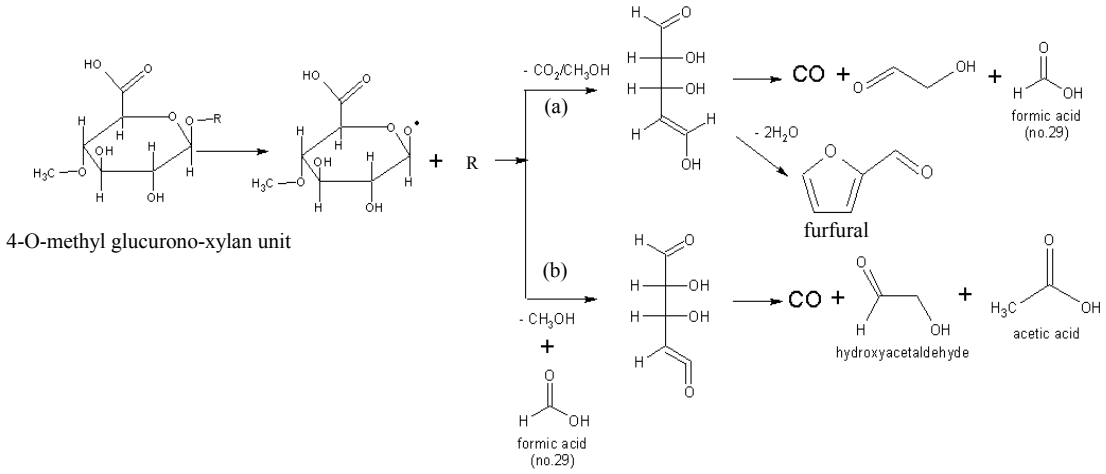

Figure C-6 The proposed pyrolytic pathway of formic acid (no.29).

VITAE

Miss Chomalee Kasiban was born on January 24, 1985 in Nakhon Phanom, Thailand. She graduated with Bachelor of Industrial Chemistry from Faculty of Applied science, King Mongkut‟s University of Technology North Bangkok in 2007. She continued her study in Petrochemistry and Polymer Science, Chulalongkorn University in 2008 and completed in 2011. She participated in 14th Asian Chemical Congress (14th ACC) on September 5-8, 2011 at Queen sirikit national convention center, Bangkok, Thailand.